UNDERDETERMINED DIRECTION OF ARRIVAL ESTIMATION WITH NESTED CIRCULAR RING ARRAYS

A THESIS SUBMITTED TO
THE GRADUATE SCHOOL OF NATURAL AND APPLIED SCIENCES
OF
MIDDLE EAST TECHNICAL UNIVERSITY

BY

HIKMET BUĞUR

IN PARTIAL FULFILLMENT OF THE REQUIREMENTS
FOR
THE DEGREE OF MASTER OF SCIENCE
IN
ELECTRICAL AND ELECTRONICS ENGINEERING

AUGUST 2024

Approval of the thesis:

UNDERDETERMINED DIRECTION OF ARRIVAL ESTIMATION WITH NESTED CIRCULAR RING ARRAYS

submitted by **HIKMET BUĞUR** in partial fulfillment of the requirements for the degree of **Master of Science in Electrical and Electronics Engineering Department, Middle East Technical University** by,

Prof. Dr. Naci Emre Altun
Dean, Graduate School of **Natural and Applied Sciences** _____

Prof. Dr. İlkay Ulusoy
Head of Department, **Electrical and Electronics Engineering** _____

Prof. Dr. Temel Engin Tuncer
Supervisor, **Electrical And Electronics Engineering, METU** _____

Examining Committee Members:

Assist. Prof. Dr. Gökhan Muzaffer Güvensen
Electrical And Electronics Engineering, METU _____

Prof. Dr. Temel Engin Tuncer
Electrical And Electronics Engineering, METU _____

Prof. Dr. Tansu Filik
Electrical And Electronics Engineering, ESTU _____

Date:27.08.2024

I hereby declare that all information in this document has been obtained and presented in accordance with academic rules and ethical conduct. I also declare that, as required by these rules and conduct, I have fully cited and referenced all material and results that are not original to this work.

Name, Surname: Hikmet Buğur

Signature :

ABSTRACT

UNDERDETERMINED DIRECTION OF ARRIVAL ESTIMATION WITH NESTED CIRCULAR RING ARRAYS

Buğur, Hikmet
M.S., Department of Electrical and Electronics Engineering
Supervisor: Prof. Dr. Temel Engin Tuncer

August 2024, 96 pages

Circular arrays are optimal for achieving an isometric DOA response in planar geometries, especially when the inter-element spacing is less than half the operating wavelength. However, in underdetermined scenarios—where the number of sources exceeds the number of sensors—these arrays often experience performance degradation due to wider beamwidths and higher sidelobe levels. These limitations are not fully addressed in the existing literature. This thesis introduces a novel array structure, the Nested Circular Ring Arrays (NCRA), which combines the benefits of sparsity and circular symmetry to improve DoA estimation accuracy in these challenging cases. NCRA provides a larger effective aperture than traditional circular arrays, resulting in a narrower beamwidth and reduced sidelobe levels, which enhance resolution and yield more accurate DoA estimates. These improvements allow NCRA to more precisely localize sources compared to a Uniform Circular Array (UCA) with the same number of sensors. The thesis investigates both overdetermined and underdetermined scenarios, with a particular focus on the challenges posed by coherent sources in underdetermined cases. Techniques such as Maximum Likelihood Estimation (MLE) for covariance matrices and Sparse Bayesian Learning (SBL) are applied

to these scenarios. Additionally, the Khatri-Rao product is used to effectively manage underdetermined cases by mapping observations to a higher dimension. A detailed analysis of NCRA's design and performance, supported by Cramér-Rao Lower Bound (CRLB) comparisons, demonstrates that NCRA not only maintains isotropic characteristics but also significantly outperforms conventional circular arrays. This makes NCRA a robust solution for underdetermined DoA estimation, particularly in environments demanding high accuracy and reliability.

Keywords: Underdetermined DoA Estimation, Sparse Bayesian Learning, Sparse Arrays

ÖZ

İÇ İÇE GEÇMİŞ DAİRESEL HALKALI DİZİLER İLE SENSÖR SAYISINDAN FAZLA GELİŞ AÇISI TAHMİNİ

Buğur, Hikmet
Yüksek Lisans, Elektrik ve Elektronik Mühendisliği Bölümü
Tez Yöneticisi: Prof. Dr. Temel Engin Tuncer

Ağustos 2024 , 96 sayfa

Dairesel diziler, elemanlar arası mesafenin dalga boyunun yarısından az olduğu düzlemsel dizi geometrilerinde izometrik DoA kestirimi için idealdir. Ancak, kaynak sayısının sensör sayısını aştığı eksik tanımlı senaryolarda, bu diziler geniş huzme genişliği ve yüksek yan lob seviyeleri nedeniyle performans düşüklüğü yaşayabilir. Bu sorunlar mevcut literatürde yeterince ele alınmamıştır. Bu tezde, eksik tanımlı DoA kestiriminde doğruluğu artırmak amacıyla seyrekliğin ve dairesel simetrinin avantajlarını birleştiren yeni bir dizi yapısı olan İç İçe Geçmiş Dairesel Halkalı Diziler (NCRA) tanıtılmaktadır. NCRA, geleneksel dairesel dizilere göre daha büyük bir efektif açıklık sağlayarak daha dar bir huzme genişliği ve azaltılmış yan lob seviyeleri sunabilmektedir, bu da daha iyi bir çözünürlük ve daha doğru DoA kestirimleri ile sonuçlanır. Bu özellikler, NCRA'nın aynı sensör sayısına sahip Dairesel Tekdüzen Dizi (UCA) ile karşılaştırıldığında, kaynakları daha doğru bir şekilde konumlandırabilmesini sağlar. Tezde, eksik tanımlı ve fazla tanımlı (overdetermined) senaryolar ile ilişkili/koherent ve ilişkisiz kaynaklar incelenmiştir. Eksik tanımlı durum, özellikle koherent kaynaklar için zorlu bir senaryodur. Bu durumları ele almak için Maksimum Olabilirlik

Kestirisicisi (MLE) kullanılarak kovaryans matrislerinin tahmini ve Seyrek Bayesian Öğrenmesi (SBL) gibi teknikler kullanılmıştır. Ayrıca, eksik tanımlı senaryoların yönetimi için gözlemleri daha yüksek bir boyuta taşımak amacıyla Khatri-Rao çarpımı kullanılmaktadır. Tezde, NCRA'nın tasarımı ve performansı, Cramér-Rao Alt Sınırı (CRLB) ile desteklenmiş çeşitli senaryolar üzerinden detaylı şekilde analiz edilmiştir. NCRA'nın izotropik özelliklerini korumanın yanı sıra geleneksel dairesel dizilere kıyasla belirgin şekilde daha iyi performans gösterdiği kanıtlanmıştır. Bu, NCRA'yı yüksek doğruluk ve güvenilirlik gerektiren ortamlarda eksik tanımlı DoA kestirimi için etkili bir çözüm haline getirmektedir.

Anahtar Kelimeler: Sensör Sayısından Fazla İşaret Geliş Açısı Kestirimi, Seyrek Bayes Öğrenmesi, Seyrek Diziler

to living memory of grandma and grandpa

ACKNOWLEDGMENTS

I would like to express my deepest gratitude to my supervisor, Prof. Dr. Temel Engin Tuncer, for his unwavering support and invaluable guidance throughout this journey. His dedication, generous commitment of time, and expertise, extending far beyond his formal responsibilities, have been essential to the completion of this study. His insightful advice and encouragement during challenging moments made this work possible, and I feel privileged to have had the benefit of his mentorship.

I am also profoundly grateful to Dr. Serkan Karakütük and Prof. Dr. Tansu Filik, for their support, and thoughtful guidance. Their suggestions have shaped my approach and broadened my perspective, playing a crucial role in the development of this thesis.

Additionally, I would like to sincerely thank my family—Tekin Buğur, Meral Buğur, Abdullah Buğur, and Yıldıray Meral—for their unwavering motivation and patience. Their support has been a cornerstone throughout this process.

I would also like to extend my appreciation to Ersoy Çalışkan, MSc, Hakan Özen, MSc, and Safa Çelik, MSc, for their assistance and support during this time.

Lastly, I am deeply thankful to my girlfriend, Gamze Şimşek, for her continuous support and patience throughout this work.

TABLE OF CONTENTS

ABSTRACT v

ÖZ vii

ACKNOWLEDGMENTS x

TABLE OF CONTENTS xi

LIST OF TABLES xiv

LIST OF FIGURES xv

LIST OF ABBREVIATIONS xviii

CHAPTERS

1 INTRODUCTION 1

1.1 Motivation and Problem Definition 1

1.2 Contributions and Novelties 3

1.3 The Outline of the Thesis 4

2 DIRECTION OF ARRIVAL ESTIMATION 7

2.1 Data Model 8

2.2 Direction Of Arrival Estimation Methods 9

2.2.1 MUltiple SIgnal Classification (MUSIC) 9

2.2.2 Sparse Bayesian Learning (SBL) 11

2.3 Maximum Likelihood(ML) Covariance Matrix Estimation using Coordinate-Wise Descent(CWD) Algorithm 15

3 UNDERDETERMINED DIRECTION OF ARRIVAL ESTIMATION OF QUASI-STATIONARY SIGNALS 19

3.1 Difference Co-Arrays 20

3.1.1 Uniform Linear Arrays 22

3.1.2 Co-Prime Arrays 24

3.1.3 Nested Arrays 27

3.1.4 Uniform Circular Arrays 29

3.2 Applying the Khatri-Rao Product to Underdetermined DoA Estimation Problems 31

3.3 Khatri-Rao MUSIC 33

3.4 Cramér-Rao Lower Bound Characteristics of Underdetermined DoA Estimation 34

4 NESTED CIRCULAR RING ARRAYS 37

5 SIMULATION RESULTS 49

5.1 Overdetermined Scenario 49

5.1.1 RMSE-SNR Simulations 50

5.1.2 RMSE-Azimuth Simulations 54

5.2 Underdetermined Scenario 56

5.2.1 RMSE-SNR Simulations 56

5.2.1.1 Non-Coherent Scenario 57

5.2.1.2 Coherent Scenario 64

5.2.2 Resolution Probability Simulations 68

6 CONCLUSIONS 73

REFERENCES 75

APPENDICES

A CRAMÉR-RAO LOWER BOUND FOR OVERDETERMINED DOA ESTIMATION 81

B CRAMÉR-RAO LOWER BOUND FOR UNDERDETERMINED DOA ESTIMATION 83

C DEGREES OF FREEDOM IN THE DIFFERENCE CO-ARRAY OF UNIFORM CIRCULAR ARRAYS 85

D KHATRI-RAO PRODUCT AND DIFFERENCE CO-ARRAY RELATION . 89

E COST FUNCTION FOR MAXIMUM LIKELIHOOD COVARIANCE MATRIX ESTIMATION 91

F OPTIMIZING APERTURE SCALING IN 4-ARM NCRA CONFIGURATIONS 93

LIST OF TABLES

TABLES

Table 3.1 Summary of 2-Level Nested Arrays [1] 27

Table 4.1 NCRA Parameters. 42

Table 4.2 UCA Parameters 46

Table 5.1 Simulation parameters for case 1. 51

Table 5.2 Simulation parameters for case 2. 53

Table 5.3 Simulation parameters. 55

Table 5.4 Simulation Parameters for Case 1 57

Table 5.5 Simulation parameters for case 2. 59

Table 5.6 Simulation parameters for case 3. 61

Table 5.7 Simulation parameters for case 4. 63

Table 5.8 Simulation parameters for case 1. 65

Table 5.9 Simulation parameters for case 2. 67

Table 5.10 Simulation parameters for case 1. 69

Table 5.11 Simulation parameters for case 2. 71

LIST OF FIGURES

FIGURES

Figure 3.1 Illustration of synthetic quasi-stationary signals with frame separations. The lines define the local stationary intervals, namely frames. Only the real parts of the signals are plotted. 20

Figure 3.2 A 7-element Uniform Linear Array (ULA) with inter-element spacing of $d = \lambda/2$, its corresponding difference co-array. 24

Figure 3.3 A 5-element Co-Prime Array with $M = 2$ and $N = 3$ elements, $d = \lambda/2$ along with its corresponding difference co-array. 26

Figure 3.4 A 8-element Co-Prime Array with $M = 3$ and $N = 5$ elements, $d = \lambda/2$ along with its corresponding difference co-array. 26

Figure 3.5 A 6-element Nested Array with $M_1 = 3$ elements for $d_1 = \lambda/2$ and $M_2 = 3$ elements for $d_2 = 2\lambda$, and its corresponding difference co-array. 28

Figure 3.6 A 5-element Nested Array with $M_1 = 2$ elements for $d_1 = \lambda/2$ and $M_2 = 3$ elements for $d_2 = 3\lambda$, and its corresponding difference co-array. 28

Figure 3.7 A 7-element Uniform Circular Array (UCA) with a radius of $r = \lambda/2$ and its corresponding difference co-array. 30

Figure 3.8 A 8-element Uniform Circular Array (UCA) with a radius of $r = \lambda/2$ and its corresponding difference co-array. 31

Figure 3.9 CRLB versus SNR for 7 Element UCA with Several Number of Sources 35

Figure 4.1 Layout of NCRA. 38

Figure 4.2 Back-forth ambiguity for $L = 2$. 40

Figure 4.3 Comparison of a non-symmetrical array and a UCA. 41

Figure 4.4 7 Element NCRA 44

Figure 4.5 9 Element NCRA 44

Figure 4.6 10 Element NCRA 45

Figure 4.7 13 Element NCRA - 6 Arms 45

Figure 4.8 Comparison of omnidirectional characteristics: Overdetermined CRLB vs. Azimuth for various NCRA configurations and UCAs 47

Figure 5.1 7 Element Arrays, 3 Uncorrelated Sources, 200 MCT 51

Figure 5.2 7 Element Arrays, 3 Coherent Sources, 200 MCT 53

Figure 5.3 Azimuth-RMSE comparison of NCRA and UCA. 55

Figure 5.4 7 Element Arrays, 9 Uncorrelated Sources, 500 MCT 58

Figure 5.5 Spatial spectrum of case 1 trials for -5dB SNR. 58

Figure 5.6 Spatial spectrum for case 2 trials. 60

Figure 5.7 10 Element Arrays, 11 Uncorrelated Sources, 500 MCT 61

Figure 5.8 Spatial spectrum of case 3 trials for -5dB SNR. 62

Figure 5.9 10 Element Arrays, 13 Uncorrelated Sources, 500 MCT 63

Figure 5.10 Spatial spectrum for case 4 trials for -5dB SNR. 64

Figure 5.11 10 element arrays, 9 uncorrelated sources, 2 coherent sources, 500 MCT. 65

Figure 5.12 Spatial spectrums for case 2 at 5dB SNR. 66

Figure 5.13 10 element arrays, 8 uncorrelated sources, 3 coherent sources, 500 MCT. 67

Figure 5.14 Spatial spectrums for case 2 at 5dB SNR. 68

Figure 5.15 7 Element Arrays, 10 Uncorrelated Sources, 500 MCT. 70

Figure 5.16 Spatial spectrums for case 1 at 15° angular separation. 70

Figure 5.17 10 Element Arrays, 11 Uncorrelated Sources, 500 MCT. 72

Figure 5.18 Spatial spectrums for case 2 at 15° angular separation. 72

Figure F.1 Scaling for ambiguity problem of 4-arm NCRA configurations. . 94

Figure F.2 Scaling effect for 4-arm NCRA configurations. 96

LIST OF ABBREVIATIONS

CRLB	Cramér–Rao Lower Bound
CWD	Coordinate-Wise Descent
DF-QSS	Direction Finding for Quasi-Stationary Signals
DoA	Direction of Arrival
DoF	Degrees of Freedom
EM	Expectation Maximization
FBSS	Forward-Backward Spatial Smoothing
FIM	Fisher Information Matrix
HPBW	Half-Power Beamwidth
KR	Khatri-Rao
ML	Maximum Likelihood
MCT	Monte-Carlo Trials
MSLL	Maximum Sidelobe Level
MUSIC	Multiple Signal Classification
NCRA	Nested Circular Ring Arrays
NB	Narrowband
RMSE	Root Mean Square Error
SBL	Sparse Bayesian Learning
SNR	Signal-to-Noise Ratio
SVD	Singular Value Decomposition
UCA	Uniform Circular Array
ULA	Uniform Linear Array

CHAPTER 1

INTRODUCTION

1.1 Motivation and Problem Definition

Estimating the direction of arrival (DoA) of plane waves at an antenna array is essential for a variety of applications, including radar, sonar, acoustics, and communications [2, 3]. Accurate DoA estimation is crucial for enhancing the effectiveness of these systems, making it a significant area of research.

Traditionally, DoA estimation relies on an overdetermined signal model, where the number of sensors in the array exceeds the number of incoming signals. In this context, conventional algorithms such as Multiple Signal Classification (MUSIC) [4] and Estimation of Signal Parameters via Rotational Invariance Technique (ESPRIT) [5] have been widely used. More recently, compressed sensing-based methods like Sparse Bayesian Learning (SBL) [6, 7, 8], Orthogonal Matching Pursuit (OMP) [9], and Least Absolute Shrinkage and Selection Operator (LASSO) [10] have also been applied to DoA estimation problems.

In scenarios involving coherent sources or multi-path propagation, the performance of traditional subspace-based algorithms tends to degrade. In such cases, the Sparse Bayesian Learning (SBL) algorithm has been shown to effectively handle coherent source scenarios, offering better performance compared to subspace-based algorithms [11, 12].

Additionally, for DoA estimation of coherent or correlated sources, the Forward-Backward Spatial Smoothing (FBSS) method [13] is commonly used. However, this method requires a Uniform Linear Array (ULA) structure and effectively reduces the

number of sensors after processing. As an alternative, the Maximum Likelihood Covariance Matrix Estimation using the Coordinate-Wise Descent algorithm [14, 15, 16] can be employed. This approach can be applied to arbitrary array geometries without losing degrees-of-freedom, making it a versatile solution for coherent source scenarios.

Despite the success of these methods in overdetermined scenarios, they encounter significant challenges in underdetermined scenarios, where the number of sources surpasses the number of sensors. Traditional models and algorithms struggle in these cases because they rely on having more sensors than sources to provide accurate DoA estimation.

To address this challenge, an alternative signal model is employed [17], which utilizes a virtual array created through the difference co-array procedure [18, 19, 20]. The difference co-array of a physical array generates a virtual array with more elements than the physical array itself, effectively increasing the Degrees of Freedom (DoF) and enabling better DoA estimation in underdetermined cases. This approach opens new possibilities for accurately estimating the DoA in scenarios where conventional methods fall short.

For underdetermined DoA estimation, the subspace-based Khatri-Rao MUSIC (KR-MUSIC) [21, 22, 23] and SBL [24, 25] algorithms can be applied to quasi-stationary signals using the corresponding signal model as explained in [21]. The signal model for quasi-stationary signals is particularly relevant for underdetermined DoA estimation within the scope of this thesis. The SBL algorithm demonstrates superior performance compared to the subspace-based KR-MUSIC algorithm, especially in coherent source scenarios.

Additionally, a 4^{th} order cumulant-based approach, as explained in [26], uses higher-order statistics of the received data. However, this method requires a large number of snapshots to accurately capture the characteristics of higher-order statistics, which can be a significant disadvantage.

The underdetermined DoA estimation problem can also be addressed using sparse array interpolation techniques, as discussed in [27, 28]. Nevertheless, fully exploiting

the correlation information of undersampled signals remains challenging due to the diverse configurations of sparse arrays and the resulting fragmented virtual arrays, leading to inevitable performance degradation.

Moreover, sparse array geometries such as Nested Arrays [1], Co-Prime Arrays [29, 30, 31], and Super Nested Sparse Circular Arrays [32] have been proposed to more effectively utilize the underdetermined DoA estimation. These geometries offer advantages for difference-array computation, array interpolation, higher-order statistics-based approaches by forming non-uniform sparse arrays with expanded apertures to address the gaps in traditional array configurations.

In this thesis, a new planar array structure, Nested Circular Ring Arrays (NCRA), is proposed. NCRA combines the benefits of Nested Arrays and circular arrays. The Nested Arrays component increases the aperture of the array, thereby reducing the beamwidth, while the circular placement ensures consistent performance across the entire spatial domain due to its isotropy. NCRA outperforms uniform circular arrays for underdetermined scenarios by achieving narrower beamwidth and lower sidelobe levels with the same number of elements. Additionally, the SBL algorithm is utilized for underdetermined scenarios in this thesis, with performance comparisons against KR-MUSIC, particularly in coherent and independent source scenarios. For all performance analyses, including both underdetermined [17, 33] and overdetermined [34, 35] cases, CRLB computations have been made as a performance benchmark.

1.2 Contributions and Novelties

The contributions of this thesis are outlined as follows:

1. A novel planar array structure is proposed for effective 2D underdetermined DoA estimation, offering improved performance in scenarios where the number of sources exceeds the number of sensors.

2. The performances and characteristics of different NCRA variants are analyzed, focusing on Degrees of Freedom (DoF), Half-Power Beamwidth (HPBW), and

Maximum Sidelobe Level (MSL). This analysis highlights how these metrics contribute to NCRA's enhanced resolution and accuracy in underdetermined DoA estimation scenarios.

3. An in-depth analysis of beamwidth and sidelobe effects is conducted, with a particular focus on their influence on the accuracy and resolution of underdetermined DoA estimation—an aspect often overlooked in the existing literature.

4. The KR-MUSIC and SBL algorithms are employed for underdetermined DoA estimation. The thesis demonstrates the robustness of SBL in handling coherent sources, even in challenging underdetermined scenarios. Using the Cramér-Rao Lower Bound (CRLB) as a benchmark, the performance of these algorithms is assessed.

5. ML Covariance Matrix estimation with CWD algorithm and SBL are used for overdetermined DoA estimation, with performance comparisons provided to highlight the advantages and disadvantages of these methods.

1.3 The Outline of the Thesis

This thesis is organized into the following chapters:

In Chapter 2, the problem definition and signal model for overdetermined direction of arrival (DoA) estimation are explained. MUSIC, SBL and ML Covariance Matrix Estimation with CWD algorithms are also discussed in detail.

Chapter 3 focuses on the problem definition for underdetermined DoA estimation of quasi-stationary signals. This chapter includes a thorough explanation of the difference co-array procedure and discusses difference co-arrays for ULA, UCA, Nested Arrays, and Co-Prime arrays. Additionally, the KR-MUSIC algorithm is derived and its application is explained. The characteristics of the Cramér-Rao Lower Bound (CRLB) in underdetermined scenarios are also explored.

In Chapter 4, the proposed novel planar array structure, Nested Circular Ring Arrays (NCRA), is discussed. The design criteria, characteristics, and advantages of NCRA are explained, along with a comparison to UCA from the perspectives of Degrees

of Freedom (DoF), Half-Power Beamwidth (HPBW), and Maximum Sidelobe Level (MSLL).

Chapter 5 presents the simulation results. SNR vs. RMSE simulations are provided for both overdetermined and underdetermined scenarios, including comparisons with the Cramér-Rao Lower Bound for different scenarios involving varying numbers of sources, both coherent and non-coherent. Additionally, resolution probability simulations are conducted to compare the spatial resolution capabilities of NCRA and UCA.

Finally, Chapter 6 offers a summary of the work, conclusions, and suggestions for future research.

CHAPTER 2

DIRECTION OF ARRIVAL ESTIMATION

Direction of Arrival (DoA) estimation is a fundamental problem in array signal processing with significant applications in radar, sonar, wireless communications, and acoustics. The primary goal of DoA estimation is to determine the direction from which a received signal arrives at an array of sensors by analyzing the phase and amplitude information captured by the sensor array [3, 2].

Accurate DoA estimation enhances the performance of communication systems, improves localization accuracy in radar and sonar, and enables efficient beamforming in wireless networks. Several algorithms have been developed over the years, each with unique advantages and limitations.

Traditional methods for DoA estimation include Correlative Interferometry, the Maximum Likelihood (ML) method, Multiple Signal Classification (MUSIC), and Estimation of Signal Parameters via Rotational Invariance Techniques (ESPRIT). Recent advancements in sparse signal processing and machine learning have introduced new approaches, such as Sparse Bayesian Learning (SBL) and Compressive Sensing (CS), which leverage the sparsity of signal representation to improve estimation accuracy and reduce computational complexity [6, 7, 8].

This chapter provides an overview of DoA estimation signal model, various DoA estimation techniques, highlighting their theoretical foundations, computational aspects, and practical applications. It explains the strengths and weaknesses of different methods and discusses their performance in various scenarios.

2.1 Data Model

Assume K narrow-band source signals $\{s_1(t), s_2(t), \ldots, s_K(t)\}$ are arriving from distinct directions $\{(\phi_1, \theta_1), (\phi_2, \theta_2), \ldots, (\phi_K, \theta_K)\}$ to an M-element antenna array. The received data from the array is given by the following equation:

$$\mathbf{y}(t) = \mathbf{A}\mathbf{s}(t) + \mathbf{n}(t), \quad t \in \{1, 2, \ldots, N\} \tag{2.1}$$

where $\mathbf{y}(t) = [y_1(t)\ y_2(t)\ \ldots\ y_M(t)]^T$, $\mathbf{A} = [\mathbf{a}(\phi_1, \theta_1)\ \mathbf{a}(\phi_2, \theta_2)\ \ldots\ \mathbf{a}(\phi_K, \theta_K)]$, $\mathbf{s}(t) = [s_1(t)\ s_2(t)\ \ldots\ s_K(t)]^T$, $\mathbf{n}(t) = [n_1(t)\ n_2(t)\ \ldots\ n_M(t)]^T$ are the received signal, array manifold, source signal vector and noise vector respectively. The array manifold contains steering vectors for corresponding source direction and it can be modeled as followings:

$$\mathbf{a}(\phi_i, \theta_i) = [v(\phi_i, \theta_i, \mathbf{p}_1)\ v(\phi_i, \theta_i, \mathbf{p}_2)\ \ldots\ v(\phi_i, \theta_i, \mathbf{p_M})]^T, \tag{2.2}$$

$$\mathbf{p}_j = [x_j\ y_j\ z_j]^T, \tag{2.3}$$

$$v(\phi_i, \theta_i, \mathbf{p}_j) = \exp(j\frac{2\pi}{\lambda}(x_j \cos(\phi_i)\sin(\theta_i) + y_j \sin(\phi_i)\sin(\theta_i) + z_j \cos(\theta_i))) \tag{2.4}$$

where $\mathbf{p}_j$ is the position vector of j^{th} sensor in the array, λ is the wavelength of operation frequency. The dimensions of parameters are $\mathbf{y}(t) \in \mathbb{C}^{M\times 1}$, $\mathbf{A} \in \mathbb{C}^{M\times K}$, $\mathbf{a}(\phi_i, \theta_i) \in \mathbb{C}^{M\times 1}$, $\mathbf{s}(t) \in \mathbb{C}^{K\times 1}$ and $\mathbf{n}(t) \in \mathbb{C}^{M\times 1}$. Using the equation 2.1 the data model can be extended to matrix form to explain the multi-snapshot case:

$$\mathbf{Y} = \mathbf{A}\mathbf{S} + \mathbf{N} \tag{2.5}$$

where $\mathbf{Y} = [\mathbf{y}(t_1)\, \mathbf{y}(t_2)\ \ldots\ \mathbf{y}(t_N)]$, $\mathbf{S} = [\mathbf{s}_1\, \mathbf{s}_2\ \ldots\ \mathbf{s}_K]^T$, $\mathbf{s}_j = [s_j(t_1)\ s_j(t_2)\ \ldots\ s_j(t_N)]$ and $\mathbf{N} = [\mathbf{n}(t_1)\, \mathbf{n}(t_2)\ \ldots\ \mathbf{n}(t_N)]$. The dimensions of the parameters are $\mathbf{Y} \in \mathbb{C}^{M\times N}$, $\mathbf{S} \in \mathbb{C}^{K\times N}$, and $\mathbf{N} \in \mathbb{C}^{M\times N}$.

The covariance matrix of the received signal from a source from (ϕ_K, θ_K) can be calculated as:

$$\mathbf{R}_\mathbf{y}(t, (\phi_K, \theta_K)) = \mathbf{E}[\mathbf{y}(t, (\phi_K, \theta_K))\mathbf{y}^H(t, (\phi_K, \theta_K))] \tag{2.6}$$

and for multi-snapshot case it can be calculated as equation 2.7.

$$\mathbf{R_Y}(\phi_K, \theta_K) = \mathbf{E}[\mathbf{Y}\mathbf{Y}^H] = \frac{1}{N}\sum_{t=1}^{N}\mathbf{R}_y(t, (\phi_K, \theta_K)) \ = \mathbf{A}\mathbf{R_s}\mathbf{A}^H + \sigma^2\mathbf{I} \qquad (2.7)$$

Where the dimensions of parameters are $\mathbf{R_y}(t, (\phi_K, \theta_K)) \in \mathbb{C}^{M\times M}$ and $\mathbf{R_Y}(\phi_K, \theta_K) \in \mathbb{C}^{M\times M}$.

2.2 Direction Of Arrival Estimation Methods

In this section, the direction-finding methods examined within the scope of this thesis are discussed. The focus is on the signal models and algorithm flows of these methods. Additionally, the strengths and weaknesses of each method are explained to provide a comprehensive understanding of their performance in different scenarios.

2.2.1 MUltiple SIgnal Classification (MUSIC)

MUSIC[4] algorithm is one of the powerful super-resolution algorithms and it can be applied to arbitrary array geometries. It requires a theoretically calculated array manifold dictionary, or one collected using a reference signal from all azimuth-elevation pairs $(\phi_K, \theta_K)\}$. While the collected dictionary accounts for phase/gain mismatches, antenna position errors, and antenna coupling errors, the theoretically calculated dictionary does not perfectly capture these effects due to the difficulty in simulating them. Therefore, the collected dictionary generally provides better performance compared to theoretical calculations. However, for analytical and expression purposes, theoretical calculations that do not account for these effects for scope of this thesis.

MUSIC algorithm stars with the computation of covariance matrix as given equation (2.7). Then Singular-Value Decomposition(SVD) is applied to covariance matrix to extract spactral compounds.

$$\mathbf{R_Y} = \mathbf{V}\mathbf{\Lambda}\mathbf{V}^H \qquad (2.8)$$

When it is assumed that there are K independent source signals are impinging to array, the parameters on the equation (2.8) will be as following equations.

$$rank(\mathbf{R_Y}) = K \tag{2.9}$$

$$\mathbf{\Lambda} = \begin{bmatrix} \lambda_1 + \sigma^2 & & & & & & \\ & \lambda_2 + \sigma^2 & & & & & \\ & & \ddots & & & & \\ & & & \lambda_K + \sigma^2 & & & \\ & & & & \sigma^2 & & \\ & & & & & \ddots & \\ & & & & & & \sigma^2 \end{bmatrix} \tag{2.10}$$

$$\mathbf{V} = [\mathbf{v}_1\ \mathbf{v}_2\ \dots\ \mathbf{v}_K\ \mathbf{v}_{K+1}\ \dots\ \mathbf{v}_M] \tag{2.11}$$

Where $\mathbf{\Lambda} \in \mathbb{R}^{M \times M}$ in equation (2.10) represents the eigenvalues of covariance matrix and the $\mathbf{V} \in \mathbb{C}^{M \times M}$ in equation (2.11) represents the eigenvectors of the covariance matrix. After applying spectral decomposition by SVD, signal subpsace $\mathbf{S} \in \mathbb{C}^{M \times K}$ and noise subspace $\mathbf{G} \in \mathbb{C}^{M \times M-K}$ are extracted as equations (2.12) and (2.13) respectively.

$$\mathbf{S} = [\mathbf{v}_1\ \mathbf{v}_2\ \dots\ \mathbf{v}_K] \tag{2.12}$$

$$\mathbf{G} = [\mathbf{v}_{K+1}\ \mathbf{v}_{K+1}\ \dots\ \mathbf{v}_M] \tag{2.13}$$

Range space of noise subspace $\mathcal{R}(\mathbf{G})$ is equal to null space of array manifold which contains source steering vectors $\mathcal{N}(\mathbf{A}^H)$; $\mathcal{R}(\mathbf{G}) = \mathcal{N}(\mathbf{A}^H)$. Then the folowing statement can be given.

$$\mathbf{R_Y G} = \mathbf{A R_s A}^H \mathbf{G} + \sigma^2 \mathbf{I G} \tag{2.14}$$

$$\mathbf{A R_s A}^H \mathbf{G} = 0 \tag{2.15}$$

Only solutions for the equation $\mathbf{a}^H(\theta_i, \phi_i)\mathbf{G}\mathbf{G}^H\mathbf{a}(\theta_i, \phi_i) = 0$ are the true DOA angles $\{\theta_i, \phi_i\}_{i=1}^K$. So the cost function of MUSIC is given on the equation (2.16).

$$f(\theta_i, \phi_i) = \frac{1}{\mathbf{a}(\theta_i, \phi_i)\mathbf{G}\mathbf{G}^H\mathbf{a}(\theta_i, \phi_i)^H} \tag{2.16}$$

Algorithm 1 MUSIC Algorithm

Inputs: $\mathbf{R_Y}, \mathbf{A}$

Output: $(\hat{\phi}, \hat{\theta})$

$\mathbf{R_Y} = \mathbf{V}\mathbf{\Lambda}\mathbf{V}^H$

$\mathbf{S} = [\mathbf{v}_1\ \mathbf{v}_2\ \ldots\ \mathbf{v}_K]$

$\mathbf{G} = [\mathbf{v}_{K+1}\ \mathbf{v}_{K+2}\ \ldots\ \mathbf{v}_M]$

for $i = 1, 2, \ldots, G_{az}$ **do**

  for $j = 1, 2, \ldots, G_{el}$ **do**

    $f(\theta_i, \phi_j) = \left(\mathbf{a}(\theta_i, \phi_j)^H\mathbf{G}\mathbf{G}^H\mathbf{a}(\theta_i, \phi_j)\right)^{-1}$

  end for

end for

$(\hat{\phi}, \hat{\theta}) = \underset{\phi_i, \theta_j}{\operatorname{argmax}}\ f(\theta_i, \phi_j)$

2.2.2 Sparse Bayesian Learning (SBL)

The Sparse Bayesian Learning (SBL) algorithm, firstly introduced in [6], has been applied to the problem of Direction of Arrival Estimation (DoAE) in [7] and [8]. It effectively handles coherent sources regardless of the array geometry. Unlike methods such as MUSIC [4], Root-MUSIC [36], and ESPRIT [5], which rely on covariance matrices for estimating DoA, SBL adopts a Bayesian statistical approach.

In DoA estimation, SBL utilizes a sparse signal representation. The source signal vector to be estimated $\hat{\mathbf{S}}$ is a complex $L \times 1$ vector, where each element is drawn from a complex L-dimensional multivariate Gaussian distribution. Here, L is significantly larger than K, the number of active sources, and L denotes the number of potential source locations, which define the grids.

For the scope of this thesis, the SBL algorithm is focused on 1D DoA estimation, specifically involving azimuth angles only. The azimuth grid interval Δ_ϕ can be uniformly spaced based on the array beamwidth, or adjusted with sectoral density if prior

information about the source direction is available. Additionally, several off-grid SBL algorithms are discussed in literature. However, due to their reliance on specific array geometries, they are not applied within the scope of this thesis [6, 12, 37].

The signal model for DoA estimation using the SBL algorithm is described as:

$$\mathbf{Y} = \mathbf{A}\hat{\mathbf{S}} + \mathbf{N} \tag{2.17}$$

where $\mathbf{A} = [\mathbf{a}(\phi_1), \ldots, \mathbf{a}(\phi_L)] \in \mathbb{C}^{M \times L}$ represents the array manifold consisting of L steering vectors corresponding to each grid angle ϕ_l, and $\hat{\mathbf{S}} \in \mathbb{C}^{L \times N}$ denotes the estimated source signals corresponding to each possible grid.

Let $\boldsymbol{\delta} = [\delta_1, \delta_2, \ldots, \delta_L]^T$ and define $\Delta = \text{diag}(\boldsymbol{\delta})$, where δ_l represents the inverse variance corresponding to the l-th possible source direction grid. The prior probability distribution $p(\hat{\mathbf{S}} \mid \boldsymbol{\delta})$ is formulated as:

$$p(\hat{\mathbf{S}} \mid \boldsymbol{\delta}) = \prod_{n=1}^{N} \mathbb{CN}(\hat{\mathbf{s}}_n \mid 0, \Delta^{-1}), \tag{2.18}$$

where N is the number of snapshots, and $\hat{\mathbf{s}}_n \in \mathbb{C}^{L \times 1}$ denotes the n-th column of $\hat{\mathbf{S}}$. To promote sparsity in $\hat{\mathbf{S}}$, the elements of $\boldsymbol{\delta}$ follow a Gamma distribution, as discussed in [6] and [11]. The prior distributions are specified as follows:

$$p(\boldsymbol{\delta}) = \prod_{l=1}^{L} \Gamma(\delta_l; 1, \rho), \tag{2.19}$$

$$p(\beta) = \Gamma(\beta; a, b), \tag{2.20}$$

where ρ is a small positive number. Here, $\beta = 1/\sigma^2$ represents the inverse of noise variance, and a, b are parameters of the Gamma distribution set close to zero. Given these models, the posterior distribution of the received signal $\mathbf{Y}$ is described by the following equation:

$$p(\mathbf{Y} \mid \hat{\mathbf{S}}; \beta) = \prod_{n=1}^{N} \mathbb{CN}(\mathbf{y}_n \mid \mathbf{A}\hat{\mathbf{s}}_n, \beta^{-1}\mathbf{I}), \tag{2.21}$$

where $\mathbf{y}_n$ represents the n-th column or snapshot of $\mathbf{Y}$.

The goal of SBL is to estimate the parameters $\boldsymbol{\delta}$ and β using the probability distribution $p(\hat{\mathbf{S}} \mid \mathbf{Y}; \boldsymbol{\delta}, \beta)$. Since this distribution cannot be computed explicitly, the Expectation Maximization (EM) algorithm is employed iteratively for its computation.

In the expectation(E) step, the posterior distribution parameters of $p(\hat{\mathbf{S}} \mid \mathbf{Y}; \boldsymbol{\delta}, \beta)$ are computed. Following Bayes' theorem, the expression can be written as:

$$\begin{aligned} p(\hat{\mathbf{S}} \mid \mathbf{Y}; \boldsymbol{\delta}, \beta) &= \frac{p(\mathbf{Y} \mid \hat{\mathbf{S}}; \beta)\, p(\hat{\mathbf{S}}; \boldsymbol{\delta})}{p(\mathbf{Y}; \boldsymbol{\delta}, \beta)} \\ &\propto p(\mathbf{Y} \mid \hat{\mathbf{S}}; \beta)\, p(\hat{\mathbf{S}}; \boldsymbol{\delta}), \end{aligned} \tag{2.22}$$

Since the posterior distribution can be approximated as Gaussian with mean $\boldsymbol{\mu} = [\mu_1, \ldots, \mu_2]^T$ and covariance matrix Σ, Equation (2.22) can be extended using the Gaussian product lemma:

$$\begin{aligned} p(\hat{\mathbf{S}} \mid \mathbf{Y}; \boldsymbol{\delta}, \beta) &\propto \prod_{n=1}^{N} \mathbb{CN}(\hat{\mathbf{s}}_n \mid (\mathbf{A}^H\mathbf{A})^{-1}\mathbf{A}^H\mathbf{y}_n, (\beta\mathbf{A}^H\mathbf{A})^{-1}) \mathbb{CN}(\hat{\mathbf{s}}_n \mid \mathbf{0}, \Delta), \\ &\propto \prod_{n=1}^{N} \mathbb{CN}(\hat{\mathbf{s}}_n \mid \boldsymbol{\mu}_n, \Sigma). \end{aligned} \tag{2.23}$$

The parameters $\boldsymbol{\mu}$ and Σ are computed as follows using the matrix inversion lemma:

$$\Sigma^{curr} = \left(\beta^{prev}\mathbf{A}^H\mathbf{A} + (\Delta^{prev})^{-1}\right)^{-1} \tag{2.24}$$

$$\boldsymbol{\mu}_n^{curr} = \beta^{prev}\Sigma^{curr}\mathbf{A}^H\mathbf{y}_n, \quad n \in \{1, 2, ..., N\} \tag{2.25}$$

In the maximization(M) step, the hyperparameters $\boldsymbol{\delta}$ and β are optimized to maximize the posterior distribution $p(\hat{\mathbf{S}} \mid \mathbf{Y}; \boldsymbol{\delta}, \beta)$. Following the derivations in [7], the hyperparameters are updated using the following equations:

$$\delta_i^{curr} = \frac{-N + \sqrt{N^2 + 4\rho \sum_{n=1}^{N} [\boldsymbol{\mu}_n^{curr}(\boldsymbol{\mu}_n^{curr})^H + \Sigma^{curr}]_{ii}}}{2\rho} \tag{2.26}$$

$$\beta^{curr} = \frac{NM + (a-1)}{b + \sum_{n=1}^{N} \|\mathbf{y}_n - \mathbf{A}\boldsymbol{\mu}_n^{curr}\|_2^2 + N \cdot \text{tr}(\mathbf{A}\Sigma^{curr}\mathbf{A}^H)} \tag{2.27}$$

where $[.]_{mn}$ denotes the $(m,n)^{th}$ element of a matrix, and tr(.) represents the trace operation. After obtaining Σ^{curr}, $\boldsymbol{\mu}_n^{curr}$ $\forall n \in \{1,\ldots,N\}$, $\boldsymbol{\delta}^{curr}$, and β^{curr}, a single iteration of the SBL procedure is completed. Iterations continue until convergence thresholds are satisfied. Once convergence is achieved, the spatial spectrum $f(\phi)$ is computed using the following equation:

$$f(\phi_k) = \delta_k^{-1}, \quad k \in \{1,\ldots,L\} \tag{2.28}$$

The estimation of DoAs can then be performed by identifying peaks in $f(\phi)$. The computational complexity of the SBL algorithm is $\mathcal{O}(ML^2)$ per iteration, as determined by equations (2.26) and (2.27), which represent the most complex processes in the SBL algorithm flow.

Before concluding the section, the advantages and disadvantages of SBL algorithm are listed below:

Advantages:

- DoA estimation is highly accurate, with RMSE-SNR performance converging asymptotically to the CRLB.
- The algorithm performs well in low SNR and small snapshot scenarios.
- It can handle correlated or coherent sources with arbitrary array geometries without requiring spatial smoothing methods like FBSS.

Disadvantages:

- The algorithm's computational complexity is high, especially due to iterative updates of signal and noise variance estimates, which involve expensive matrix operations. This can be particularly burdensome for large arrays.
- Fine-grid search requires off-grid SBL iterations, often necessitating specific array geometries and larger dictionaries.

The algorithm steps of SBL are provided in the following algorithm block.

Algorithm 2 SBL Algorithm for DoA Estimation

Inputs: $\mathbf{Y}, \mathbf{A}$

Output: $f(\phi)$

Initialization: $\boldsymbol{\delta}^0 = \mathbf{1}_{L\times 1},\ \beta^0 = 1,\ a = b = 10^{-4},\ \rho = 10^{-2},\ \epsilon^{thrs},\ j^{max}$

$j \leftarrow 0$

repeat

  Compute Σ^j and $\boldsymbol{\mu}_n^j\ \forall n \in \{1, \ldots, N\}$ using (2.24) and (2.25).

  Compute β^j and $\boldsymbol{\delta}^j$ using (2.27) and (2.26).

  $\epsilon^{curr} \leftarrow \frac{\|\boldsymbol{\delta}^j - \boldsymbol{\delta}^{j-1}\|}{\|\boldsymbol{\delta}^{j-1}\|}$

  $j \leftarrow j + 1$

until $j \geq j^{max}$ **OR** $\epsilon^{curr} < \epsilon^{thrs}$

Compute $f(\phi_k)\ \forall k \in \{1, \ldots, L\}$ using (2.28)

2.3 Maximum Likelihood(ML) Covariance Matrix Estimation using Coordinate-Wise Descent(CWD) Algorithm

Coherent sources are a fundamental problem for conventional algorithms such as MUSIC and Correlative Interferometry (CI) because they use the covariance matrix. When coherent signals come from different directions, the sample covariance matrix, as shown in equations (2.6) and (2.7), becomes rank-deficient [38]. This rank deficiency causes problems in detecting the number of sources and makes singular value decomposition difficult due to involving singular matrices.

Some conventional spatial smoothing methods, such as Forward-Backward Spatial Smoothing (FBSS), can resolve coherent source directions. However, they generally require specific array geometries like uniform linear arrays (ULA) and effectively reduce the number of sensors in the array. This reduction leads to less accurate DoA estimations [13, 2].

To address the issue of coherent source directions without needing a specific array geometry and without reducing the number of sensors, the covariance matrix can be estimated using the maximum likelihood method. For the cost function derivation,

see Appendix E. Since ML computation is computationally expensive, an optimized computation procedure called Coordinate-Wise Descent (CWD) optimization is provided by [14, 15, 16]. This procedure computes the ML estimate with Rank-1 update iterations. The procedure and derivations are given in the following equations.

The maximum likelihood cost function for the estimation of the covariance matrix is given in Appendix E as follows:

$$f(\boldsymbol{\gamma}) = \ln|\mathbf{A}\boldsymbol{\Gamma}\mathbf{A}^H + \sigma^2\mathbf{I}| + \mathrm{tr}((\mathbf{A}\boldsymbol{\Gamma}\mathbf{A}^H + \sigma^2\mathbf{I})^{-1}\mathbf{R}_\mathbf{Y}) \tag{2.29}$$

where $\mathbf{A} = [\mathbf{a}_1\ \mathbf{a}_2 \dots \mathbf{a}_G] \in \mathbb{C}^{M\times G}$ is the array manifold, G is the number of steering vectors in the array manifold, $\boldsymbol{\gamma} = [\gamma_1\ \gamma_2 \dots \gamma_G]^T \in \mathbb{R}^{G\times 1}$ represents the variances of each grid, and $\boldsymbol{\Gamma} = \mathrm{diag}(\boldsymbol{\gamma})$.

Since the computation of $f(\boldsymbol{\gamma})$ is a complex operation, it can be efficiently computed iteratively with Rank-1 updates by CWD algorithm. For each coordinate, namely for each grid k, we define a function $f_k(d) = f(\boldsymbol{\gamma} + d\mathbf{e}_k)$ where $\mathbf{e}_k$ is the k-th canonical basis vector. Defining $\boldsymbol{\Sigma} = \boldsymbol{\Sigma}(\boldsymbol{\gamma}) = \mathbf{A}\boldsymbol{\Gamma}\mathbf{A}^H + \sigma^2\mathbf{I}$, and using the Sherman-Morrison Identity for matrix inversion [39], we obtain:

$$(\boldsymbol{\Sigma} + d\mathbf{a}_k\mathbf{a}_k^H)^{-1} = \boldsymbol{\Sigma}^{-1} - \frac{d\boldsymbol{\Sigma}^{-1}\mathbf{a}_k\mathbf{a}_k^H\boldsymbol{\Sigma}^{-1}}{1 + d\mathbf{a}_k^H\boldsymbol{\Sigma}^{-1}\mathbf{a}_k} \tag{2.30}$$

Using equation (2.30) and applying the determinant identity, we derive:

$$|\boldsymbol{\Sigma} + d\mathbf{a}_k\mathbf{a}_k^H| = (1 + d\mathbf{a}_k^H\boldsymbol{\Sigma}^{-1}\mathbf{a}_k)|\boldsymbol{\Sigma}| \tag{2.31}$$

Substituting equations (2.30) and (2.31) into $f_k(d)$, we get:

$$f_k(d) = \ln(|\boldsymbol{\Sigma}|) + \mathrm{tr}(\boldsymbol{\Sigma}^{-1}\mathbf{R}_\mathbf{Y}) + \ln(1 + d\mathbf{a}_k^H\boldsymbol{\Sigma}^{-1}\mathbf{a}_k) - \frac{d\mathbf{a}_k^H\boldsymbol{\Sigma}^{-1}\mathbf{R}_\mathbf{Y}\boldsymbol{\Sigma}^{-1}\mathbf{a}_k}{1 + d\mathbf{a}_k^H\boldsymbol{\Sigma}^{-1}\mathbf{a}_k} \tag{2.32}$$

The solution for d can be computed by taking the derivative of $f_k(d)$ with respect to d and setting it to zero:

$$f_k{}'(d) = \frac{\mathbf{a}_k^H \boldsymbol{\Sigma}^{-1} \mathbf{a}_k}{1 + d\mathbf{a}_k^H \boldsymbol{\Sigma}^{-1} \mathbf{a}_k} - \frac{\mathbf{a}_k^H \boldsymbol{\Sigma}^{-1} \mathbf{R}_\mathbf{Y} \boldsymbol{\Sigma}^{-1} \mathbf{a}_k}{(1 + d\mathbf{a}_k^H \boldsymbol{\Sigma}^{-1} \mathbf{a}_k)^2} \tag{2.33}$$

Solving for d, we obtain:

$$d^* = \frac{\mathbf{a}_k^H \boldsymbol{\Sigma}^{-1} \mathbf{R}_\mathbf{Y} \boldsymbol{\Sigma}^{-1} \mathbf{a}_k - \mathbf{a}_k^H \boldsymbol{\Sigma}^{-1} \mathbf{a}_k}{(\mathbf{a}_k^H \boldsymbol{\Sigma}^{-1} \mathbf{a}_k)^2} \tag{2.34}$$

Since the output covariance matrix estimate is not rank deficient, it can be utilized with any algorithm that operates on the covariance matrix.

Before concluding the section, the advantages and disadvantages of the algorithm are listed below:

Advantages:

- The algorithm can be applied to arbitrary array geometries, unlike the FBSS algorithm.
- The algorithm does not reduce the effective number of sensors while estimating the covariance matrix in coherent source scenarios, unlike traditional spatial smoothing methods.
- The computational complexity of the algorithm is lower than that of the SBL algorithm.

Disadvantages:

- The computational complexity is higher than the traditional FBSS method due to the iterative process required for convergence.
- The algorithm depends on accurate array manifold data, unlike the traditional FBSS algorithm.

The flow of the algorithm is provided below.

Algorithm 3 CWD Optimization for ML Covariance Matrix Estimation

Inputs: $\mathbf{R_Y} = \frac{1}{N}\mathbf{Y}\mathbf{Y}^H$, $\mathbf{A} = [\mathbf{a}_1\ \mathbf{a}_2\ ...\ \mathbf{a}_G]$

1: **Initialization**: $\mathbf{\Sigma} = \sigma^2\mathbf{I}, \gamma = \mathbf{0} = [0\ 0\ ...\ 0]^T$

2: **for** $i = 1, 2, ...$

3: A random or systematically chosen index $k \in [1, 2, ..., N]$ is selected from the array manifold matrix, and the corresponding steering vector $\mathbf{a}_k$ and variance γ_k are drawn.

4: $d^* = \max\{\frac{\mathbf{a}_k{}^H\mathbf{\Sigma}^{-1}\mathbf{R_Y}\mathbf{\Sigma}^{-1}\mathbf{a}_k - \mathbf{a}_k{}^H\mathbf{\Sigma}^{-1}\mathbf{a}_k}{(\mathbf{a}_k{}^H\mathbf{\Sigma}^{-1}\mathbf{a}_k)^2}, -\gamma_k\}$

5: ${\gamma_k}^{new} = \gamma_k + d^*$

6: $\mathbf{\Sigma}^{new} = \mathbf{\Sigma} + d^*\mathbf{a}_k\mathbf{a}_k{}^H$

7: **end for**

Outputs: $\mathbf{\Sigma}$, γ

CHAPTER 3

UNDERDETERMINED DIRECTION OF ARRIVAL ESTIMATION OF QUASI-STATIONARY SIGNALS

This chapter focuses on estimating the Direction of Arrival (DoA) for quasi-stationary signals, a process also known as direction finding of quasi-stationary signals (DF-QSS) [21]. Quasi-stationary signals exhibit stable statistics over short periods but vary across different time frames, and they represent a category of signals commonly encountered in various applications, such as microphone array speech processing [40] and electroencephalogram analysis [41]. Typical examples include speech and audio signals, which maintain consistent yet evolving characteristics over time.

Estimating the DoA of audio signals is crucial for practical applications, such as monitoring birds at airports to prevent collisions with aircraft and enhancing microphone arrays for improved speech signal processing [42]. These real-world applications highlight the importance and relevance of studying DF-QSS.

Moreover, the quasi-stationary nature of signals aids in identifying sources in scenarios where there are fewer sensors than sources. This underdetermined DoA estimation is particularly challenging but essential in many practical situations. In this chapter, the estimation of DoA when the number of sources exceeds the number of sensors, specifically for quasi-stationary signals, is addressed. By leveraging the quasi-stationary properties, the aim is to improve the accuracy and reliability of source identification under these challenging conditions.

Various techniques and methodologies for underdetermined DoA estimation will be explored, their theoretical foundations discussed, and their effectiveness demonstrated through practical examples and simulations. The aim is to provide a comprehensive

understanding of how quasi-stationary signals can be utilized to achieve accurate DoA estimation even in underdetermined scenarios.

Before presenting the signal model and algorithms, this chapter explains the difference co-array procedure as it is directly related to underdetermined DoA estimation. Following the explanation of the difference co-array procedure, the data model and DoA estimation algorithms will be discussed, and the Cramer-Rao Lower Bound (CRLB) characteristics of underdetermined DoA estimation will be examined.

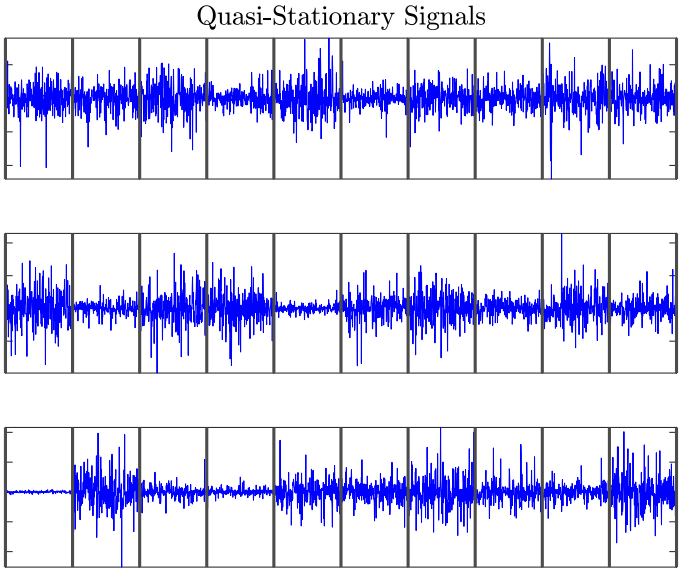

Figure 3.1: Illustration of synthetic quasi-stationary signals with frame separations. The lines define the local stationary intervals, namely frames. Only the real parts of the signals are plotted.

3.1 Difference Co-Arrays

Consider an M-element antenna array where each sensor, indexed by j, with position vector $\mathbf{p}_j = [x_j \; y_j \; z_j]^T$ in the xyz coordinate system. Define the set:

$$D = \{\mathbf{p}_j - \mathbf{p}_i\}, \quad \forall i, j \in \{1, \ldots, M\} \tag{3.1}$$

where $\mathbf{p}_j$ and $\mathbf{p}_i$ are the posioton vector of i-th and j-th sensors. Since the set D may contain repetitions, define a set $D_u = \{\mathbf{p}_1^d, \mathbf{p}_2^d, \ldots\}$ which contains the distinct position vectors in D, where $\mathbf{p}_i^d$ is the position vector of the i-th element of the difference co-array. The difference co-array of a given array is the array with elements located at the positions in D_u as explained in [1, 18, 19, 20].

The number of elements in the difference co-array (set D_u) affects the cross-correlation values in the covariance matrix of the signal received by an antenna array. By using these values in different ways, we can resolve more incoming sources than number of sensors in the array. Each method uses part or all of the difference co-array to estimate the DoA. The maximum number of sources we can detect depends on the number of elements in the co-array, which is called the degrees of freedom (DoF). By using the Difference Co-Array approach with suitable assumptions, it is possible to localize $O(M^2)$ sources. The difference co-array also virtually creates an array with more sensors and a greater array aperture. There is also a "sum co-array," but it is not considered within the scope of this thesis [43].

Define a weight function $w(\mathbf{p})$, which counts the number of times the position vector $\mathbf{p}$ appears in the difference co-array calculation, namely defines the number of covariance lags of each element position. This function helps us understand the following properties of the co-array:

1. $w(\mathbf{0}) = M$:
    - This happens when $\mathbf{p}_i = \mathbf{p}_k$ for $i = k = 1, \ldots, M$.
2. $1 \leq w(\mathbf{p}) \leq M - 1,\ \forall \mathbf{p} \in D_u \setminus \{\mathbf{0}\}$:
    - Consider $\mathbf{p}$ from the difference between the i-th and k-th sensors, expressed as $\mathbf{p} = \mathbf{p}_i - \mathbf{p}_k$. It follows that $\mathbf{p} \neq \mathbf{p}_i - \mathbf{p}_k$ for any $k \neq i$. Therefore, $\mathbf{p}$ can occur only once when comparing positions between a specific sensor (e.g., the i-th) and the others. So, $\mathbf{p}$ can appear at most once for each $i = 1, \ldots, M$, and up to $M - 1$ times overall. For example, in a Uniform Linear Array (ULA) with M elements and unit spacing, the difference of 1 appears $M - 1$ times.
3. $w(\mathbf{p}) = w(-\mathbf{p}),\ \forall \mathbf{p} \in D_u$:

- Each time $\mathbf{p} = \mathbf{p}_i - \mathbf{p}_k$ occurs, it is matched by $-\mathbf{p} = \mathbf{p}_k - \mathbf{p}_i$. Thus, these happen the same number of times.

4. $\sum_{\mathbf{p}\in D_u, \mathbf{p}\neq \mathbf{0}} w(\mathbf{p}) = M(M-1)$:

   - The total number of distinct position differences equals the number of all possible pairs of positions from the set $\{\mathbf{p}_1, \ldots, \mathbf{p}_M\}$, which is $M(M-1)$.

It's important to understand how the number of unique positions in D_u, which represents the difference co-array of an antenna array, affects the degrees of freedom it provides. According to Property 4, we find that regardless of the array's shape, the maximum degrees of freedom achievable from its difference co-array is $M(M-1)+1$ for an array with M elements. This shows the potential of using second-order statistics and leveraging the co-array's degrees of freedom to potentially achieve up to $O(M^2)$ degrees of freedom using physical elements.

The maximum degrees of freedom sets a global upper limit on what can be achieved across all array types using their difference co-array. Additionally, there's a trade-off with the weight function's value: if a position difference occurs multiple times, it reduces the number of unique positions and therefore reduces the degrees of freedom available.

3.1.1 Uniform Linear Arrays

Consider a linear array with M elements, each spaced evenly by a distance d. These type of arrays called as Uniform Linear Arrays (ULA). The positions of the elements along the axis can be written as follows:

$$\begin{aligned} P_{ULA} &= \{p_1, p_2, \ldots, p_M\} \\ &= \left\{ \frac{-(M-1)}{2}d, \frac{-(M-1)}{2}d + d, \ldots, \frac{-(M-1)}{2}d + (M-1)d \right\} \end{aligned} \tag{3.2}$$

This set P_{ULA} shows the positions of each element in the array, starting from the leftmost element to the rightmost element, with the same spacing d between each pair of elements.

To find the difference co-array for this ULA, we calculate all possible differences between the positions of the elements. This can be expressed as:

$$D_{ULA} = \{p_j - p_i \mid \forall i, j \in \{1, \ldots, M\}\} \tag{3.3}$$

The set D_{ULA} includes all the differences between the positions of the elements in the ULA. Since some of these differences might be repeated, we define D_u to include only the unique position differences. This set is given by:

$$D_{uULA} = \{-(M-1)d, -(M-1)d + d, \ldots, (M-1)d\} \tag{3.4}$$

The set D_{uULA} shows the unique elements of the difference co-array, ranging from $-(M-1)d$ to $(M-1)d$ in steps of d.

It is important to note that the difference co-array of an M-element ULA has $2M-1$ unique elements, as shown in (3.4). This follows the property stated in 4, which says that the upper limit of the total number of unique position differences for an array with M elements is $M(M-1)+1$. The difference co-array creates more elements and a larger aperture than the original array, which improves its ability to estimate the DoA and increases its DoF.

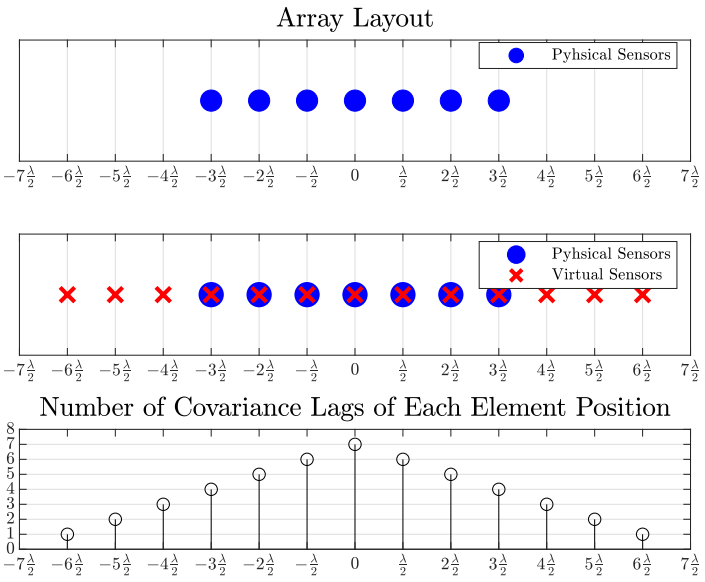

Figure 3.2: A 7-element Uniform Linear Array (ULA) with inter-element spacing of $d = \lambda/2$, its corresponding difference co-array.

As Figure 3.2 shows, a 7-element ULA generates a virtual array with 13 elements. The figure also depicts the number of covariance lags for each position, revealing repeating elements (weights greater than 1) that indicate sub-optimality in terms of DoF. These repetitions mean not all positions in the difference co-array are unique, reducing the potential DoF.

3.1.2 Co-Prime Arrays

Co-prime arrays, explained in [30] [44] [31] [29], are sparse arrays that provide more DoF than ULA. Created by combining two ULAs with co-prime inter-element spacing, a co-prime array with M and N element sub-arrays, Co-prime(M, N), where M and N are co-prime integers, has sensor positions as follows:

$$
\begin{aligned}
P_{SA1} &= \{Mnd \mid n = 0, \ldots, N-1\} \\
P_{SA2} &= \{Nmd \mid m = 1, \ldots, 2M-1\} \\
P_{Coprime} &= P_{SA1} \cup P_{SA2}
\end{aligned}
\tag{3.5}
$$

where d is the fundamental inter-element spacing, resulting in a co-prime array with $2M + N - 1$ physical elements. The difference co-array of co-prime arrays can be calculated by the following equation:

$$
\begin{aligned}
D_{Coprime} = \{\{Mnd - Nmd\} \cup \{Nmd - Mnd\} \cup \{-Mnd + Nmd\} \\
\cup \{-Nmd + Mnd\} \mid n \in \{0, \ldots, N-1\}, m \in \{1, \ldots, 2M-1\}\}
\end{aligned}
\tag{3.6}
$$

Figures 3.3 and 3.4 show the difference co-array of co-prime arrays. These figures indicate that the difference co-array may have gaps and lacks a complete ULA structure but includes a central hole-free part. The element positions in this hole-free range are given by:

$$
P_{HF} = \{kd \mid -(MN + (N-1)) \leq k \leq (MN + (N-1))\} \tag{3.7}
$$

Equation (3.7) shows that the hole-free range provides $2(MN + (N-1)) + 1$ DoF. The total DoF for the entire difference co-array is not analytically trackable.

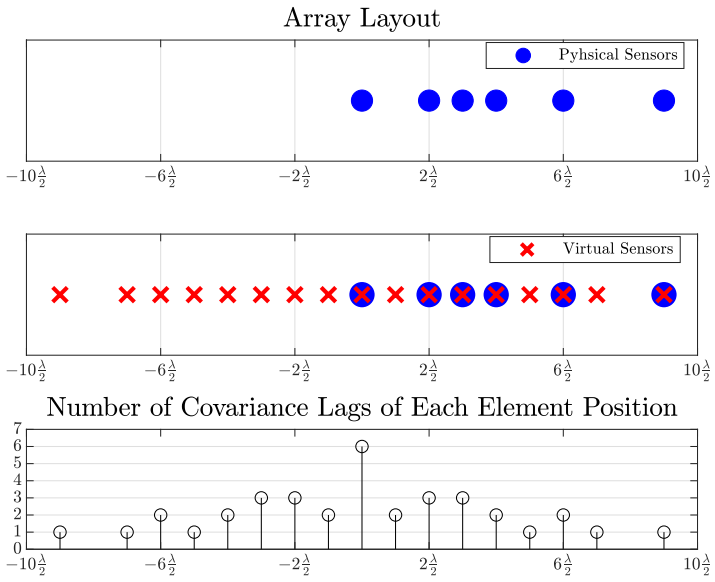

Figure 3.3: A 5-element Co-Prime Array with $M = 2$ and $N = 3$ elements, $d = \lambda/2$ along with its corresponding difference co-array.

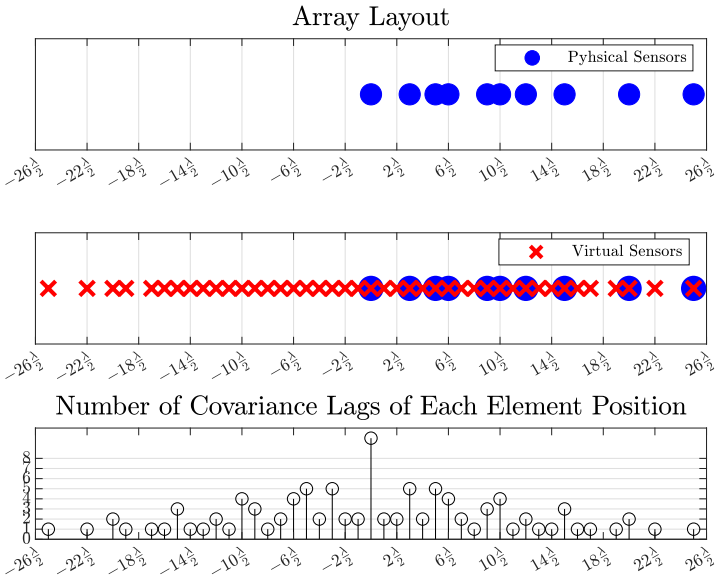

Figure 3.4: A 8-element Co-Prime Array with $M = 3$ and $N = 5$ elements, $d = \lambda/2$ along with its corresponding difference co-array.

3.1.3 Nested Arrays

Nested arrays, a type of sparse arrays, as proposed by [1], can provide more DoF compared to ULA. These arrays are created by concatenating two ULAs with different inter-element spacing end to end. The structure is defined such that one ULA is nested within the other. This results in a larger aperture and a higher number of unique position differences in the difference co-array. This leads to an increased DoF, enhancing the array's ability to estimate the DoA of multiple sources.

As previously mentioned, nested arrays are generated by concatenating two sub-arrays which are ULAs. One ULA has M_1 elements with d_1 inter-element spacing, and the other has M_2 elements with $d_2 = (M_1 + 1)d_1$ inter-element spacing. The positions of these sub-arrays are given by:

$$\begin{aligned} P_{SA1} &= \{md_1 \mid m = 1, 2, \ldots, M_1\} \\ P_{SA2} &= \{k(M_1 + 1)d_1 \mid k = 1, 2, \ldots, M_2\} \\ P_{Nested} &= P_{SA1} \cup P_{SA2} \end{aligned} \tag{3.8}$$

In nested arrays with 2 levels of nesting (2 sub-arrays), the difference co-array contains $2M_2(M_1 + 1) - 1$ unique elements, which determine its degrees of freedom. The structure of the difference co-array in nested arrays is analogous to that of a Uniform Linear Array (ULA) in terms of its properties. The properties of the difference co-array for nested arrays are summarized in the table 3.1, [1].

Table 3.1: Summary of 2-Level Nested Arrays [1]

Pyhsical Elements (M)	*Optimal M_1, M_2*	*DoF*
Even	$M_1 = M_2 = \frac{M}{2}$	$\frac{M^2-2}{2} + M$
Odd	$M_1 = \frac{M-1}{2}, M_2 = \frac{M+1}{2}$	$\frac{M^2-1}{2} + M$

Also, Figures 3.6 and 3.5 depict 5-element and 6-element Nested Arrays, respectively.

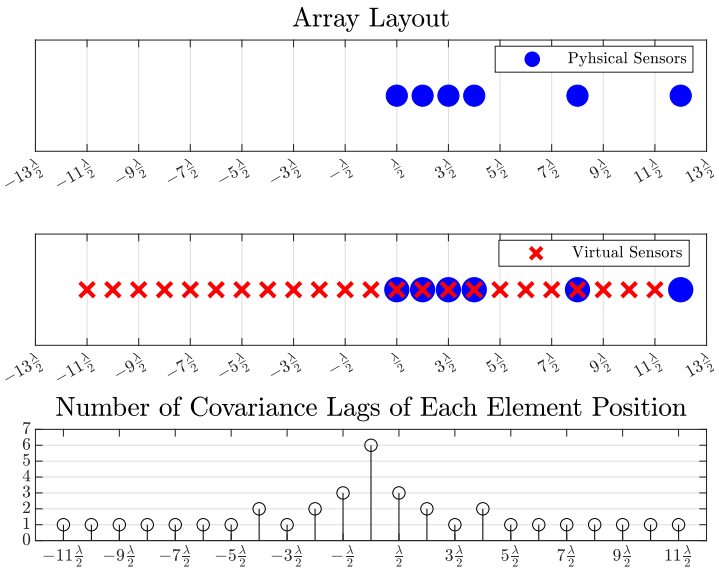

Figure 3.5: A 6-element Nested Array with $M_1 = 3$ elements for $d_1 = \lambda/2$ and $M_2 = 3$ elements for $d_2 = 2\lambda$, and its corresponding difference co-array.

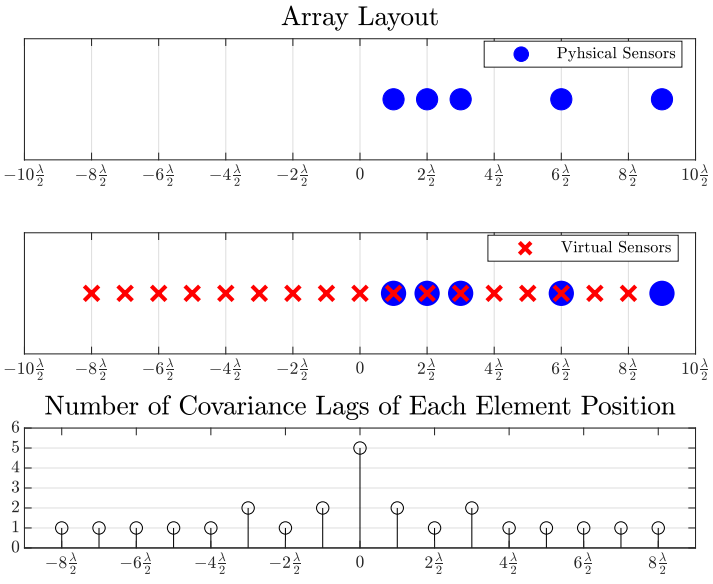

Figure 3.6: A 5-element Nested Array with $M_1 = 2$ elements for $d_1 = \lambda/2$ and $M_2 = 3$ elements for $d_2 = 3\lambda$, and its corresponding difference co-array.

3.1.4 Uniform Circular Arrays

Uniform Circular Arrays (UCAs) are another widely used array structure in array signal processing. Unlike Uniform Linear Arrays (ULAs) and Nested Arrays, which are linear configurations, UCAs arrange their elements in a circular configuration with uniform angular spacing, creating a planar array where the elements are located on a 2D axis. This unique structure offers distinct advantages, particularly in terms of azimuthal symmetry, enabling the array to resolve signals from any direction in the azimuth plane with consistent performance.

For a UCA with M elements, the position vectors of the elements are given by:

$$\mathbf{p}_m = R \begin{bmatrix} \cos\left(\frac{2\pi(m-1)}{M}\right) \\ \sin\left(\frac{2\pi(m-1)}{M}\right) \end{bmatrix}, \quad m = 1, 2, \ldots, M,$$

where R is the radius of the circular array.

The difference co-array of a UCA is formed by considering all possible pairwise differences between the positions of the array elements. It contains all possible vector differences between these positions:

$$D_{UCA} = \{p_j - p_i \mid \forall i, j \in \{1, \ldots, M\}\} \tag{3.9}$$

This results in a set of difference vectors that exhibit circular symmetry. One key property of the difference co-array of a UCA is that it tends to have a higher number of unique difference vectors compared to its linear counterpart. The DoF provided by a UCA depends on the number of elements and whether the number of elements is even or odd. As proven by [45] and summarized in Appendix C, the details are given below:

- For an odd number of elements M:

$$\text{DoF} = M^2 - M + 1$$

- For an even number of elements M:

$$\text{DoF} = \frac{M^2}{2} + 1$$

It can be noted that a UCA with an odd number of elements reaches the global maximum DoF limit achievable by its difference co-array. However, a UCA with an even number of elements cannot achieve this due to having an element exactly opposite (shifted $180°$), which creates redundancies. Examples of UCAs with odd and even numbers of elements are shown in Figures 3.7 and 3.8, respectively.

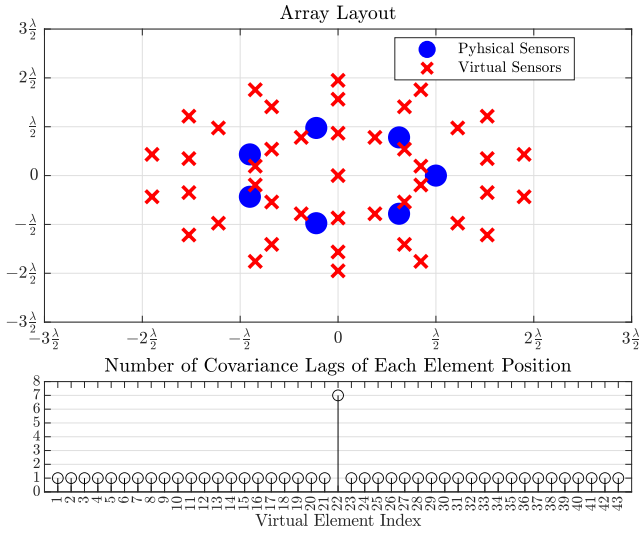

Figure 3.7: A 7-element Uniform Circular Array (UCA) with a radius of $r = \lambda/2$ and its corresponding difference co-array.

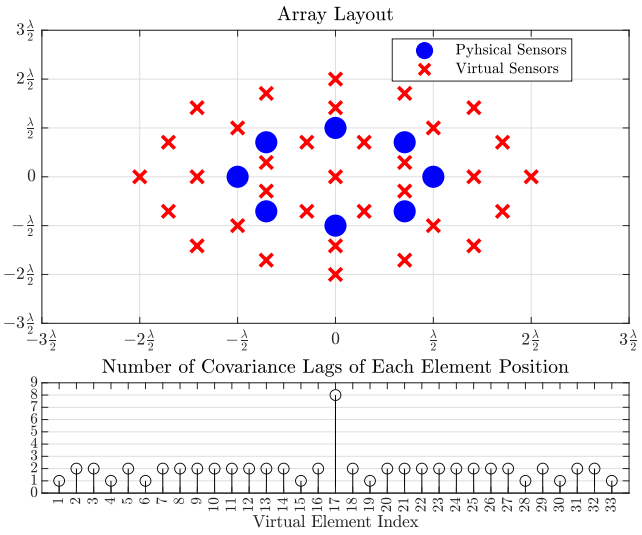

Figure 3.8: A 8-element Uniform Circular Array (UCA) with a radius of $r = \lambda/2$ and its corresponding difference co-array.

3.2 Applying the Khatri-Rao Product to Underdetermined DoA Estimation Problems

Assume K narrow-band quasi-stationary source signals $\{s_1(t), s_2(t), \ldots, s_K(t)\}$ are arriving from distinct directions $\{(\phi_1), (\phi_2), \ldots, (\phi_K)\}$ to an M-element antenna array. The received data from the array is given by the following equation, which is the same with equation (2.1):

$$\mathbf{y}(t) = \mathbf{A}\mathbf{s}(t) + \mathbf{n}(t), \quad t \in \{1, 2, \ldots\} \tag{3.10}$$

Since the signal characteristics are quasi-stationary, the received signal can be divided into F frames, each containing L snapshots. Each local covariance matrix is shown below:

$$\begin{aligned}\mathbf{R}_{\mathbf{Y}}^{m} &= \mathbf{E}[\mathbf{y}(t)\mathbf{y}^{H}(t)], \quad t \in \{(m-1)L, \ldots, mL-1\} \\ &= \frac{1}{L}\sum_{t=(m-1)L}^{mL-1} \mathbf{y}(t)\mathbf{y}^{H}(t) = \mathbf{A}\mathbf{R}_{\mathbf{S}}^{m}\mathbf{A}^{H} + \sigma^{2}\mathbf{I}\end{aligned} \tag{3.11}$$

Here, $\mathbf{R}_{\mathbf{Y}}^{m} \in \mathbb{C}^{M\times M}$ represents the covariance matrix of the received signal in the m-th frame, $\mathbf{R}_{\mathbf{S}}^{m} \in \mathbb{C}^{K\times K}$ is the covariance matrix of the source signals in the m-th frame, and $\sigma^{2} \in \mathbb{R}$ denotes the noise variance.

For the underdetermined DoA estimation problem, the covariance matrix of each frame on equation (3.11) is vectorized as follows:

$$\begin{aligned}\mathbf{r}_{m} &= \text{vec}(\mathbf{R}_{\mathbf{Y}}^{m}) \\ &= \text{vec}(\mathbf{A}\mathbf{R}_{\mathbf{S}}^{m}\mathbf{A}^{H}) + \text{vec}(\sigma^{2}\mathbf{I}) \\ &= \sum_{i=1}^{K} p_{i}^{m}\text{vec}(\mathbf{a}(\phi_{i})\mathbf{a}^{H}(\phi_{i})) \\ &\quad + \sum_{\substack{j=1\\ j\neq z}}^{K}\sum_{\substack{z=1\\ z\neq j}}^{K} \rho_{jz}^{m}\sqrt{p_{j}^{m}p_{z}^{m}}\text{vec}(\mathbf{a}(\phi_{j})\mathbf{a}^{H}(\phi_{z})) + \text{vec}(\sigma^{2}\mathbf{I})\end{aligned} \tag{3.12}$$

where p_{i}^{m} is the power of the i-th signal for m-th frame, and ρ_{jz}^{m} is the correlation coefficient between the j-th and z-th sources for m-th frame. If it is assumed that the sources are uncorrelated, namely $\rho_{jz}^{m} = 0,\ \forall j, z \in \{1, \ldots, K\}, j \neq z$; equation (3.12) can be rewritten as follows:

$$\begin{aligned}\mathbf{r}_{m} &= \sum_{i=1}^{K} p_{i}^{m}\text{vec}(\mathbf{a}(\phi_{i})\mathbf{a}^{H}(\phi_{i})) + \text{vec}(\sigma^{2}\mathbf{I}) \\ &= \sum_{i=1}^{K} p_{i}^{m}\mathbf{a}^{*}(\phi_{i}) \otimes \mathbf{a}(\phi_{i}) + \text{vec}(\sigma^{2}\mathbf{I}) \\ &= [\mathbf{A}^{*} \odot \mathbf{A}]\,\mathbf{p}_{m} + \mathbf{i}_{n} \\ &= \mathbf{A}_{d}\mathbf{p}_{m} + \mathbf{i}_{n}\end{aligned} \tag{3.13}$$

where $(.)^{*}$ denotes complex conjugation, $\otimes$ is the Kronecker product, $\odot$ is the Khatri-Rao product, $\mathbf{A}_{d}$ represents the array manifold of the difference co-array (see Ap-

pendix D for derivation) explained in Section 3.1 of a sensor array with repeating elements, $\mathbf{p}_m = \text{diag}(\mathbf{R}_{\mathbf{S}}^m)$, and $\mathbf{i}_n = \sigma^2 \left[\mathbf{e}_1^T, \ldots, \mathbf{e}_M^T\right]^T$, where $\mathbf{e}_j$ denotes the j-th canonical basis vector in an M-dimensional space. The covariance matrix for a single frame is given by equation (3.13). For multiple frames, the concatenated data model is as follows:

$$\begin{aligned} \mathbf{Z} &= [r_1, \ldots, \mathbf{r}_F] \in \mathbb{C}^{M^2 \times F} \\ &= \mathbf{A}_d \mathbf{P}^T + \mathbf{i}_n \end{aligned} \tag{3.14}$$

where $\mathbf{P} = [\mathbf{p}_1, \ldots, \mathbf{p}_F]^T$. Assuming that the source power distributions across the time frames vary sufficiently so that $\mathbf{P}$ maintains a full column rank condition [21, 22, 46, 1].

3.3 Khatri-Rao MUSIC

Underdetermined DoA estimation using Khatri-Rao MUSIC (KR-MUSIC) is proposed by [21, 22]; it uses the signal model explained in Section 3.2.

Consider performing SVD on concatenated local covariance matrices $\mathbf{Z}$ given in equation (3.14):

$$\begin{aligned} \mathbf{Z} &= \mathbf{U}\mathbf{\Sigma}\mathbf{V}^H \\ &= \begin{bmatrix} \mathbf{U}_s & \mathbf{U}_n \end{bmatrix} \begin{bmatrix} \mathbf{\Sigma}_s & \mathbf{0} \\ \mathbf{0} & \mathbf{0} \end{bmatrix} \begin{bmatrix} \mathbf{V}_s^H \\ \mathbf{V}_n^H \end{bmatrix}, \end{aligned} \tag{3.15}$$

where $\mathbf{U}_s \in \mathbb{C}^{M^2 \times K}$ and $\mathbf{V}_s \in \mathbb{C}^{F \times K}$ are the left and right singular matrices that define the signal subspace corresponding to non-zero singular values; $\mathbf{U}_n \in \mathbb{C}^{M^2 \times (M^2 - K)}$ and $\mathbf{V}_n \in \mathbb{C}^{F \times (M^2 - K)}$ are the left and right singular matrices that define the noise subspace corresponding to zero singular values; and $\mathbf{\Sigma}_s \in \mathbb{R}^{K \times K}$ is the diagonal matrix of non-zero singular values. According to the SVD results, $\mathcal{R}(\mathbf{A}^* \odot \mathbf{A}) = \mathcal{R}(\mathbf{U}_s)$, where $\mathcal{R}(\cdot)$ denotes the range space and $\mathbf{U}_s \perp \mathbf{U}_n$. Using these results, the following expression can be formulated:

$$\mathbf{U}_n^H \left[\mathbf{A}^* \odot \mathbf{A}\right]_{k=1}^K = \mathbf{U}_n^H \left[\mathbf{a}^*(\phi_k) \otimes \mathbf{a}(\phi_k)\right]_{k=1}^K = 0 \tag{3.16}$$

Using the expression given in (3.16), the cost function of KR-MUSIC can be written as follows:

$$f(\phi_k) = \frac{1}{||\mathbf{U}_n^H \left(\mathbf{a}^*(\phi_k) \otimes \mathbf{a}(\phi_k)\right)||^2} \tag{3.17}$$

The estimation of DoAs can then be performed by identifying peaks in $f(\phi)$. The algorithm steps of KR-MUSIC are given in the following algorithm block.

Algorithm 4 KR-MUSIC Algorithm

Inputs: $\mathbf{Z} = [\mathbf{r}_1, \ldots, \mathbf{r}_F] = \left[\text{vec}(\mathbf{R}_Y^1), \ldots, \text{vec}(\mathbf{R}_Y^F)\right], \mathbf{A} = [\mathbf{a}(\phi_1), \ldots, \mathbf{a}(\phi_G)]$

Output: $\hat{\phi}$

1: $\mathbf{Z} = \mathbf{U}\mathbf{\Sigma}\mathbf{V}^H$

2: $\mathbf{U}_n = [\mathbf{u}_{K+1}, \ldots, \mathbf{u}_{M^2}]$

3: **for** $i = 1, 2, \ldots, G$ **do**

4: $\quad f(\phi_i) = ||\mathbf{U}_n^H \left(\mathbf{a}^*(\phi_i) \otimes \mathbf{a}(\phi_i)\right)||^{-2}$

5: **end for**

6: $\hat{\phi} = \underset{\phi}{\text{argmax}}\, f(\phi)$

3.4 Cramér-Rao Lower Bound Characteristics of Underdetermined DoA Estimation

As explained in previous parts of this chapter, underdetermined DoA estimation can be handled by the virtually created difference co-array of a physical array. However, when the number of sources equals or exceeds the number of antennas, the system reaches saturation due to being a virtual operation, as explained in [47].

Figure 3.9 illustrates the effect of saturation in underdetermined DoA estimation. The plot shows the Cramér-Rao Lower Bound (CRLB) [17, 33, 48, 47, 46] versus SNR for both underdetermined and overdetermined scenarios.

In the underdetermined scenario, where the number of sources is equal to or greater than the number of antennas, saturation occurs. This happens because the physical array does not have enough sensors to uniquely determine the directions of all sources. The difference co-array helps mitigate this problem by creating a virtual array with more elements, but its performance saturates after a certain SNR level. This saturation is a consequence of relying on virtual elements, which cannot fully replicate the performance of additional physical sensors.

In contrast, the overdetermined scenario, where the number of antennas exceeds the number of sources, does not exhibit saturation in the CRLB values.

Figure 3.9 clearly shows that while the difference co-array technique allows to underdetermined DoA estimation, the system's performance saturates if number of sources are greater or equal to number of sensors in the array.

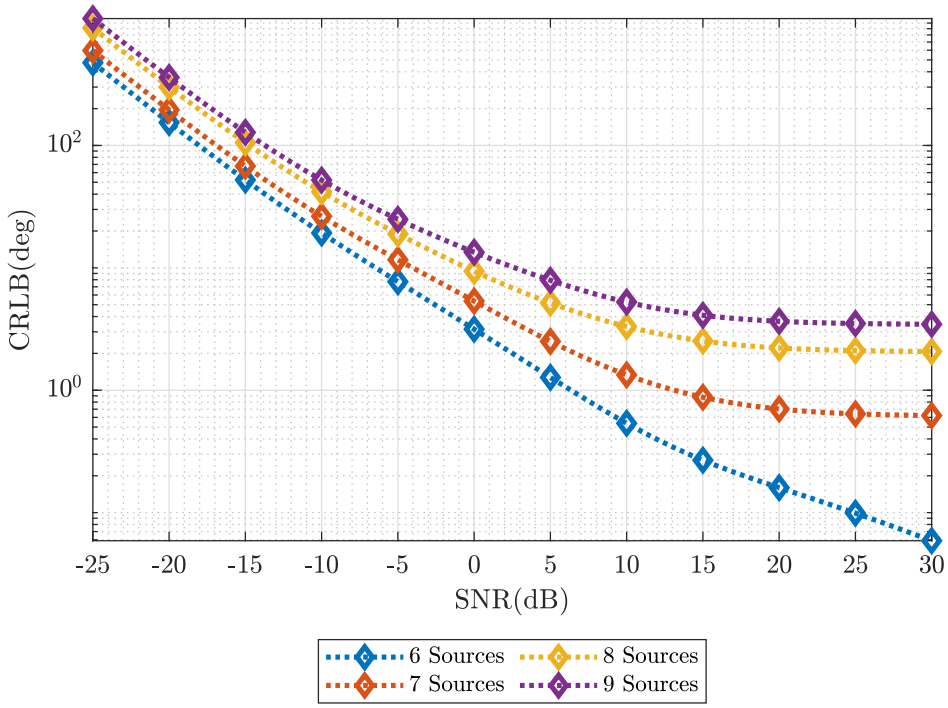

Figure 3.9: CRLB versus SNR for 7 Element UCA with Several Number of Sources

CHAPTER 4

NESTED CIRCULAR RING ARRAYS

In this chapter, the proposed Nested Circular Ring Arrays (NCRA) are explained, detailing the design approach and criteria. Additionally, NCRA is compared with conventional Uniform Circular Arrays (UCA) by evaluating half-power beamwidth, maximum sidelobe level, and degrees of freedom to highlight the advantages and disadvantages of each configuration.

The effects of beamwidth and sidelobe levels on underdetermined DoA estimation are generally overlooked in the literature. In array processing, narrow beamwidths and lower sidelobe levels are crucial for improving DoA estimation accuracy. Simulations have shown that the performance of one of the most commonly used conventional planar array structures, the UCA, may not be sufficient for underdetermined scenarios due to its wider beamwidth.

The main motivation behind NCRA is to create a sparse (to achieve a wider aperture and hence a narrower beamwidth), planar (to obtain a 360° azimuthal coverage), circular isotropic (to ensure consistent performance across the entire azimuthal spectrum) array to achieve more accurate DoA estimation performance, especially in underdetermined scenarios.

The proposed NCRA is a sparse planar array consisting of multiple circularly arranged linear nested arrays. These Linear Nested Arrays, detailed in Section 3.1.3, are positioned with uniform angular shifts, as shown in Figure 4.1.

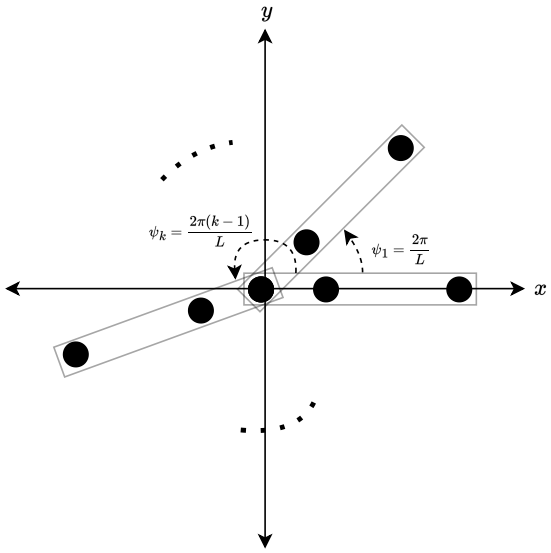

Figure 4.1: Layout of NCRA.

The main advantages and disadvantages of NCRA are listed below:

- **Advantages:**
  - Narrower beamwidth compared to conventional planar array structures like UCA, achieved through the use of sparsity.
  - Enhanced DoA estimation performance for both coherent (an important challenge in underdetermined DoA estimation) and non-coherent source scenarios, attributed to its narrower beamwidth and comparable sidelobe levels.
  - Consistent DoA performance across the entire azimuthal spectrum, due to its isotropic geometry [49].
- **Disadvantages:**
  - NCRA is not applicable for all sensor configurations. Specifically, **Number of Sensors** - 1 must not be a prime number, as will be explained in subsequent sections of this chapter.

- Due to having sparsities, namely interelement distances greater than $\lambda/2$, robustness at low SNR levels may be reduced.

As shown in Figure 4.1, the sparsity of NCRA is achieved through the use of multiple Linear Nested Arrays arranged in a circular pattern. Since each nested array is shifted around the center, the first element of each array is located at the same position. This element, placed at the center, serves as a common element, allowing for the implementation of multiple nested arrays without increasing the total number of elements. The requirement for a central element is the main reason why NCRA cannot be constructed for every possible number of total sensors, which is explained as a disadvantage of NCRA.

After presenting the motivation, introduction, and a brief review of NCRA, the general design criteria for NCRA can be summarized as follows:

1. **Omni-directional characteristics**: This criterion ensures that the DoA estimation performance remains consistent regardless of the source direction. Arrays that meet this criterion are known as isotropic arrays [49], achieved by designing the array with circular symmetry.

2. **2-level Nested Sub-Arrays placed on arms**: Nested arrays are sparse arrays that provide a wider aperture and more degrees of freedom in the difference co-array, as explained in Section 3.1.3 and in [1]. Therefore, nested arrays are chosen for this design.

3. **An element placed at the center**: The central element serves as the common element for each linear nested array. This design ensures a larger aperture without increasing the total number of elements in the physical array.

Consider a NCRA comprising L linear nested arrays which are called as **arm**, each consisting of K elements. The total number of physical elements M can be expressed as:

$$M = LK - (L - 1) \tag{4.1}$$

The term $(L-1)$ is subtracted to account for the common element located at the center. As shown in equation (4.1), this structure is not applicable for **A prime number + 1** number of physical elements. The angular shift step for placing the linear nested arrays can be calculated as follows:

$$\begin{aligned} \psi_{step} &= \frac{2\pi}{L}, \\ \psi_k &= \frac{2\pi(k-1)}{L} \end{aligned} \tag{4.2}$$

By considering Design Criteria 1 and equations (4.1), (4.2), the number of arms L must satisfy $L > 2$. For a design where $L \leq 2$, the array will become a linear array and have back-forth ambiguity similar to a ULA [3], as shown in Figure 4.2. Additionally, to create a nested array that contains multiple concatenated uniform linear arrays, the number of elements must satisfy $K \geq 3$ elements in a single linear nested array. This means the minimum number of physical elements required to create a NCRA is $M = 7$ by equation (4.1) for $L = 3$ and $K = 3$.

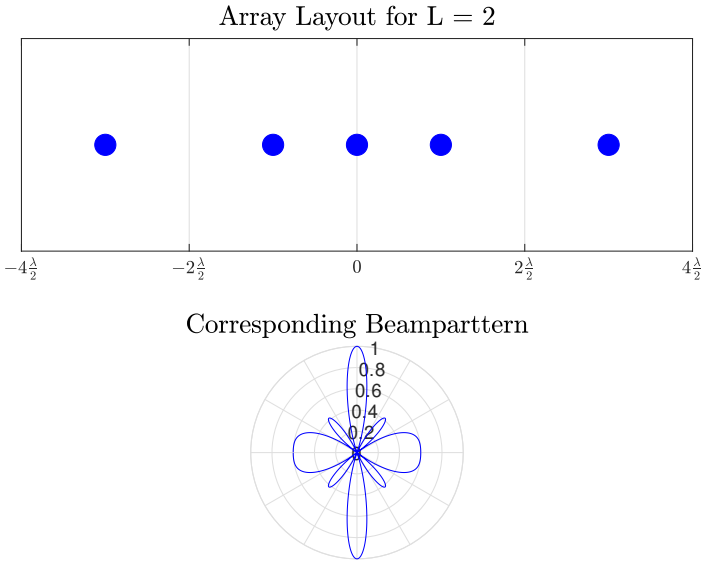

Figure 4.2: Back-forth ambiguity for $L = 2$.

Furthermore, the omni-directional property is achieved by having circular symmetry with circularly placed nested linear arrays. This design ensures uniform performance

in all directions for DoA estimation. The importance of this circular symmetry is illustrated in Figure 4.3, which compares the CRLB [34][35][3] across all azimuth planes for a non-symmetrical array and a UCA. The figure demonstrates how the lack of symmetry can lead to performance fluctuations, whereas a symmetrical design like NCRA maintains consistent performance, similar to that of a UCA [50, 51].

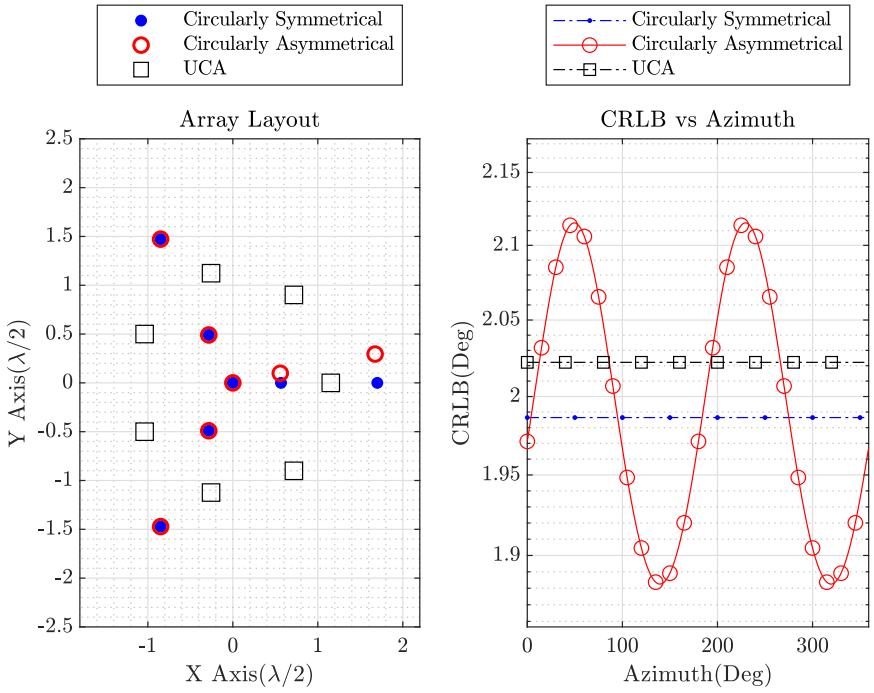

Figure 4.3: Comparison of a non-symmetrical array and a UCA.

The Table 4.1 presents various NCRA configurations with different numbers of physical elements and configuration options. It provides details on the number of arms, corresponding to the number of linear nested arrays used, as well as the specific nested array configuration, the degrees of freedom (DoF) provided by the difference co-array, the half-power beamwidth (HPBW), and the maximum sidelobe level (MSLL). The nested array layouts indicated by [.] represent the optimal sub-array element number selection, as given in Table 3.1, to maximize DoF.

Figures 4.4, 4.5, 4.6, and 4.7 illustrate different NCRA configurations explained in Table 4.1 with various numbers of physical elements and their corresponding difference co-arrays with number of covariance lags.

Table 4.1: NCRA Parameters.

Number of Pyhsical Sensors	*Number of Arms*	*Corresponding Nested Array for Each Arm* ($\frac{\lambda}{2}$)	*Number of Sensors on Difference Co-Array*	*HPBW (Deg) (Simulation Result)*	*MSLL (Simulation Result)*
7	3	[0 1 3]*	43	21.78	0.62
8	M-1 = 7 is a prime number.				
9	4	0.9×[0 1 3]*	37	24.03	0.77
10	3	[0 1 3 5]	85	14.25	0.65
		[0 1 2 5]*	85	15.45	0.52
11	5	[0 1 3]*	111	20.99	0.50
12	M-1 = 11 is a prime number.				
13	3	[0 1 2 5 8]*	145	10.45	0.56
		[0 1 3 5 7]	139	10.73	0.67
		[0 1 2 3 7]	139	12.75	0.49
	4	0.9×[0 1 3 5]	69	15.91	0.84
		0.9×[0 1 2 5]*	69	17.63	0.63
	6	[0 1 3]*	67	20.82	0.55
14	M-1 = 13 is a prime number.				
15	7	[0 1 3]*	211	20.69	0.5
16	3	[0 1 2 3 7 11]*	217	8.65	0.55
		[0 1 2 5 8 11]	217	7.85	0.63
		[0 1 3 5 7 9]	205	8.95	0.68
	5	[0 1 2 5]*	231	15.25	0.54
		[0 1 3 5]	231	13.91	0.49
17	4	0.9×[0 1 2 5 8]*	113	11.80	0.66
		0.9×[0 1 2 3 7]	109	14.65	0.61
		0.9×[0 1 3 5 7]	109	12	0.88
	8	[0 1 3]*	137	20.59	0.64

As seen in Table 4.1, several NCRA configurations can be created with different numbers of arms. The selection of the number of arms, i.e., the number of nested arrays placed on the NCRA, critically impacts performance by directly affecting the beamwidth and sidelobe characteristics due to changes in the array layout and aperture.

Increasing the number of arms with the same number of elements reduces the aperture, leading to a wider beamwidth, which can degrade the resolution performance in underdetermined DoA estimation. For optimal resolution performance, it is recommended to choose the lowest number of arms and the longest nested linear array structure.

Additionally, sidelobe levels—an important parameter for underdetermined DoA estimation, especially with coherent sources or in low SNR conditions—do not have a straightforward linear relationship with the number of arms or the sparsity of the array structure. Therefore, sidelobe levels should be measured or computed and appropriately selected based on the specific requirements.

The design process for constructing a Nested Circular Ring Array (NCRA) with a specified number of sensors M involves the following steps:

1. Determine the number of arms L and the corresponding number of sensors per arm, guided by equation (4.1) and Table 4.1. The selection of L significantly impacts the array's performance.

2. Calculate the angular shift step for positioning the nested arrays around the circular structure using equation (4.2), ensuring even distribution and maintaining circular symmetry.

3. Select the appropriate Linear Nested Array for each arm of the NCRA, based on optimal configurations in Table 3.1 and the design goals in Table 4.1.

4. Upon completing these steps, the NCRA design is finalized, resulting in an array with enhanced degrees of freedom (DoF), improved beamwidth, and optimized sidelobe levels for the intended application.

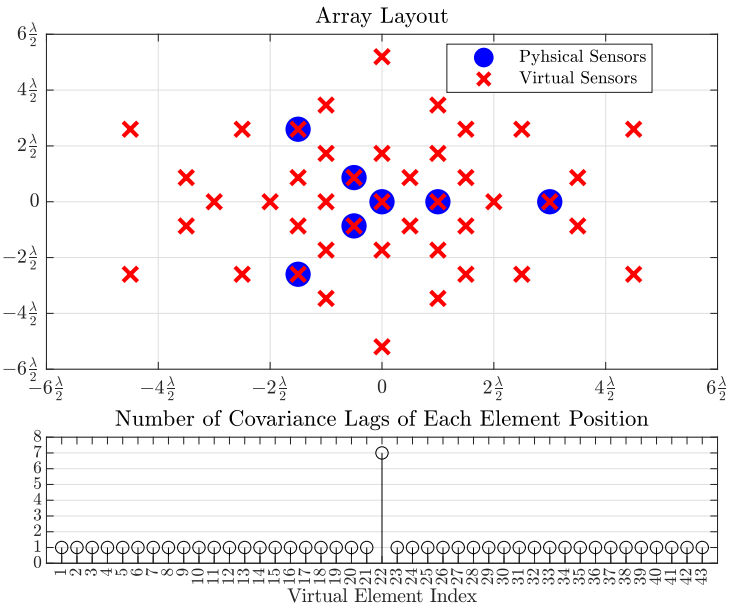

Figure 4.4: 7 Element NCRA

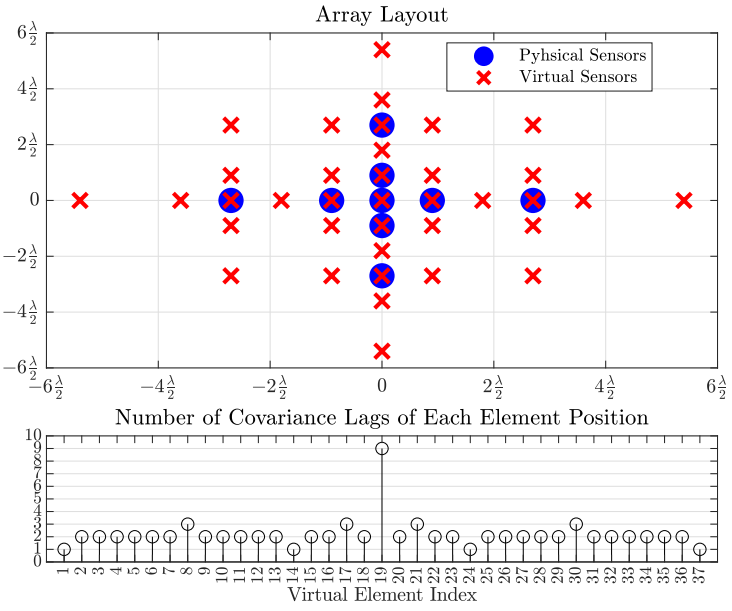

Figure 4.5: 9 Element NCRA

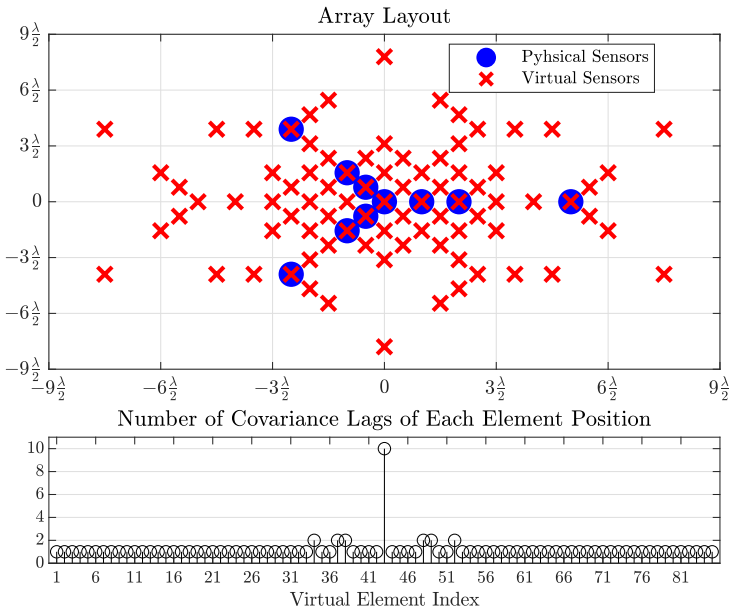

Figure 4.6: 10 Element NCRA

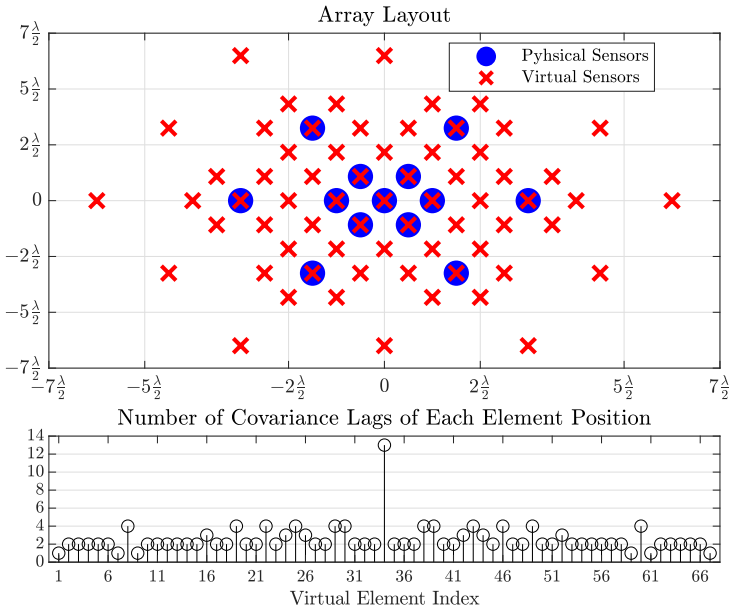

Figure 4.7: 13 Element NCRA - 6 Arms

Table 4.2: UCA Parameters

Number of Pyhsical Sensors	*Max. Radius* ($\frac{\lambda}{2}$)	*Number of Sensors on Difference Co-Array*	*HPBW (Deg)*		*MSLL (Simulation Result)*
			Simulation Result	*Approximation in [52]*	
7	1.152	43	36.75	36.44	0.59
8	1.306	33	32.49	32.14	0.62
9	1.461	73	29.13	28.72	0.50
10	1.618	51	26.41	25.95	0.69
11	1.774	111	24.15	23.66	0.50
12	1.931	73	22.27	21.74	0.50
13	2.089	157	20.65	20.10	0.50
14	2.247	99	19.27	18.69	0.54
15	2.404	211	18.07	17.46	0.50
16	2.562	129	17.01	16.38	0.55
17	2.72	273	16.09	15.43	0.49

Table 4.2 lists the maximum unambiguous radius, DoF of the difference co-array, half-power beamwidth (HPBW), and maximum sidelobe level (MSLL) for various uniform circular arrays, allowing comparison with NCRA configurations in Table 4.1. HPBW results are provided from both an approximation [52] and simulations, with similar outcomes verifying the simulation. MSLL is also determined via simulation from the beampattern.

Figure 4.8 illustrates the omnidirectional characteristics of different NCRA configurations listed in Table 4.1 by plotting the Cramér-Rao Lower Bound (CRLB) versus azimuth angles. This comparison shows how the symmetrical design of NCRA, as defined by Design Criterion 1, ensures uniform performance across all azimuth angles, similar to uniform circular arrays (UCAs). The subfigures in Figure 4.8 present CRLB vs. azimuth plots for various NCRA configurations with different numbers of elements, confirming that the omnidirectional characteristic is preserved in NCRA designs, making them suitable for robust DoA estimation in diverse scenarios.

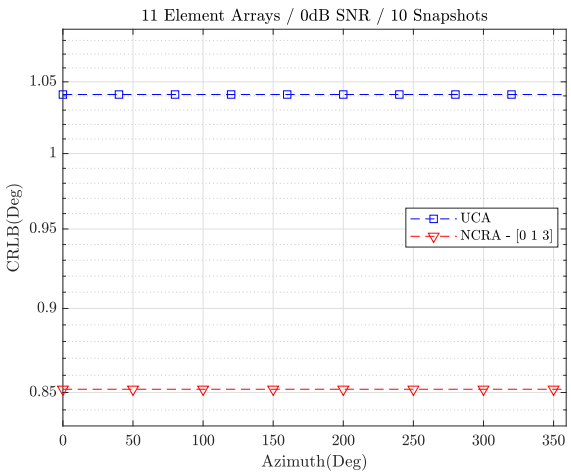

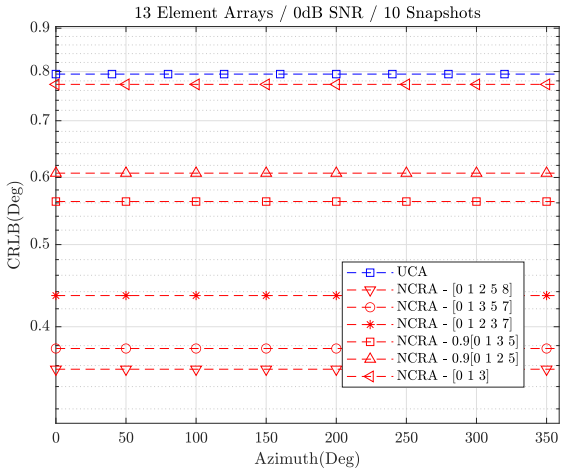

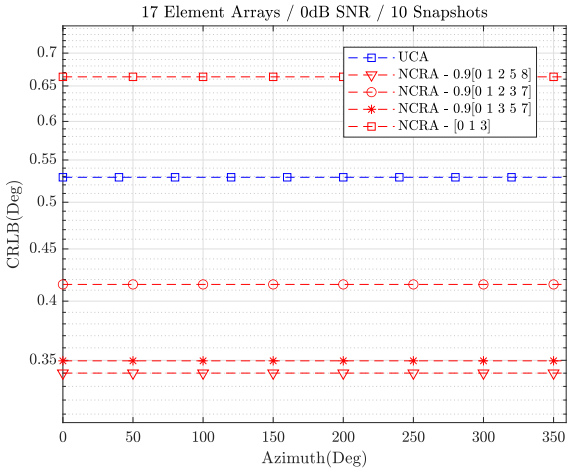

Figure 4.8: Comparison of omnidirectional characteristics: Overdetermined CRLB vs. Azimuth for various NCRA configurations and UCAs

CHAPTER 5

SIMULATION RESULTS

In this section, the performances of the proposed NCRA are investigated using Covariance Matrix Estimation with CWD, MUSIC, and SBL algorithms for the overdetermined case, and SBL and KR-MUSIC algorithms for the underdetermined case, with varying numbers of sources, including both coherent and non-coherent sources.

The first part examines overdetermined DoA estimation performance through RMSE-SNR and Azimuth-RMSE analysis, with all RMSE analyses supported by corresponding CRLB computations as a theoretical benchmark of algorithm performance, as detailed in [34, 17] and further explained in Appendices A and B. The second part focuses on underdetermined DoA estimation performance, comparing NCRA with UCA through RMSE-SNR and Resolution probability analysis. This analysis not only highlights the potential advantages and limitations of NCRA but also evaluates how effectively NCRA can detect individual sources. The performance of NCRA is assessed in terms of its ability to identify the presence and direction of more sources than sensors, demonstrating its robustness and reliability, particularly when compared to UCA. The benefits of NCRA's greater aperture and narrower beamwidth in enhancing detection performance in challenging scenarios are also emphasized, offering valuable insights into its practical applications.

5.1 Overdetermined Scenario

In this section, performance comparisons between the proposed NCRA and UCA are conducted using 7-element configurations within an overdetermined scenario and signal model. The comparison includes RMSE-SNR analysis for both coherent and

non-coherent source cases to assess the SNR dependency of the algorithms and arrays, as well as Azimuth-RMSE analysis to evaluate the omni-directional characteristics of the arrays. To provide a theoretical benchmark for algorithm performances, CRLB results [34, 35] are included in all analyses.

The Maximum Likelihood (ML) Covariance Matrix Estimation with the CWD algorithm is employed to estimate the covariance matrix, which is then used as an input for the MUSIC algorithm. Additionally, the SBL algorithm and the traditional MUSIC algorithm with the sample covariance matrix are utilized for the simulations. These three algorithms were used to provide a comprehensive evaluation, allowing for an assessment of both the performance of the array configurations and the algorithms themselves across a broad scope.

5.1.1 RMSE-SNR Simulations

Case 1: RMSE-SNR Performance Comparison of 7-Element NCRA and UCA with 3 Uncorrelated Sources in an Overdetermined Scenario

In this case, a 7-element configuration of both NCRA and UCA is evaluated in an overdetermined scenario with 3 uncorrelated sources. The sources are positioned with a uniform angular separation of 75°. The SNR is varied from -20 dB to 10 dB to assess the robustness of the arrays under different noise conditions. For each SNR level, 100 snapshots are collected, and 200 Monte Carlo iterations are performed to compute the RMSE values. In this scenario, the performance of NCRA and UCA is compared using the MUSIC algorithm with both the ML Covariance Matrix Estimation and the sample covariance matrix, as well as the SBL algorithm. This analysis aims to highlight the advantages of the NCRA design in terms of accuracy and resilience against noise when compared to the traditional UCA in an overdetermined setting.

Table 5.1: Simulation parameters for case 1.

Simulation Parameters	
Number of sensors	7
SNR	-20 to 10dB
Number of sources	3
Angular Separation	$75°$
Number of snapshots	100
Number of Iterations	200

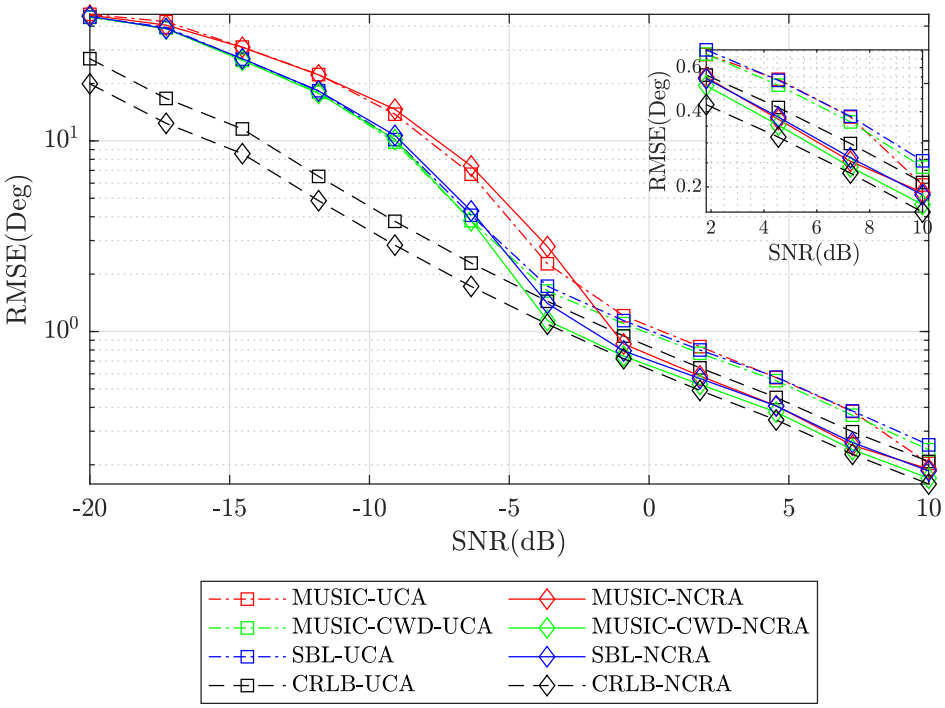

Figure 5.1: 7 Element Arrays, 3 Uncorrelated Sources, 200 MCT

As can be seen from Figure 5.1, all algorithms demonstrate a general trend of decreasing RMSE with increasing SNR, reflecting improved accuracy as the signal-to-noise ratio improves.

For SNR levels below 0 dB, the MUSIC algorithm, whether applied to UCA or

NCRA, shows slightly higher RMSE values compared to the SBL and CWD algorithms, indicating that SBL and CWD provide better robustness in low SNR conditions. The use of the CWD approach with MUSIC improves performance, reducing RMSE compared to the standard MUSIC algorithm.

At higher SNR levels (above 0 dB), the RMSE values for all algorithms converge to the CRLB, but RMSE values for NCRA are consistently lower than those for UCA across all algorithm results. This indicates that NCRA, with its narrower beamwidth and lower sidelobe levels, performs better than UCA.

In summary, the results demonstrate that NCRA offers superior DoA estimation accuracy compared to UCA.

Case 2: RMSE-SNR Performance Comparison of 7-Element NCRA and UCA with 3 Coherent Sources in an Overdetermined Scenario

In this case, the simulation involves a 7-element configuration for both NCRA and UCA arrays, with 3 coherent sources positioned at an angular separation of 75°. Coherent sources present a more challenging scenario for DoA estimation algorithms due to the high correlation between signals. The Signal-to-Noise Ratio (SNR) is varied from -20 dB to 10 dB, and 200 Monte Carlo iterations are performed at each SNR level with 100 snapshots per iteration to compute the RMSE values. Given the coherence among the sources, the MUSIC algorithm is not used in this case, as it is known to perform poorly under such conditions. Instead, the SBL and CWD algorithm is utilized to assess the performance of NCRA and UCA under these challenging conditions.

Table 5.2: Simulation parameters for case 2.

Simulation Parameters	
Number of sensors	7
SNR	-20 to 10dB
Number of coherent sources	3
Angular Separation	75°
Number of snapshots	100
Number of Iterations	200

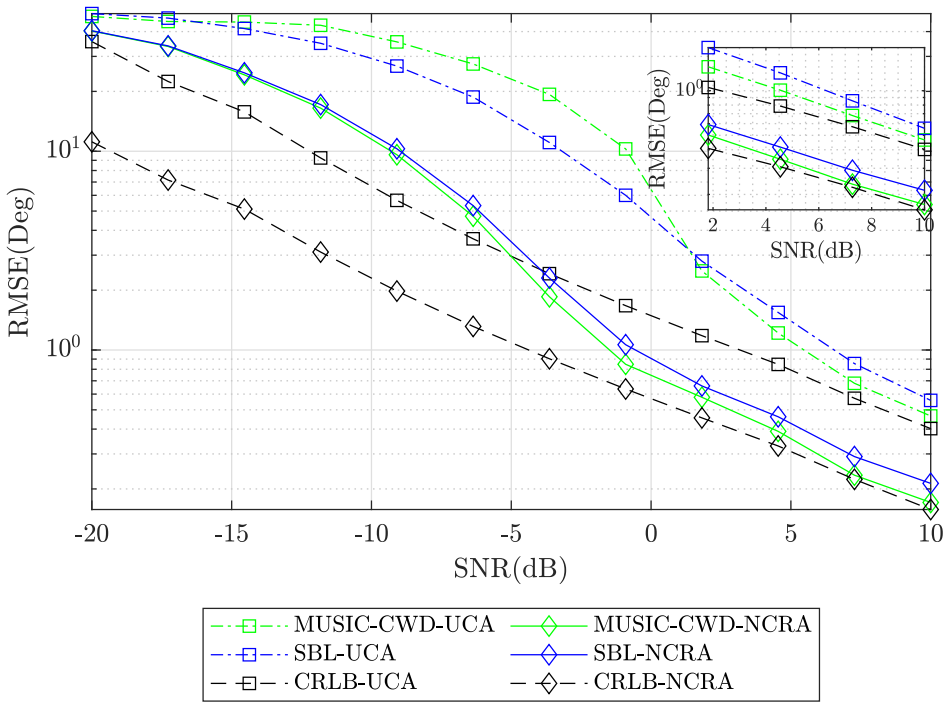

Figure 5.2: 7 Element Arrays, 3 Coherent Sources, 200 MCT

As shown in Figure 5.2, the RMSE-SNR analysis reveals that the SBL algorithm performs better than the CWD algorithm at SNR levels above 0 dB for UCA, while its performance is worse than CWD below 0 dB SNR. Additionally, for NCRA, both algorithms perform similarly below -10 dB SNR, but the CWD algorithm outperforms

SBL above the -10 dB SNR level. When comparing Figure 5.2 with Figure 5.1, it is evident that the algorithms converge to the CRLB more slowly in the coherent source scenario than in the uncorrelated case.

The performance of NCRA consistently surpasses that of UCA across all SNR levels, showcasing NCRA's advantage in handling coherent sources effectively due to its narrower beamwidth. As SNR increases, the RMSE values for all methods gradually approach the CRLB, with NCRA achieving closer proximity to the CRLB than UCA, indicating superior accuracy. Notably, at higher SNR levels, the gap between the NCRA and UCA results becomes more pronounced, further highlighting the benefits of using NCRA in coherent source scenarios. Overall, this analysis underscores the robustness of NCRA in challenging overdetermined DoA estimation scenarios involving coherent sources.

5.1.2 RMSE-Azimuth Simulations

In this subsection, RMSE-Azimuth simulations are conducted to evaluate the omni-directional performance of the proposed NCRA and UCA, utilizing a 7-element configuration. The simulation parameters are detailed in table given below. This analysis is performed with a single source, covering azimuth angles from 0° to 359°, at an SNR level of 7 dB. A total of 100 snapshots are used, and 500 Monte Carlo iterations are conducted for each azimuth angle.

Three algorithms—MUSIC, SBL, and MUSIC with CWD covariance matrix estimation—are employed to assess the performance of both arrays. The primary objective of this analysis is to verify the omni-directional characteristics of NCRA and compare its performance with UCA across the entire azimuthal spectrum. The results aim to demonstrate that both NCRA and UCA maintain consistent performance regardless of the direction of the incoming signal, thereby confirming their suitability for applications requiring omni-directional DoA estimation.

Table 5.3: Simulation parameters.

Simulation Parameters	
Number of sensors	7
SNR	7dB
Number of sources	1
Azimuth Coverage	0° to 359°
Number of snapshots	100
Number of Iterations	500

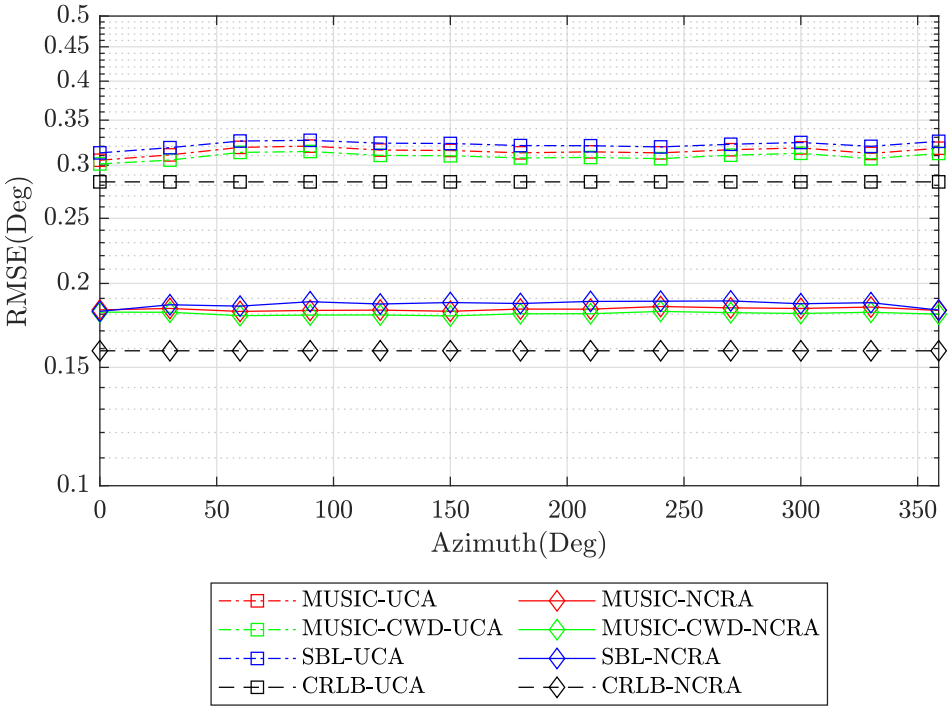

Figure 5.3: Azimuth-RMSE comparison of NCRA and UCA.

As shown in Figure 5.3, the RMSE values remain relatively constant across all azimuth angles for both the NCRA and UCA configurations, confirming that both arrays exhibit omni-directional characteristics. This consistency indicates that the performance of the arrays does not depend on the direction of the incoming signal, val-

idating their suitability for applications requiring uniform DoA estimation across the azimuthal spectrum.

The slight variations observed in the RMSE curves for different algorithms, particularly in the SBL and MUSIC with CWD results, are primarily due to the limited number of iterations (500) and sparse grids are used in the simulations. These minor fluctuations are expected and would likely diminish with an increased number of iterations. Nonetheless, the overall flatness of the RMSE curves demonstrates that both arrays maintain consistent performance across all directions, fulfilling the design criterion for omni-directionality.

5.2 Underdetermined Scenario

This section presents a performance comparison between the proposed NCRA and UCA using 7-element and 10-element configurations in an underdetermined scenario with the corresponding signal model. The analysis includes RMSE-SNR evaluation for both coherent and non-coherent sources to determine how the algorithms and array configurations respond to varying SNR levels. Additionally, resolution performance is assessed to examine the relationship between beamwidth and resolution for each array. To ensure a thorough evaluation, CRLB results [17, 33] are provided as a theoretical benchmark across all analyses.

The simulations employ both the SBL and KR-MUSIC algorithms. Utilizing these two algorithms allows for a well-rounded assessment, offering insights into the performance of both the array designs and the algorithms themselves under a variety of conditions.

5.2.1 RMSE-SNR Simulations

This section presents the RMSE-SNR simulations to assess the performance of the proposed NCRA in underdetermined scenarios involving both coherent and non-coherent sources, using the KR-MUSIC and SBL algorithms. The performance of NCRA is compared against that of UCA to underscore the enhancements in accuracy

and robustness in direction-of-arrival estimation offered by NCRA. For this analysis, 7-element and 10-element NCRA configurations are evaluated and compared with UCAs containing the same number of sensors. Furthermore, the underdetermined CRLB, as explained in Appendix B, is plotted to provide a theoretical performance benchmark.

5.2.1.1 Non-Coherent Scenario

Case 1: RMSE-SNR Performance Comparison of 7-Element NCRA and UCA with 9 Sources in an Underdetermined Scenario

In this case, a 7-element configuration of both NCRA and UCA is utilized. Nine uncorrelated sources are positioned with a uniform angular spacing of 38°. For quasi-stationary signal generation, 30 frames and 250 snapshots are used. The performance of NCRA and UCA is compared using the KR-MUSIC and SBL algorithms, with the results benchmarked against the Cramér-Rao Lower Bound (CRLB). The Signal-to-Noise Ratio (SNR) is varied from -15dB to 15dB, and 500 Monte Carlo iterations are performed at each SNR level to compute the RMSE values.

Table 5.4: Simulation Parameters for Case 1

Simulation Parameters	
Number of sensors	7
SNR	-15 to 15dB
Number of sources	9
Angular Separation	38°
Number of frames	30
Number of snapshots per frame	250
Number of iterations	500

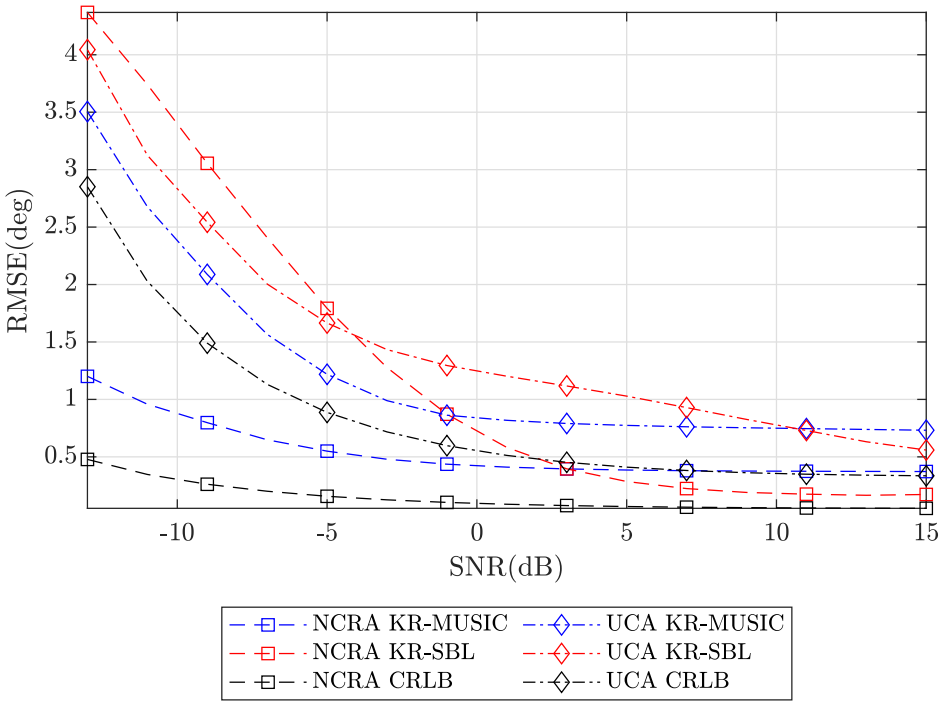

Figure 5.4: 7 Element Arrays, 9 Uncorrelated Sources, 500 MCT

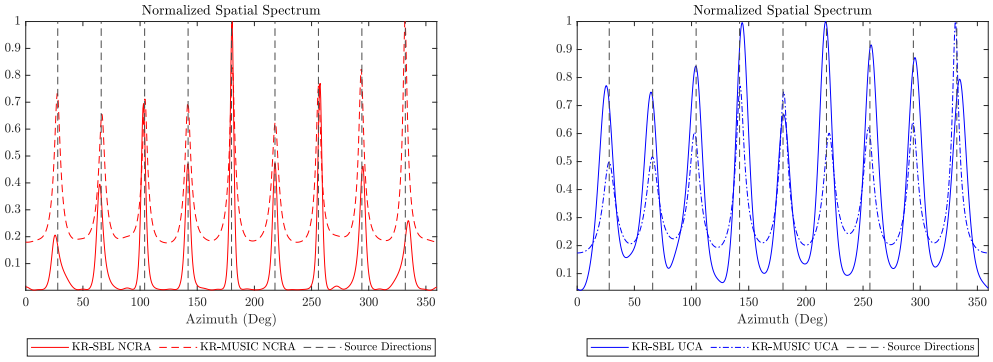

(a) 7 Element NCRA

(b) 7 Element UCA

Figure 5.5: Spatial spectrum of case 1 trials for -5dB SNR.

As shown in Figure 5.4, the 7-element NCRA has lower RMSE and CRLB compared to the 7-element UCA with maximum unambiguous radius due to its greater aper-

ture, as explained in Tables 4.2 and 4.1. This increased aperture enhances the array's resolution. Additionally, it can be observed that KR-MUSIC has a gap between its performance and the CRLB for both arrays, similar to the results in [23], while SBL asymptotically converges to the CRLB. However, KR-MUSIC performs better than SBL at lower SNR levels for this simulation scenario. Figure 5.5 also illustrates the spatial spectrum for this simulation scenario at -5 dB SNR.

Case 2: Spatial Spectrum Comparison of 7-Element NCRA and UCA with 16 Sources in an Underdetermined Scenario

In this case, the spatial spectrum performance of 7-element NCRA and UCA arrays is compared in an underdetermined scenario with 16 sources, each separated by an angular spacing of 20°. Unlike the previous cases, RMSE-SNR analysis is not performed here due to the inability of UCA to resolve the sources effectively. Therefore, the Cramér-Rao Lower Bound (CRLB) is not presented. Instead, the focus is on the spatial spectrum results at an SNR of 15 dB for both arrays. The KR-MUSIC and KR-SBL algorithms are applied to illustrate the differences in source detection capabilities between NCRA and UCA under these challenging conditions.

Table 5.5: Simulation parameters for case 2.

Simulation Parameters	
Number of sensors	7
SNR	15dB
Number of sources	16
Angular Separation	20°
Number of frames	40
Number of snapshots per frame	200

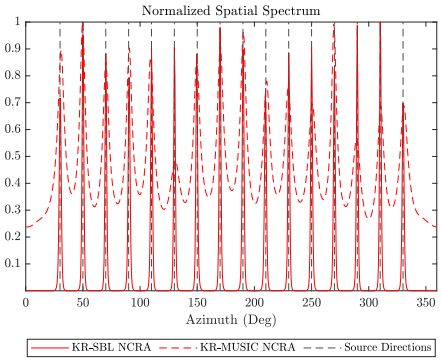

(a) 7 Element NCRA

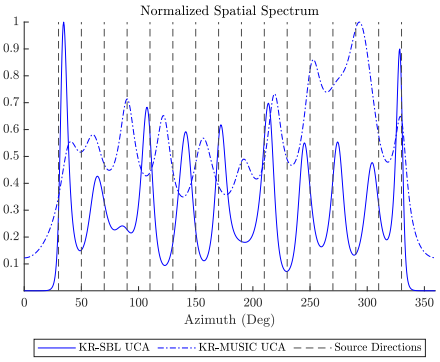

(b) 7 Element UCA

Figure 5.6: Spatial spectrum for case 2 trials.

Figure 5.6b illustrates an example of the beamwidth limitation of a UCA. The DoF provided by the difference co-array of the 7-element UCA is 43, but it cannot handle the 16 sources with 20° angular separation. In contrast, the 7-element NCRA can manage this scenario and accurately estimate the direction of the sources due to having a wider aperture and hence narrower beamwidth, as depicted in Figure 5.6a. This demonstrates NCRA's effectiveness in scenarios where traditional UCA fails, highlighting its advantage in increasing aperture and reducing beamwidth.

Case 3: RMSE-SNR Performance Comparison of 10-Element NCRA and UCA with 11 Sources in an Underdetermined Scenario

In this scenario, a 10-element configuration is applied to both NCRA and UCA arrays. 11 uncorrelated sources are placed with a uniform angular spacing of $30°$. For the generation of quasi-stationary signals, 20 frames and 100 snapshots are utilized. The comparison between NCRA and UCA is conducted using the KR-MUSIC and SBL algorithms, with the performance evaluated against the Cramér-Rao Lower Bound (CRLB) as a theoretical benchmark. The Signal-to-Noise Ratio (SNR) is varied between -15dB and 15dB, with 500 Monte Carlo iterations executed at each SNR level to calculate the RMSE values.

Table 5.6: Simulation parameters for case 3.

Simulation Parameters	
Number of sensors	10
SNR	-15 to 15dB
Number of sources	11
Angular Separation	30°
Number of frames	20
Number of snapshots per frame	100
Number of iterations	500

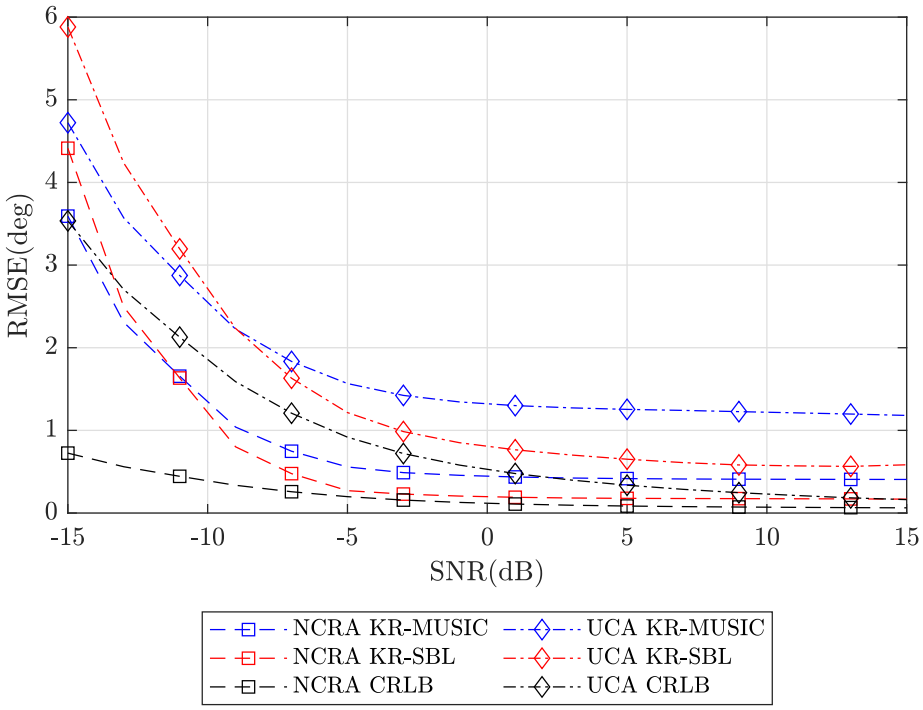

Figure 5.7: 10 Element Arrays, 11 Uncorrelated Sources, 500 MCT

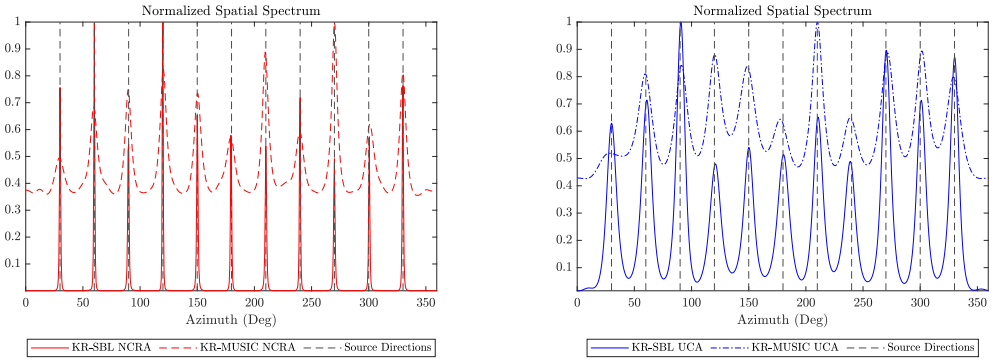

(a) 10 Element NCRA

(b) 10 Element UCA

Figure 5.8: Spatial spectrum of case 3 trials for -5dB SNR.

Figure 5.7 illustrates an 11-source scenario, showing that the 10-element NCRA achieves lower RMSE and CRLB compared to the 10-element UCA with maximum unambiguous radius, as detailed in Tables 4.2 and 4.1. The larger aperture of NCRA significantly enhances its resolution capabilities. Additionally, KR-MUSIC exhibits a noticeable gap from the CRLB for both arrays, while SBL tends to converge closely to the CRLB. Figure 5.8 visualizes the spatial spectrum for this scenario at -5 dB SNR, highlighting the performance differences.

Case 4: RMSE-SNR Performance Comparison of 10-Element NCRA and UCA with 13 Sources in an Underdetermined Scenario

In this scenario, both NCRA and UCA arrays are configured with 10 elements. 13 uncorrelated sources are arranged with a uniform angular spacing of $27°$. Quasi-stationary signals are generated using 30 frames and 100 snapshots. The performance of NCRA and UCA is assessed using the KR-MUSIC and SBL algorithms, with results compared against the Cramér-Rao Lower Bound (CRLB) for a theoretical benchmark. The Signal-to-Noise Ratio (SNR) ranges from -15dB to 15dB, and RMSE values are obtained by performing 500 Monte Carlo iterations at each SNR level.

Table 5.7: Simulation parameters for case 4.

Simulation Parameters	
Number of sensors	10
SNR	-10 to 15dB
Number of sources	13
Angular Separation	27°
Number of frames	30
Number of snapshots per frame	100
Number of iterations	500

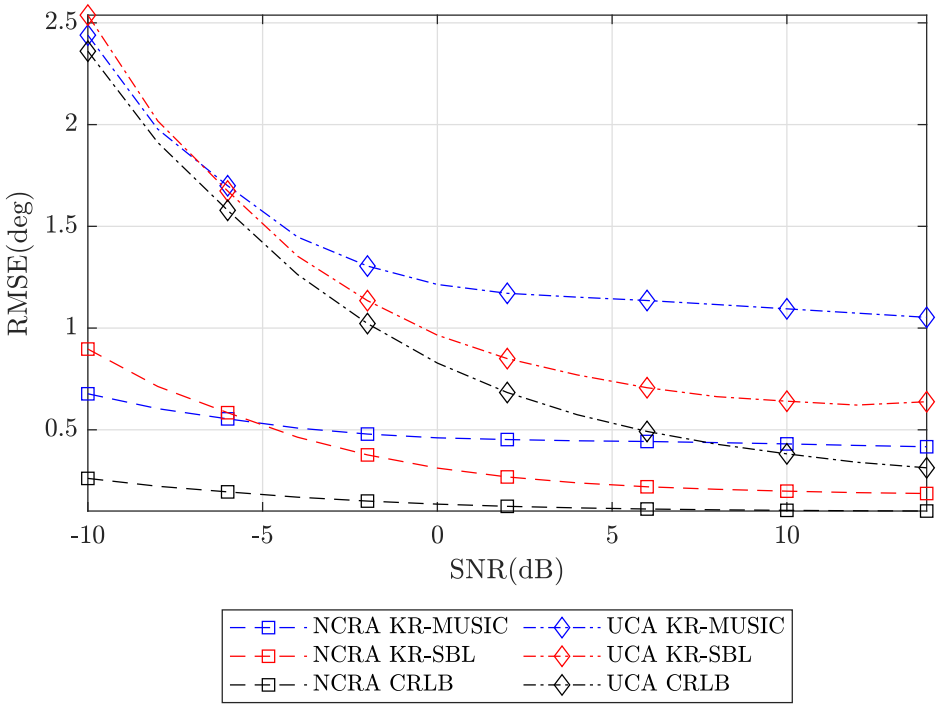

Figure 5.9: 10 Element Arrays, 13 Uncorrelated Sources, 500 MCT

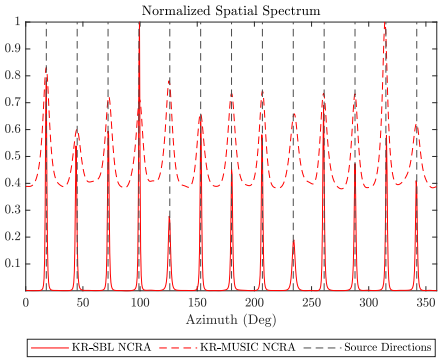

(a) 10 Element NCRA

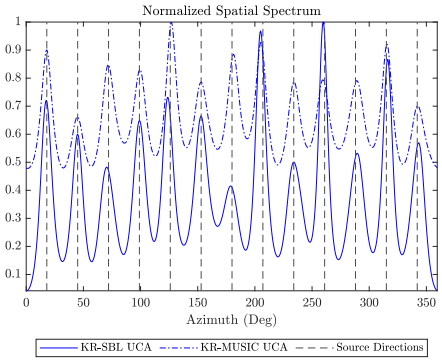

(b) 10 Element UCA

Figure 5.10: Spatial spectrum for case 4 trials for -5dB SNR.

In a 13-source scenario, as depicted in Figure 5.9, the 10-element NCRA demonstrates superior performance with lower RMSE and CRLB compared to the 10-element UCA with maximum unambiguous radius. This is attributed to the larger aperture of NCRA, as explained in Tables 4.2 and 4.1, which significantly enhances its resolution capabilities. Additionally, Figure 5.10 shows the spatial spectrum for this scenario at -5 dB SNR, highlighting the differences in performance between the two arrays. The spatial spectra for NCRA and UCA, shown in Figures 5.10a and 5.10b respectively, further emphasize the improved resolution and detection capabilities of NCRA in this challenging scenario.

5.2.1.2 Coherent Scenario

Case 1: RMSE-SNR Comparison of 10-Element NCRA and UCA with 9 Uncorrelated Sources and 2 Coherent Sources in an Underdetermined Scenario

In this analysis, both NCRA and UCA are configured with 10 elements. The scenario involves nine uncorrelated sources and two coherent sources, all spaced uniformly by 30°. For the generation of quasi-stationary signals, 30 frames and 100 snapshots are used. Given that KR-MUSIC struggles with coherent sources, the SBL algorithm is employed to evaluate the performance of the arrays. The results are benchmarked against the Cramér-Rao Lower Bound (CRLB). The Signal-to-Noise Ratio (SNR) is

adjusted from -15dB to 15dB, with 500 Monte Carlo iterations performed at each SNR level to determine the RMSE.

Table 5.8: Simulation parameters for case 1.

Simulation Parameters	
Number of sensors	10
SNR	-15 to 15dB
Number of sources	11
Number of Coherent Sources	2
Angular Separation	30°
Number of frames	30
Number of snapshots per frame	100
Number of iterations	500

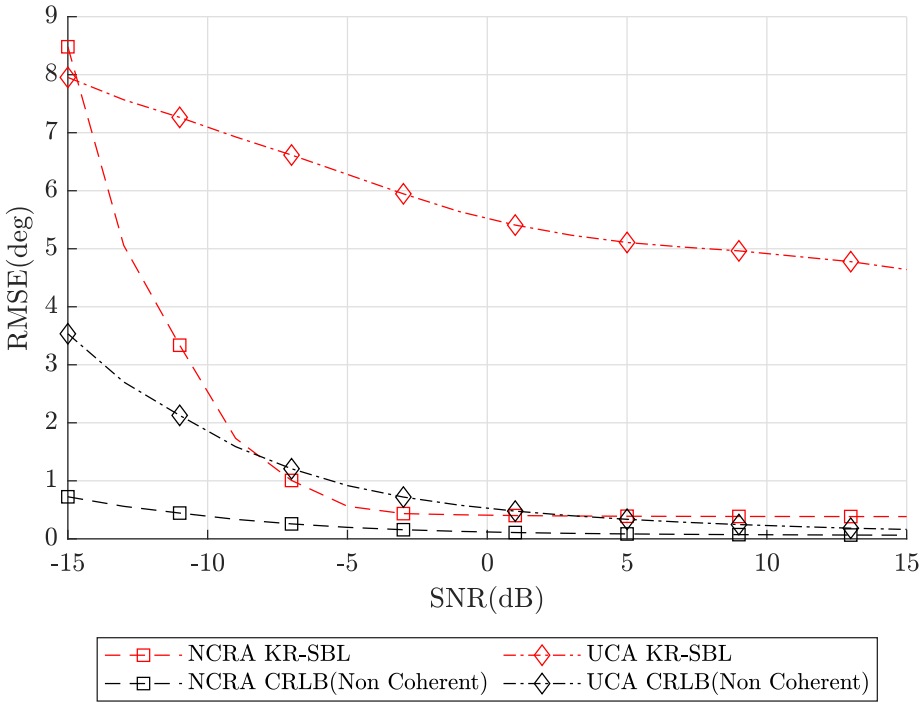

Figure 5.11: 10 element arrays, 9 uncorrelated sources, 2 coherent sources, 500 MCT.

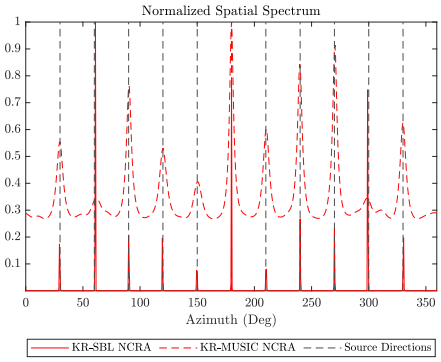

(a) 10 Element NCRA

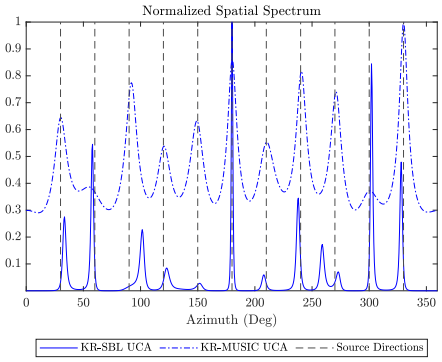

(b) 10 Element UCA

Figure 5.12: Spatial spectrums for case 2 at 5dB SNR.

The simulation results in Figures 5.11 and 5.12 demonstrate the performance of the 10-element NCRA and UCA configurations in an underdetermined DoA estimation scenario with 2 coherent sources. The 10-element NCRA shows superior RMSE and CRLB performance compared to the 10-element UCA, benefiting from its larger aperture and lower sidelobe level which enhances resolution capabilities. Additionally, the spatial spectrum plots in Figures 5.12a and 5.12b illustrate that the NCRA provides more accurate direction estimates, particularly at lower SNR levels.

Case 2: RMSE-SNR Comparison of 10-Element NCRA and UCA with 8 Uncorrelated Sources and 3 Coherent Sources in an Underdetermined Scenario

In this scenario, both NCRA and UCA arrays are configured with 10 elements each. The setup includes 8 uncorrelated sources and 3 coherent sources, all arranged with an angular separation of $30°$. For generating quasi-stationary signals, 30 frames and 100 snapshots per frame are used. Due to the challenges KR-MUSIC faces with coherent sources, the SBL algorithm is employed to compare the performance of NCRA and UCA. The evaluation spans a range of Signal-to-Noise Ratios (SNR) from -15dB to 15dB, with 500 Monte Carlo iterations conducted at each SNR level to compute the resulting spatial spectra and assess the arrays' performance.

Table 5.9: Simulation parameters for case 2.

Simulation Parameters	
Number of sensors	10
SNR	-15 to 15dB
Number of sources	11
Number of coherent sources	3
Angular Separation	30°
Number of frames	30
Number of snapshots per frame	100
Number of iterations	500

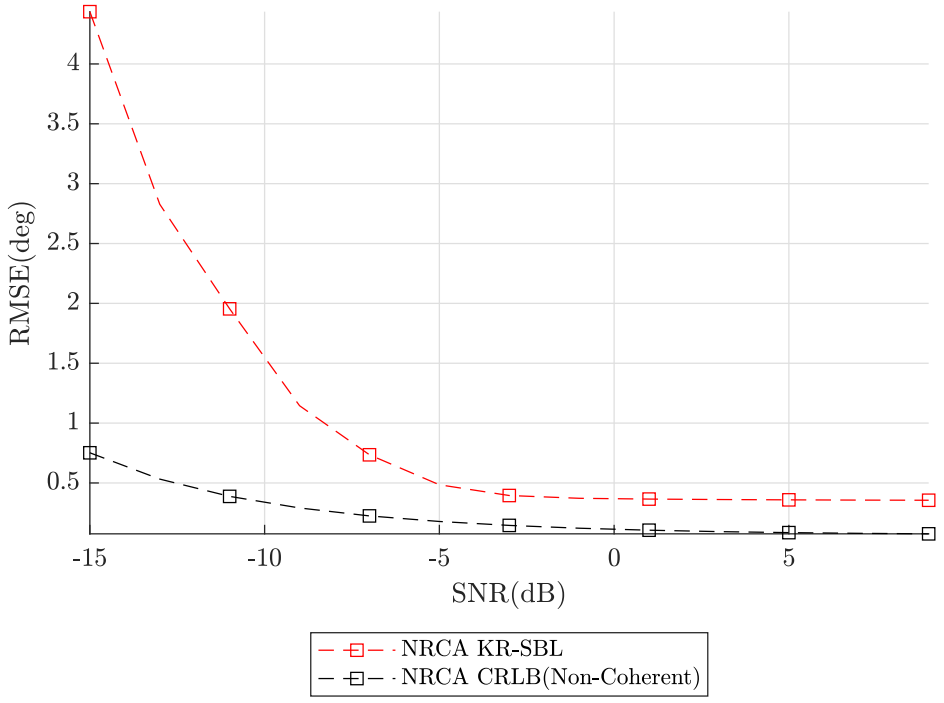

Figure 5.13: 10 element arrays, 8 uncorrelated sources, 3 coherent sources, 500 MCT.

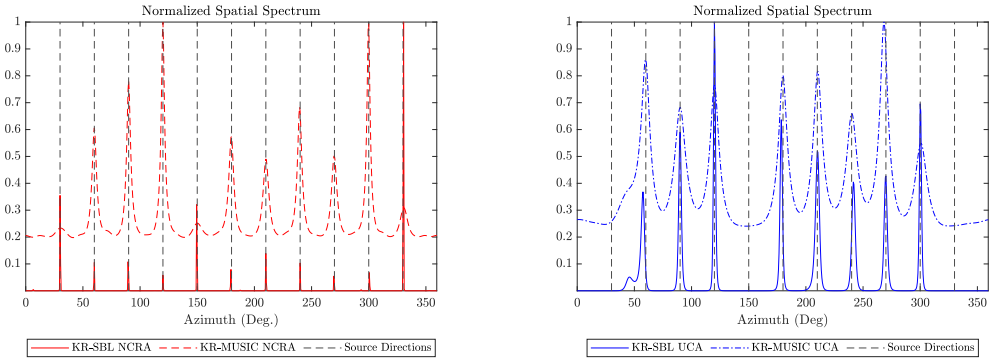

(a) 10 Element NCRA

(b) 10 Element UCA

Figure 5.14: Spatial spectrums for case 2 at 5dB SNR.

As can be seen from Figures 5.13 and 5.14a, the NCRA structure can effectively perform DoA estimation using the SBL algorithm under a scenario involving 3 coherent sources in an underdetermined situation. In contrast, the UCA configuration fails to resolve the coherent sources, as demonstrated in Figure 5.14b. This analysis highlights the critical role of beamwidth and sidelobe levels in the performance of underdetermined DoA estimation. The narrower beamwidth and lower sidelobe levels of the NCRA contribute to its superior performance, enabling it to accurately resolve sources in challenging scenarios where the UCA struggles. These results underscore the importance of array design in underdetermined DoA estimation, with NCRA proving to be a more effective configuration than UCA for scenarios involving coherent sources.

5.2.2 Resolution Probability Simulations

In this section, the resolution probability performance of the proposed NCRA is analyzed and compared with that of a traditional UCA with the same number of elements. The analysis considers varying angular separations between sources to evaluate how effectively NCRA can detect multiple sources in challenging scenarios, emphasizing its advantages over the UCA in terms of resolution capabilities.

Both the SBL and KR-MUSIC algorithms are employed in this analysis to ensure a

comprehensive comparison. The detection criterion used in these simulations requires that all sources must be detected. The resolution probability (P_r) is calculated as follows:

$$P_r = \frac{\text{Number of successful detections}}{\text{Number of trials}} \tag{5.1}$$

Case 1: Resolution Probability Comparison of 7-Element NCRA and UCA with 10 Uncorrelated Sources in an Underdetermined Scenario

This scenario evaluates the resolution probability of 7-element NCRA and UCA configurations with 10 uncorrelated sources in an underdetermined scenario. Both the Sparse Bayesian Learning (SBL) and KR-MUSIC algorithms are applied to compare the effectiveness of NCRA and UCA in resolving multiple sources under challenging conditions. The simulations are conducted at an SNR of 5 dB, with 20 frames and 400 snapshots per frame, and 500 Monte Carlo iterations are performed to ensure the reliability of the results. The goal is to determine how effectively NCRA and UCA can resolve closely spaced sources, with the resolution probability calculated based on the detection of all sources.

Table 5.10: Simulation parameters for case 1.

Simulation Parameters	
Number of sensors	7
SNR	5dB
Number of sources	10
Number of frames	20
Number of snapshots per frame	400
Number of iterations	500

Figure 5.15 illustrates the resolution probability for a 7-element NCRA in an underdetermined (UD) model scenario with 10 non-coherent sources at 5 dB SNR. The simulation is conducted using 400 snapshots over 20 frames. As the angular separation increases, the resolution probability improves, showcasing NCRA's effectiveness

in resolving sources even at lower angular separations compared to UCA. The higher probability of detection at smaller angular separations underscores NCRA's superior performance in challenging scenarios. Additionally, Figure 5.16 corroborates the resolution probability analysis by presenting the spatial spectrums corresponding to the same simulation parameters.

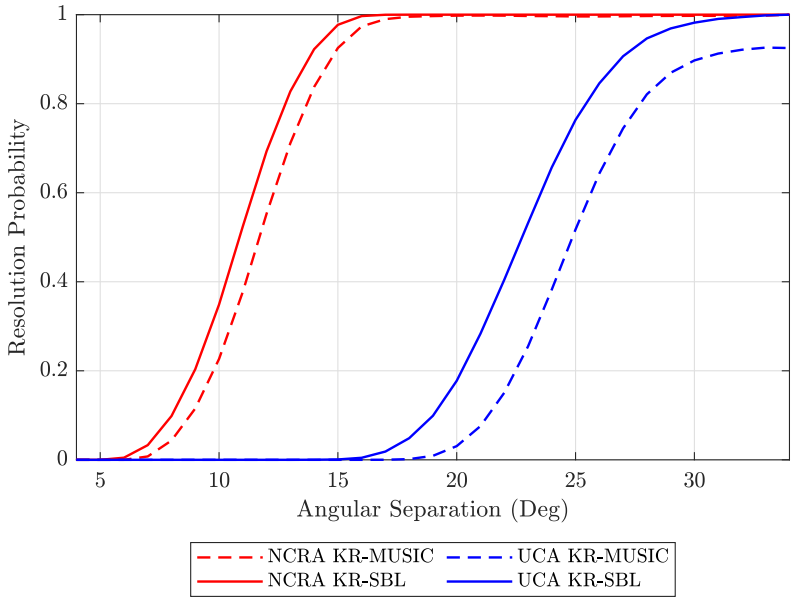

Figure 5.15: 7 Element Arrays, 10 Uncorrelated Sources, 500 MCT.

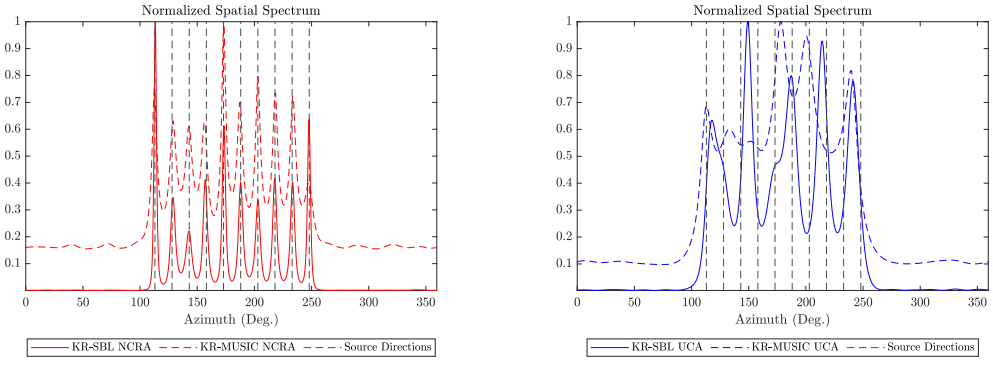

(a) 7 Element NCRA

(b) 7 Element UCA

Figure 5.16: Spatial spectrums for case 1 at 15° angular separation.

Case 2: Resolution Probability Comparison of 10-Element NCRA and UCA with 11 Uncorrelated Sources in an Underdetermined Scenario

In this scenario, the resolution probability of 10-element NCRA and UCA configurations is assessed with 11 uncorrelated sources in an underdetermined scenario. Both Sparse Bayesian Learning (SBL) and KR-MUSIC algorithms are utilized to compare the performance of NCRA and UCA in resolving multiple sources under challenging conditions. The simulations are conducted at an SNR of 0 dB, with 20 frames and 400 snapshots per frame, and 500 Monte Carlo iterations are carried out to ensure robust results. The objective is to evaluate how effectively NCRA and UCA can resolve closely spaced sources, with resolution probability calculated based on the successful detection of all sources.

Table 5.11: Simulation parameters for case 2.

Simulation Parameters	
Number of sensors	10
SNR	0dB
Number of sources	11
Number of frames	20
Number of snapshots per frame	400
Number of iterations	500

Figure 5.17 presents the resolution probability for a 10-element NCRA with a specific configuration $[0, 1, 2, 5]$ in an underdetermined (UD) model scenario with 11 non-coherent sources at 0 dB SNR. The simulation uses 400 snapshots over 20 frames. The plot demonstrates that NCRA maintains a high probability of resolving sources even at low SNR levels. The steep curve in the resolution probability indicates that NCRA excels in resolving closely spaced sources compared to UCA, highlighting its robustness and effectiveness in practical applications. Additionally, Figure 5.18 supports the resolution probability analysis by presenting the spatial spectrums corresponding to the same simulation parameters.

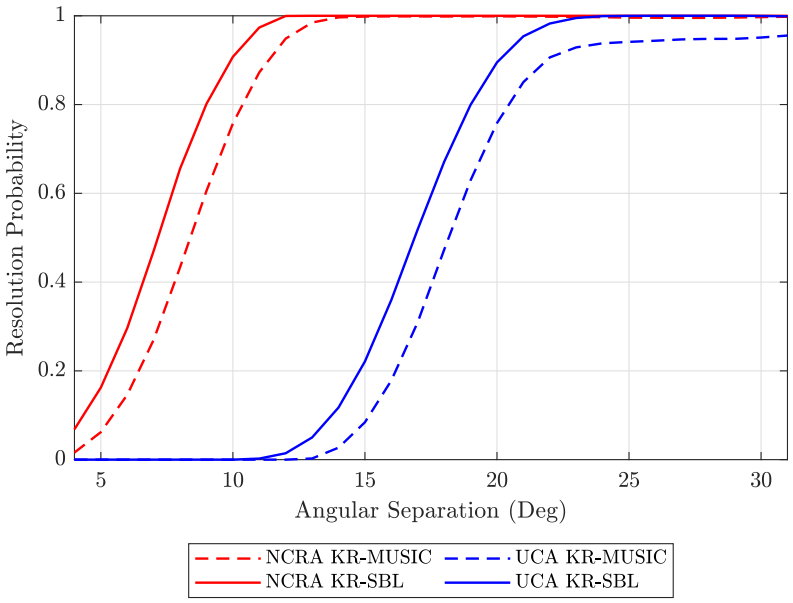

Figure 5.17: 10 Element Arrays, 11 Uncorrelated Sources, 500 MCT.

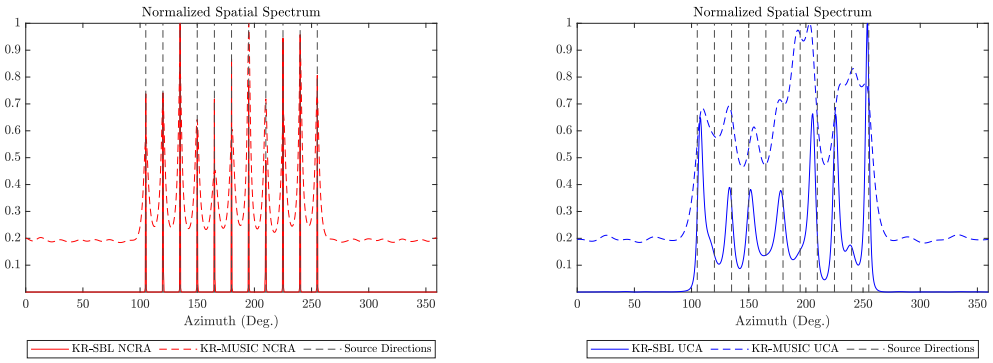

(a) 10 Element NCRA

(b) 10 Element UCA

Figure 5.18: Spatial spectrums for case 2 at 15° angular separation.

These figures collectively demonstrate that NCRA significantly enhances the resolution probability for multiple sources under various conditions, outperforming traditional UCA configurations.

CHAPTER 6

CONCLUSIONS

This thesis addresses the complex challenge of Direction of Arrival (DoA) estimation in underdetermined scenarios, where the number of source signals exceeds the number of sensors in the array. While various signal models, algorithms, and array configurations have been proposed for underdetermined DoA estimation, this study emphasizes the often-overlooked effects of beamwidth and sidelobe levels in such scenarios.

Additionally, the thesis introduces a novel planar array structure that uniquely combines the advantages of sparsity and circular symmetry, offering a solution to the limitations of traditional array configurations. Common array geometries, such as Uniform Circular Arrays (UCA) and Uniform Linear Arrays (ULA), are widely used in array processing but have inherent limitations when applied to underdetermined DoA estimation. These traditional arrays often suffer from broader beamwidths and higher sidelobe levels, which can significantly hinder their ability to accurately estimate the directions of multiple sources, particularly in environments with closely spaced or coherent signals.

To overcome these challenges, this thesis proposes the Nested Circular Ring Arrays (NCRA) as a novel solution. The NCRA structure integrates the principles of sparsity—exemplified by configurations like nested and co-prime arrays—with the benefits of circular symmetry, which ensures uniform performance across all azimuth angles. This approach results in a larger effective aperture, leading to narrower beamwidths and reduced sidelobe levels compared to traditional UCAs. Consequently, NCRA enhances the array's resolution capabilities and improves the accuracy of DoA estimation in underdetermined scenarios.

Extensive simulations presented in this thesis demonstrate that the proposed NCRA structure offers significant improvements over traditional arrays. Specifically, the results show that NCRA, when used with advanced algorithms like Sparse Bayesian Learning (SBL), provides superior performance in terms of Root Mean Square Error (RMSE) and Cramér-Rao Lower Bound (CRLB), particularly in scenarios where the number of sources exceeds the number of sensors. The robustness of SBL in handling coherent sources further underscores the effectiveness of the proposed approach.

In conclusion, this thesis advances the field of DoA estimation in underdetermined scenarios by addressing the critical issues of beamwidth and sidelobe effects, proposing a new array structure, and demonstrating its practical benefits through rigorous analysis and simulation. The Nested Circular Ring Arrays (NCRA) offer a promising solution for high-resolution DoA estimation in complex environments.

For future work, developing a fast DoA algorithm that eliminates the need for grid searches when using NCRA could significantly enhance its practical utility. While the grid-based approach in the SBL algorithm is effective, increasing the grid size to improve accuracy leads to higher computational costs. To address this, applying off-grid methodologies—previously developed for specific array geometries like ULA—to NCRA could allow for more accurate DoA estimation without the need to increase grid density. This approach would leverage the benefits of off-grid techniques to maintain computational efficiency while improving accuracy, making the system more effective in real-world applications.

REFERENCES

[1] P. Pal and P. P. Vaidyanathan, "Nested arrays: A novel approach to array processing with enhanced degrees of freedom," *IEEE Transactions on Signal Processing*, vol. 58, no. 8, pp. 4167–4181, 2010.

[2] T. Tuncer and B. Friedlander, *Classical and Modern Direction-of-Arrival Estimation*. 07 2009.

[3] H. Van Trees, *Optimum Array Processing*. Wiley-Interscience, 2001.

[4] R. Schmidt, "Multiple emitter location and signal parameter estimation," *IEEE Transactions on Antennas and Propagation*, vol. 34, no. 3, pp. 276–280, 1986.

[5] R. Roy and T. Kailath, "Esprit-estimation of signal parameters via rotational invariance techniques," *IEEE Transactions on Acoustics, Speech, and Signal Processing*, vol. 37, no. 7, pp. 984–995, 1989.

[6] M. E. Tipping, "Sparse bayesian learning and the relevance vector machine," *J. Mach. Learn. Res.*, vol. 1, p. 211–244, sep 2001.

[7] J. Dai, X. Bao, W. Xu, and C. Chang, "Root sparse bayesian learning for off-grid doa estimation," *IEEE Signal Processing Letters*, vol. 24, no. 1, pp. 46–50, 2017.

[8] P. Gerstoft, C. Mecklenbräuker, and A. Xenaki, "Multi snapshot sparse bayesian learning for doa estimation," 02 2016.

[9] M. Emadi, E. Miandji, and J. Unger, "Omp-based doa estimation performance analysis," *Digital Signal Processing*, vol. 79, pp. 57–65, 2018.

[10] A. Panahi and M. Viberg, "On the resolution of the lasso-based doa estimation method," in *2011 International ITG Workshop on Smart Antennas*, pp. 1–5, 2011.

[11] S. Ji, Y. Xue, and L. Carin, "Bayesian compressive sensing," *IEEE Transactions on Signal Processing*, vol. 56, no. 6, pp. 2346–2356, 2008.

[12] H. Wang, X. Wang, M. Huang, and L. Wan, "Off-grid doa estimation with unknown nonuniform noise via covariance sbl strategy," in *2020 IEEE International Conference on Computational Electromagnetics (ICCEM)*, pp. 187–189, 2020.

[13] S. Pillai and B. Kwon, "Forward/backward spatial smoothing techniques for coherent signal identification," *IEEE Transactions on Acoustics, Speech, and Signal Processing*, vol. 37, no. 1, pp. 8–15, 1989.

[14] A. Fengler, S. Haghighatshoar, P. Jung, and G. Caire, "Non-bayesian activity detection, large-scale fading coefficient estimation, and unsourced random access with a massive mimo receiver," *IEEE Transactions on Information Theory*, vol. 67, no. 5, pp. 2925–2951, 2021.

[15] S. Haghighatshoar, P. Jung, and G. Caire, "Improved scaling law for activity detection in massive mimo systems," in *2018 IEEE International Symposium on Information Theory (ISIT)*, pp. 381–385, 2018.

[16] S. Haghighatshoar, P. Jung, and G. Caire, "A new scaling law for activity detection in massive mimo systems," 2018.

[17] M. Wang and A. Nehorai, "Coarrays, music, and the cramér–rao bound," *IEEE Transactions on Signal Processing*, vol. 65, no. 4, pp. 933–946, 2017.

[18] D. Linebarger, I. Sudborough, and I. Tollis, "Difference bases and sparse sensor arrays," *IEEE Transactions on Information Theory*, vol. 39, no. 2, pp. 716–721, 1993.

[19] C.-L. Liu and P. P. Vaidyanathan, "Remarks on the spatial smoothing step in coarray music," *IEEE Signal Processing Letters*, vol. 22, no. 9, pp. 1438–1442, 2015.

[20] R. Hoctor and S. Kassam, "The unifying role of the coarray in aperture synthesis for coherent and incoherent imaging," *Proceedings of the IEEE*, vol. 78, no. 4, pp. 735–752, 1990.

[21] W.-K. Ma, T.-H. Hsieh, and C.-Y. Chi, "Doa estimation of quasi-stationary signals with less sensors than sources and unknown spatial noise covariance: A khatri–rao subspace approach," *IEEE Transactions on Signal Processing*, vol. 58, no. 4, pp. 2168–2180, 2010.

[22] W.-K. Ma, T.-H. Hsieh, and C.-Y. Chi, "Doa estimation of quasi-stationary signals via khatri-rao subspace," in *2009 IEEE International Conference on Acoustics, Speech and Signal Processing*, pp. 2165–2168, 2009.

[23] J. Li and X. Zhang, "Direction of arrival estimation of quasi-stationary signals using unfolded coprime array," *IEEE Access*, vol. 5, pp. 6538–6545, 2017.

[24] N. Hu, B. Sun, Y. Zhang, J. Dai, J. Wang, and C. Chang, "Underdetermined doa estimation method for wideband signals using joint nonnegative sparse bayesian learning," *IEEE Signal Processing Letters*, vol. 24, no. 5, pp. 535–539, 2017.

[25] A. Al Hilli, L. Najafizadeh, and A. Petropulu, "Weighted sparse bayesian learning (wsbl) for basis selection in linear underdetermined systems," *IEEE Transactions on Vehicular Technology*, vol. 68, no. 8, pp. 7353–7367, 2019.

[26] P. Gupta and M. Agrawal, "Doa estimation of non-circular signals using fourth order cumulant in underdetermined cases," in *2018 IEEE International Workshop on Signal Processing Systems (SiPS)*, pp. 25–30, 2018.

[27] M. Guo, T. Chen, and B. Wang, "An improved doa estimation approach using coarray interpolation and matrix denoising," *Sensors*, vol. 17, no. 5, 2017.

[28] C. Zhou, Y. Gu, Y. D. Zhang, and Z. Shi, *Sparse Array Interpolation for Direction-of-Arrival Estimation*, pp. 41–74. 2024.

[29] T. Mahmud, Z. Ye, K. Shabir, R. Zheng, and M. Islam, "Off-grid doa estimation aiding virtual extension of coprime arrays exploiting fourth order difference coarray with interpolation," *IEEE Access*, vol. 6, pp. 1–1, 08 2018.

[30] P. Pal and P. P. Vaidyanathan, "Coprime sampling and the music algorithm," in *2011 Digital Signal Processing and Signal Processing Education Meeting (DSP/SPE)*, pp. 289–294, 2011.

[31] P. P. Vaidyanathan and P. Pal, "Sparse sensing with coprime arrays," in *2010 Conference Record of the Forty Fourth Asilomar Conference on Signals, Systems and Computers*, pp. 1405–1409, 2010.

[32] S. Wandale, T. Basikolo, and K. Ichige, "Super nested sparse circular array for high resolution doa estimation," in *2019 IEEE International Symposium on Circuits and Systems (ISCAS)*, pp. 1–5, 2019.

[33] A. Koochakzadeh and P. Pal, "Cramér–rao bounds for underdetermined source localization," *IEEE Signal Processing Letters*, vol. 23, no. 7, pp. 919–923, 2016.

[34] P. Stoica, E. Larsson, and A. Gershman, "The stochastic crb for array processing: a textbook derivation," *IEEE Signal Processing Letters*, vol. 8, no. 5, pp. 148–150, 2001.

[35] P. Stoica and A. Nehorai, "Performance study of conditional and unconditional direction-of-arrival estimation," *IEEE Transactions on Acoustics, Speech, and Signal Processing*, vol. 38, no. 10, pp. 1783–1795, 1990.

[36] B. Rao and K. Hari, "Performance analysis of root-music," *IEEE Transactions on Acoustics, Speech, and Signal Processing*, vol. 37, no. 12, pp. 1939–1949, 1989.

[37] H. Wang, X. Wang, M. Huang, and L. Wan, "A novel variational sbl approach for off-grid doa detection under nonuniform noise," *Digital Signal Processing*, vol. 128, p. 103622, 2022.

[38] S. Smith, "Covariance, subspace, and intrinsic crame/spl acute/r-rao bounds," *IEEE Transactions on Signal Processing*, vol. 53, no. 5, pp. 1610–1630, 2005.

[39] J. Sherman and W. J. Morrison, "Adjustment of an inverse matrix corresponding to a change in one element of a given matrix," *The Annals of Mathematical Statistics*, vol. 21, no. 1, pp. 124–127, 1950.

[40] F. Asano, S. Hayamizu, T. Yamada, and S. Nakamura, "Speech enhancement based on the subspace method," *IEEE Transactions on Speech and Audio Processing*, vol. 8, no. 5, pp. 497–507, 2000.

[41] L. Rankine, N. Stevenson, M. Mesbah, and B. Boashash, "A nonstationary model of newborn eeg," *IEEE Transactions on Biomedical Engineering*, vol. 54, no. 1, pp. 19–28, 2007.

[42] C. Kwan, K. Ho, G. Mei, Y. Li, Z. Ren, R. Xu, Y. Zhang, D. Lao, M. Stevenson, V. Stanford, and C. Rochet, "An automated acoustic system to monitor and classify birds," *EURASIP Journal on Applied Signal Processing*, vol. 2006, pp. 52–52, 12 2006.

[43] J. Li, F. Wang, and D. Jiang, "Direction of arrival estimation using sum co-array of coprime arrays," in *2017 International Applied Computational Electromagnetics Society Symposium (ACES)*, pp. 1–2, 2017.

[44] A. M. Elbir, "Coprime arrays with enhanced degrees of freedom," *Anadolu University Journal of Science and Technology A - Applied Sciences and Engineering*, vol. 19, no. 2, p. 235–241, 2018.

[45] M.-Y. Cao, L. Huang, C. Qian, J.-Y. Xue, and H. So, "Underdetermined doa estimation of quasi-stationary signals via khatri–rao structure for uniform circular array," *Signal Processing*, vol. 106, pp. 41–48, 2015.

[46] Y. Liang, W. Liu, Q. Shen, W. Cui, and S. Wu, "On the cramér-rao bound and the number of resolvable sources in the presence of nonuniform noise for underdetermined doa estimation," in *2020 15th IEEE International Conference on Signal Processing (ICSP)*, vol. 1, pp. 93–98, 2020.

[47] T. Basikolo, K. Ichige, and H. Arai, "A note on crlb formulation for underdetermined doa estimation in circularly configured planar arrays," *IEICE Electronics Express*, vol. 15, 03 2018.

[48] Z.-Q. He, Z.-P. Shi, and L. Huang, "Covariance sparsity-aware doa estimation for nonuniform noise," *Digital Signal Processing*, vol. 28, pp. 75–81, 2014.

[49] U. Baysal and R. Moses, "On the geometry of isotropic arrays," *IEEE Transactions on Signal Processing*, vol. 51, no. 6, pp. 1469–1478, 2003.

[50] F. Keskin and T. Filik, "An optimum volumetric array design approach for both azimuth and elevation isotropic doa estimation," *IEEE Access*, vol. 8, pp. 183903 – 183912, 10 2020.

[51] I. Peshkov and Y. Nechaev, “Estimation and minimization of the cramer-rao lower bound for radio direction-finding on the azimuth and elevation of planar antenna arrays,” *Journal of Communications Software and Systems*, vol. 15, 11 2019.

[52] H. Tang, Z. Nie, and X. Zong, “Approximate calculation of hpbw for uniform circular array,” in *2018 Cross Strait Quad-Regional Radio Science and Wireless Technology Conference (CSQRWC)*, pp. 1–3, 2018.

APPENDIX A

CRAMÉR-RAO LOWER BOUND FOR OVERDETERMINED DOA ESTIMATION

Assume an array of M elements receives signals emitted from K far-field narrowband sources, where $K < M$, coming from directions $\{\phi_1, \ldots, \phi_K\}$. In this scenario, the array output matrix is given by:

$$\mathbf{Y} = \mathbf{AS} + \mathbf{N} \tag{A.1}$$

where

$$\mathbf{Y} = [\mathbf{y}(1) \ \ldots \ \mathbf{y}(N)] \in \mathbb{C}^{M \times N},$$

$$\mathbf{A} = [\mathbf{a}(\phi_1) \ \ldots \ \mathbf{a}(\phi_K)] \in \mathbb{C}^{M \times K},$$

$$\mathbf{S} = [\mathbf{s}_1 \ \ldots \ \mathbf{s}_K]^T \in \mathbb{C}^{K \times N},$$

$$\mathbf{s}_j = [s_j(1) \ s_j(2) \ \ldots \ s_j(N)] \in \mathbb{C}^{1 \times N},$$

$$\mathbf{N} = [\mathbf{n}(1) \ \mathbf{n}(2) \ \ldots \ \mathbf{n}(N)] \in \mathbb{C}^{M \times N}$$

are the array output matrix, array manifold containing steering vectors, source signal matrix, and AWGN, respectively.

Under the assumptions that the noise is spatially and temporally white, and the sources are uncorrelated, the array output covariance matrix is given by:

$$\mathbf{R}_Y = \mathbb{E}[\mathbf{Y}\mathbf{Y}^H] = \mathbf{A}\mathbf{R}_S\mathbf{A}^H + \sigma^2\mathbf{I}_M \tag{A.2}$$

where $\mathbf{R}_Y$ is the array output covariance matrix, $\mathbf{R}_S = \mathbb{E}[\mathbf{S}\mathbf{S}^H]$ is the source signal covariance matrix, σ^2 is the noise variance, and $\mathbf{I}_M$ is the $M \times M$ identity matrix.

Let $\boldsymbol{\alpha} = [\boldsymbol{\phi}^T \ \mathbf{p}^T \ \sigma^2]^T$ be the unknown parameter vector, where $\boldsymbol{\phi} = [\phi_1, \ldots, \phi_K]^T$, $\mathbf{p}$ contains the diagonal and upper elements of $\mathbf{R}_S$ and σ^2 is the noise variance. Following the derivations given in [3], [34], or [35], the (k, l)-th element of the Fisher Information Matrix (FIM) for the unknown parameter vector $\boldsymbol{\alpha}$ is:

$$\text{FIM}_{k,l} = N\text{tr}\left(\frac{d\mathbf{R}_Y}{d\alpha_k}\mathbf{R}_Y^{-1}\frac{d\mathbf{R}_Y}{d\alpha_l}\mathbf{R}_Y^{-1}\right) \quad \text{for } k, l \in \{1, \ldots, K + K^2 + 1\} \tag{A.3}$$

where $\text{tr}(\cdot)$ denotes the trace operation. Since the Cramér-Rao Lower Bound (CRLB) is $\text{CRLB} = \text{FIM}^{-1}$, and we are interested in $\boldsymbol{\phi}$, denoted as $\text{CRLB}(\boldsymbol{\phi})$, it is calculated as:

$$\text{CRLB}(\boldsymbol{\phi}) = \frac{\sigma^2}{2N}\left\{\text{Re}(\mathbf{D}^H\boldsymbol{\Pi}_{\mathbf{A}}^{\perp}\mathbf{D}) \circ \left(\mathbf{R}_S\mathbf{A}^H\mathbf{R}_Y^{-1}\mathbf{A}\mathbf{R}_S\right)^T\right\}^{-1} \tag{A.4}$$

where

$$\begin{aligned}
\circ &= \text{Hadamard-Schur Product}, \\
\mathbf{D} &= \left[\frac{d\mathbf{a}(\phi_1)}{d\phi_1} \ \cdots \ \frac{d\mathbf{a}(\phi_K)}{d\phi_K}\right], \\
\boldsymbol{\Pi}_{\mathbf{A}}^{\perp} &= \mathbf{I} - \boldsymbol{\Pi}_{\mathbf{A}}, \\
\boldsymbol{\Pi}_{\mathbf{A}} &= \mathbf{A}(\mathbf{A}^H\mathbf{A})^{-1}\mathbf{A}^H.
\end{aligned}$$

APPENDIX B

CRAMÉR-RAO LOWER BOUND FOR UNDERDETERMINED DOA ESTIMATION

Since the number of sources can exceed the number of sensors for underdetermined DoA estimation, the CRLB formulation in (A.4) cannot be applied directly. The derivation of the CRLB for underdetermined DoA estimation is explained by several sources [17, 33, 48, 47, 46]. The unknown parameter vector $\boldsymbol{\alpha}$ can be given as follows:

$$\boldsymbol{\alpha} = [\phi_1, \ldots, \phi_K, p_1, \ldots, p_K, \sigma^2]^T \tag{B.1}$$

Following the derivations given in [3], [34], and [35], the (k, l)-th element of the Fisher Information Matrix (FIM) for the unknown parameter vector $\boldsymbol{\alpha}$ is given by the following equation, which is the same as (A.3):

$$\text{FIM}_{k,l} = N\text{tr}\left(\frac{d\mathbf{R}_Y}{d\alpha_k}\mathbf{R}_Y^{-1}\frac{d\mathbf{R}_Y}{d\alpha_l}\mathbf{R}_Y^{-1}\right) \tag{B.2}$$

where N is the number of snapshots. The underdetermined DoA estimation signal model is given by the following equation:

$$\mathbf{r} = \mathbf{A}_d\mathbf{p} + \sigma^2\mathbf{i} \tag{B.3}$$

$$\mathbf{r} = \text{vec}(\mathbf{R}_Y),$$

$$\mathbf{A}_d = \mathbf{A}^* \odot \mathbf{A} = \text{vec}(\mathbf{A}\mathbf{A}^H),$$

$$\mathbf{p} = \text{diag}(\mathbf{R}_S),$$

where $\odot$ denotes the Khatri-Rao product, and $\mathbf{i} = \text{vec}(\mathbf{I})$.

Since $\text{tr}(\mathbf{AB}) = \text{vec}(\mathbf{A}^T)^T\text{vec}(\mathbf{B})$ and $(\mathbf{AXB}) = (\mathbf{B}^T \otimes \mathbf{A})\text{vec}(\mathbf{X})$, where $\otimes$ is the Kronecker product, (B.2) can be rewritten as:

$$\text{FIM}_{k,l} = N \left(\frac{d\mathbf{r}}{d\alpha_k} \right)^H (\mathbf{R}_Y^T \otimes \mathbf{R}_Y) \frac{d\mathbf{r}}{d\alpha_l} \tag{B.4}$$

The derivatives in (B.4) are placed as follows:

$$\frac{d\mathbf{r}}{d\boldsymbol{\alpha}} = \left[\frac{d\mathbf{r}}{d\phi_1} \ \cdots \ \frac{d\mathbf{r}}{d\phi_K} \ \frac{d\mathbf{r}}{dp_1} \ \cdots \ \frac{d\mathbf{r}}{dp_K} \ \frac{d\mathbf{r}}{d\sigma^2} \right] \tag{B.5}$$

$$\frac{d\mathbf{r}}{d\boldsymbol{\alpha}} = \left[\dot{\mathbf{A}}_d \mathbf{R}_S \ \ \mathbf{A}_d \ \ \mathbf{i} \right] \tag{B.6}$$

$$\dot{\mathbf{A}}_d = \dot{\mathbf{A}}^* \odot \mathbf{A} + \mathbf{A}^* \odot \dot{\mathbf{A}} = \text{vec}(\mathbf{A}\dot{\mathbf{A}}^H + \dot{\mathbf{A}}\mathbf{A}^H),$$

$$\dot{\mathbf{A}} = \left[\frac{d\mathbf{a}(\phi_1)}{d\phi_1} \ \cdots \ \frac{d\mathbf{a}(\phi_K)}{d\phi_K} \right]$$

$$\text{FIM} = \left(\frac{d\mathbf{r}}{d\boldsymbol{\alpha}} \right)^H (\mathbf{R}_Y^T \otimes \mathbf{R}_Y) \frac{d\mathbf{r}}{d\boldsymbol{\alpha}} \tag{B.7}$$

(B.6) can be divided into two parts which are DoAs and powers of noise and sources:

$$\begin{aligned} \mathbf{M}_{\boldsymbol{\phi}} &= (\mathbf{R}_Y^T \otimes \mathbf{R}_Y)^{-1/2} \dot{\mathbf{A}}_d \mathbf{R}_S, \\ \mathbf{M}_{\mathbf{s}} &= (\mathbf{R}_Y^T \otimes \mathbf{R}_Y)^{-1/2} \left[\mathbf{A}_d \ \mathbf{i} \right] \end{aligned} \tag{B.8}$$

where $\otimes$ is the Kronecker product. Using the partition given by (B.8), (B.7) can be rewritten as follows:

$$\text{FIM} = N \begin{bmatrix} \mathbf{M}_{\boldsymbol{\phi}}^H \mathbf{M}_{\boldsymbol{\phi}} & \mathbf{M}_{\boldsymbol{\phi}}^H \mathbf{M}_{\mathbf{s}} \\ \mathbf{M}_{\mathbf{s}}^H \mathbf{M}_{\boldsymbol{\phi}} & \mathbf{M}_{\mathbf{s}}^H \mathbf{M}_{\mathbf{s}} \end{bmatrix} \tag{B.9}$$

And the CRLB can be found by the following equation:

$$\text{CRLB}(\phi) = \frac{1}{N} \left(\mathbf{M}_{\boldsymbol{\phi}}^H \Pi_{\mathbf{M}_{\mathbf{s}}}^{\perp} \mathbf{M}_{\boldsymbol{\phi}} \right)^{-1} \tag{B.10}$$

$$\Pi_{\mathbf{M}_{\mathbf{s}}}^{\perp} = \mathbf{I} - \mathbf{M}_{\mathbf{s}} \left(\mathbf{M}_{\mathbf{s}}^H \mathbf{M}_{\mathbf{s}} \right)^{-1} \mathbf{M}_{\mathbf{s}}^H$$

APPENDIX C

DEGREES OF FREEDOM IN THE DIFFERENCE CO-ARRAY OF UNIFORM CIRCULAR ARRAYS

Number of distinct virtual elements of the Difference Co-Array of UCA is proven by [45]. Assume an M-element uniform circular array with the steering vector $\mathbf{a}(\phi)$. Its co-array steering vector is defined as:

$$\begin{aligned}\mathbf{a}_d(\phi) &= \mathbf{a}^*(\phi) \otimes \mathbf{a}(\phi) = \text{vec}(\mathbf{a}(\phi)\mathbf{a}^H(\phi)) \\ &= \begin{bmatrix} e^{-j(2\pi r/\lambda)cos(\phi-\psi_1)} \\ \vdots \\ e^{-j(2\pi r/\lambda)cos(\phi-\psi_M)} \end{bmatrix} \otimes \begin{bmatrix} e^{j(2\pi r/\lambda)cos(\phi-\psi_1)} \\ \vdots \\ e^{j(2\pi r/\lambda)cos(\phi-\psi_M)} \end{bmatrix} \\ &= \begin{bmatrix} \mathbf{a}_d^{11}(\phi) \\ \vdots \\ \mathbf{a}_d^{kl}(\phi) \\ \vdots \\ \mathbf{a}_d^{MM}(\phi) \end{bmatrix}\end{aligned} \tag{C.1}$$

$$\begin{aligned}\mathbf{a}_d^{kl}(\phi) &= e^{j(2\pi r/\lambda)(cos(\phi-\psi_k)-cos(\phi-\psi_l))} \\ &= e^{j(4\pi r/\lambda)sin((\psi_l-\psi_k)/2)sin(\phi-(\psi_l+\psi_k)/2)} \\ &= e^{jz_{kl}sin(\beta_{kl})}\end{aligned} \tag{C.2}$$

where $\psi_k = \frac{2\pi k}{M}$, $z_{kl} = (4\pi r/\lambda)sin((\psi_l - \psi_l)/2)$, $\beta_{kl} = \phi - (\psi_l + \psi_k)/2$ and $\eta_{kl} = (\psi_l + \psi_k)/2$. $\mathbf{a}_d^{kl}(\phi)$ can be rewritten as following using the Jacobi-Anger expansion:

$$\begin{aligned}\mathbf{a}_d^{kl}(\phi) &= \sum_{h=\infty}^{\infty} \mathbf{J}_h(z_{kl}) e^{jh\beta_{kl}} \\ &= \sum_{h=\infty}^{\infty} \mathbf{J}_h(z_{kl}) e^{-jh\eta_{jl}} e^{jh\phi}\end{aligned} \tag{C.3}$$

The number of distinct elements of $\mathbf{a}_d(\phi)$ defines the Degrees of Freedom (DOF) of the Difference Co-array. Distinct elements must satisfy the following statement:

$$a_d^{i_1}(\phi) \neq a_d^{i_2}(\phi) \tag{C.4}$$

where $a_d^{i_1}(\phi)$ defines the i_1^{th} element of $\mathbf{a}_d(\phi)$, and $i_1, i_2 \in \{1, 2, \ldots, M^2\}$. The coefficients of h^{th} modes of $a_d^{i_1}(\phi)$ and $a_d^{i_2}(\phi)$ can be calculated by (C.3) as follows:

$$\frac{1}{2\pi} \int_0^{2\pi} a_d^{i_1}(\phi) e^{jh\phi}\, d\phi = \mathbf{J}_h(z_{i_1}) e^{-j\eta_{i_1}} \tag{C.5}$$

$$\frac{1}{2\pi} \int_0^{2\pi} a_d^{i_2}(\phi) e^{jh\phi}\, d\phi = \mathbf{J}_h(z_{i_2}) e^{-j\eta_{i_2}} \tag{C.6}$$

The equivalent expression of (C.4) is obtained by substituting (C.4) into (C.5) and (C.6) as:

$$\mathbf{J}_h(z_{i_1}) e^{-j\eta_{i_1}} = \mathbf{J}_h(z_{i_2}) e^{-j\eta_{i_2}}, \;\; i_1 \neq i_2 \tag{C.7}$$

where $h = -\infty, \ldots, \infty$. Recall that $\mathbf{J}_h(z) \in \mathbb{R}$, $\mathbf{J}_h(zi_2)/\mathbf{J}_h(zi_1) = e^{-jh(\eta_{i_1} - \eta_{i_2})}$ is a real number with an absolute value of 1. Depending on the value of z, there are two scenarios:

Scenario 1: $z \neq 0$**.** This leads to two possible outcomes:

$$\mathbf{J}_h(z_{i_1}) = \mathbf{J}_h(z_{i_2}) \tag{C.8}$$

$$\mathbf{J}_h(z_{i_1}) = -\mathbf{J}_h(z_{i_2}) \tag{C.9}$$

First consider the $\mathbf{J}_h(z_{i_1}) = \mathbf{J}_h(z_{i_2})$. With respect to definitions of z and η in (C.2) we get:

$$\begin{cases} \sin\left(\frac{\psi l_{i_1} - \psi k_{i_1}}{2}\right) = \sin\left(\frac{\psi l_{i_2} - \psi k_{i_2}}{2}\right) \\ \frac{\psi k_{i_1} + \psi l_{i_1}}{2} = \frac{\psi k_{i_2} + \psi l_{i_2}}{2} \end{cases} \tag{C.10}$$

Reorganizing (C.10) and following the derivations given [45] we get following expression:

$$\begin{cases} k_{i_1} = \frac{M}{2} + l_{i_2}, \quad 1 \leq l_{i_2}, k_{i_1} \leq M \\ l_{i_1} = \frac{M}{2} + k_{i_2}, \quad 1 \leq l_{i_1}, k_{i_2} \leq M \end{cases} \tag{C.11}$$

The solutions of k_{i_1} are $\{l_{i_2}, k_{i_1}\} = \{1, (M/2)+1\}, \ldots, \{(M/2), M\}$ and the solutions of l_{i_1} are $\{l_{i_1}, k_{i_2}\} = \{1, (M/2)+1\}, \ldots, \{(M/2), M\}$ and there are $M^2/4$ total solutions; after extracting solutions also lead to $z = 0$ which are $M/2$, we get $M^2/4 - M/2$ solutions.

Scenario 2: $z = 0$**.** This leads to $k = l$ and there are $M - 1$ non-unique elements.

The cases given above are related to the parity of M, which is the number of physical sensors in the array. The number of virtual sensors is determined as follows:

1. If M is even, the total number of virtual sensors is given by:

$$M^2 - \left(\frac{M^2}{4} - \frac{M}{2}\right) - \left(\frac{M^2}{4} - \frac{M}{2}\right) - (M-1) = \frac{M^2}{2} + 1 \tag{C.12}$$

2. If M is odd, Case 1 does not apply. Therefore, the total number of virtual sensors is:

$$M^2 - M + 1 \tag{C.13}$$

APPENDIX D

KHATRI-RAO PRODUCT AND DIFFERENCE CO-ARRAY RELATION

Assume a sensor array of M elements with element positions of $\{\mathbf{p}_1, \mathbf{p}_2, \ldots, \mathbf{p}_M\}$, where $\mathbf{p}_j = [x_j, y_j, z_j]^T$. The steering vector corresponding to the azimuth-elevation angle pair (ϕ_i, θ_i) can be calculated as in equations (2.2) and (2.4), given by the following equations:

$$\mathbf{a}(\phi_i, \theta_i) = [v(\phi_i, \theta_i, \mathbf{p}_1)\ v(\phi_i, \theta_i, \mathbf{p}_2)\ \ldots\ v(\phi_i, \theta_i, \mathbf{p}_M)]^T, \tag{D.1}$$

$$v(\phi_i, \theta_i, \mathbf{p}_j) = \exp\left(j\frac{2\pi}{\lambda}(x_j \cos(\phi_i)\sin(\theta_i) + y_j \sin(\phi_i)\sin(\theta_i) + z_j \cos(\theta_i))\right) \tag{D.2}$$

The vectorization term in equation (3.13), $vec(\mathbf{a}(\phi_i, \theta_i)\mathbf{a}^H(\phi_i, \theta_i))$, can be written in terms of the Kronecker product as follows:

$$vec(\mathbf{a}(\phi_i, \theta_i)\mathbf{a}^H(\phi_i, \theta_i)) = \mathbf{a}^*(\phi_i, \theta_i) \otimes \mathbf{a}(\phi_i, \theta_i) \tag{D.3}$$

where $\otimes$ denotes the Kronecker product. The Khatri-Rao product, which is the column-wise Kronecker product, is explained in the following equation before explaining the main concept:

$$\begin{aligned} \mathbf{C} &= [\mathbf{c}_1, \mathbf{c}_2, \mathbf{c}_3], \\ \mathbf{D} &= [\mathbf{d}_1, \mathbf{d}_2, \mathbf{d}_3], \\ \mathbf{C} \odot \mathbf{D} &= [\mathbf{c}_1 \otimes \mathbf{d}_1, \mathbf{c}_2 \otimes \mathbf{d}_2, \mathbf{c}_3 \otimes \mathbf{d}_3], \end{aligned} \tag{D.4}$$

where $\odot$ denotes the Khatri-Rao product. Now, let's revisit equation (D.3) with the

understanding from equations (D.1) and (D.2):

$$\begin{aligned}\mathbf{a}^*(\phi_i,\theta_i)\otimes\mathbf{a}(\phi_i,\theta_i) &= \begin{bmatrix} v^*(\phi_i,\theta_i,\mathbf{p}_1)v(\phi_i,\theta_i,\mathbf{p}_1) \\ v^*(\phi_i,\theta_i,\mathbf{p}_1)v(\phi_i,\theta_i,\mathbf{p}_2) \\ \vdots \\ v^*(\phi_i,\theta_i,\mathbf{p}_1)v(\phi_i,\theta_i,\mathbf{p}_M) \\ v^*(\phi_i,\theta_i,\mathbf{p}_2)v(\phi_i,\theta_i,\mathbf{p}_1) \\ \vdots \\ v^*(\phi_i,\theta_i,\mathbf{p}_M)v(\phi_i,\theta_i,\mathbf{p}_M) \end{bmatrix} \\ &= \begin{bmatrix} v(\phi_i,\theta_i,\mathbf{p}_1-\mathbf{p}_1) \\ v(\phi_i,\theta_i,\mathbf{p}_1-\mathbf{p}_2) \\ \vdots \\ v(\phi_i,\theta_i,\mathbf{p}_1-\mathbf{p}_M) \\ v(\phi_i,\theta_i,\mathbf{p}_2-\mathbf{p}_1) \\ \vdots \\ v(\phi_i,\theta_i,\mathbf{p}_M-\mathbf{p}_M) \end{bmatrix}\end{aligned} \tag{D.5}$$

As seen from equation (D.5), by computing $\text{vec}(\mathbf{a}(\phi_i,\theta_i)\mathbf{a}^H(\phi_i,\theta_i))$, the steering vector of the difference co-array is obtained, which utilizes the position differences to form a steering vector. For a multi-source case, equation (D.5) can be extended to matrix notation and explained by the Khatri-Rao product using equation (D.4):

$$\mathbf{A} = [\mathbf{a}(\phi_1,\theta_1),\ldots,\mathbf{a}(\phi_K,\theta_K)] \tag{D.6}$$

$$\mathbf{A}^*\odot\mathbf{A} = [\mathbf{a}^*(\phi_1,\theta_1)\otimes\mathbf{a}(\phi_1,\theta_1),\ldots,\mathbf{a}^*(\phi_K,\theta_K)\otimes\mathbf{a}(\phi_K,\theta_K)] \tag{D.7}$$

The array manifold of the difference co-array of the physical array can be calculated using equation (D.7).

APPENDIX E

COST FUNCTION FOR MAXIMUM LIKELIHOOD COVARIANCE MATRIX ESTIMATION

Assume an antenna array with M elements, N snapshots are collected from the received signal $\mathbf{Y} \in \mathbb{C}^{M \times N}$. Assuming each row of $\mathbf{Y}$ has zero mean, the sample covariance matrix of the received signal can be computed as follows:

$$\mathbf{R}_{\mathbf{Y}} = \frac{1}{N}\mathbf{Y}\mathbf{Y}^{H} \tag{E.1}$$

Using the sample covariance matrix $\mathbf{R}_{\mathbf{Y}}$, the maximum likelihood (ML) estimation covariance matrix $\mathbf{\Sigma}$ can be derived through the following steps. First, the likelihood function is written as:

$$\mathcal{L}_1(\mathbf{\Sigma}) = (2\pi)^{-\frac{NM}{2}} \prod_{i=1}^{N} |\mathbf{\Sigma}|^{-\frac{1}{2}} \exp\left(-\frac{1}{2}\mathbf{y}_i^H \mathbf{\Sigma}^{-1}\mathbf{y}_i\right) \tag{E.2}$$

where $|\cdot|$ denotes the determinant, and $\mathbf{y}_i$ is the i-th column of the received signal $\mathbf{Y}$. By eliminating the scaling term $(2\pi)^{-\frac{NM}{2}}$ and computing the product, the likelihood function simplifies to:

$$\mathcal{L}_2(\mathbf{\Sigma}) = |\mathbf{\Sigma}|^{-\frac{N}{2}} \exp\left(-\frac{1}{2}\sum_{i=1}^{N} \mathbf{y}_i^H \mathbf{\Sigma}^{-1}\mathbf{y}_i\right) \tag{E.3}$$

To further simplify, we apply the trace operation ($\mathrm{tr}(\cdot)$), which allows us to rewrite the sum of quadratic forms as a trace. Thus, equation (E.3) transforms into:

$$\mathcal{L}_3(\boldsymbol{\Sigma}) = |\boldsymbol{\Sigma}|^{-\frac{N}{2}} \exp\left(-\frac{1}{2}\operatorname{tr}(N\mathbf{R}_{\mathbf{Y}}\boldsymbol{\Sigma}^{-1})\right) \tag{E.4}$$

Taking the natural logarithm of equation (E.4) simplifies the product inside the exponential and the determinant term, yielding:

$$\ln \mathcal{L}_4(\boldsymbol{\Sigma}) = -\frac{N}{2}\ln|\boldsymbol{\Sigma}| - \frac{1}{2}\operatorname{tr}(N\mathbf{R}_{\mathbf{Y}}\boldsymbol{\Sigma}^{-1}) \tag{E.5}$$

By taking the constant N outside the trace operation and eliminating the scaling term $-\frac{N}{2}$, we further simplify the expression to obtain the final cost function:

$$\mathcal{L}_5(\boldsymbol{\Sigma}) = \ln|\boldsymbol{\Sigma}| + \operatorname{tr}(\mathbf{R}_{\mathbf{Y}}\boldsymbol{\Sigma}^{-1}) \tag{E.6}$$

Equation (E.6) represents the cost function for maximum likelihood covariance matrix estimation.

APPENDIX F

OPTIMIZING APERTURE SCALING IN 4-ARM NCRA CONFIGURATIONS

As shown in Table 4.1, the 4-arm configurations of the Nested Circular Ring Array (NCRA) are scaled by a factor of 0.9. This adjustment is necessary to address an ambiguity problem inherent in the 4-arm structure. Consider a 4-arm configuration with a 2-element Uniform Linear Array (ULA) on each arm, as illustrated in Figure F.1.

The steering vectors for a 90° elevation angle can be calculated using the following equations:

$$\mathbf{a}(\phi) = \begin{bmatrix} e^{j\frac{2\pi}{\lambda}(x_1\cos(\phi)+y_1\sin(\phi))} \\ e^{j\frac{2\pi}{\lambda}(x_2\cos(\phi)+y_2\sin(\phi))} \\ e^{j\frac{2\pi}{\lambda}(x_3\cos(\phi)+y_3\sin(\phi))} \\ e^{j\frac{2\pi}{\lambda}(x_4\cos(\phi)+y_4\sin(\phi))} \\ e^{j\frac{2\pi}{\lambda}(x_5\cos(\phi)+y_5\sin(\phi))} \end{bmatrix} = \begin{bmatrix} e^{j\frac{2\pi}{\lambda}(0\cos(\phi)+0\sin(\phi))} \\ e^{j\frac{2\pi}{\lambda}(\frac{\lambda}{2}\cos(\phi)+0\sin(\phi))} \\ e^{j\frac{2\pi}{\lambda}(0\cos(\phi)+\frac{\lambda}{2}\sin(\phi))} \\ e^{j\frac{2\pi}{\lambda}(-\frac{\lambda}{2}\cos(\phi)+0\sin(\phi))} \\ e^{j\frac{2\pi}{\lambda}(0\cos(\phi)+-\frac{\lambda}{2}\sin(\phi))} \end{bmatrix} = \begin{bmatrix} 1 \\ e^{j\pi\cos(\phi)} \\ e^{j\pi\sin(\phi)} \\ e^{-j\pi\cos(\phi)} \\ e^{-j\pi\sin(\phi)} \end{bmatrix} \tag{F.1}$$

$$\mathbf{a}(0^\circ) = \mathbf{a}(180^\circ) = \begin{bmatrix} 1 \\ -1 \\ 1 \\ -1 \\ 1 \end{bmatrix}, \quad \mathbf{a}(90^\circ) = \mathbf{a}(270^\circ) = \begin{bmatrix} 1 \\ 1 \\ -1 \\ 1 \\ -1 \end{bmatrix} \tag{F.2}$$

As shown in equation (F.2), the configuration given in Figure F.1 is ambiguous due to its geometry. This ambiguity can be resolved by reducing the array aperture. Assume the sensor positions are multiplied by 0.9, effectively reducing the array aperture by

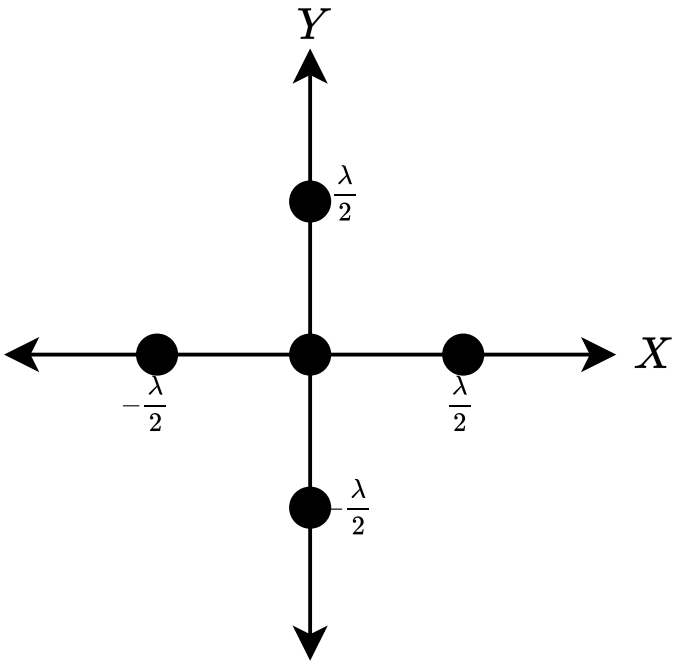

Figure F.1: Scaling for ambiguity problem of 4-arm NCRA configurations.

10%. The steering vectors for azimuth angles $0°, 90°, 180°, 270°$ of the scaled array are given in the following equations:

$$\mathbf{a}(0°) = \begin{bmatrix} 1 \\ -0.951 + j0.309 \\ 1 \\ -0.951 - j0.309 \\ 1 \end{bmatrix}, \quad \mathbf{a}(180°) = \begin{bmatrix} 1 \\ -0.951 - j0.309 \\ 1 \\ -0.951 + j0.309 \\ 1 \end{bmatrix}$$

$$\mathbf{a}(90°) = \begin{bmatrix} 1 \\ 1 \\ -0.951 + j0.309 \\ 1 \\ -0.951 - j0.309 \end{bmatrix}, \quad \mathbf{a}(270°) = \begin{bmatrix} 1 \\ 1 \\ -0.951 - j0.309 \\ 1 \\ -0.951 + j0.309 \end{bmatrix} \tag{F.3}$$

As seen in equation (F.3), the ambiguity problem for the 4-arm NCRA is resolved by reducing the aperture, while still maintaining a wider aperture than a UCA with the same number of elements and maximum unambiguous radius. Figure F.2 illustrates the scaling effect for all 4-arm NCRA configurations.

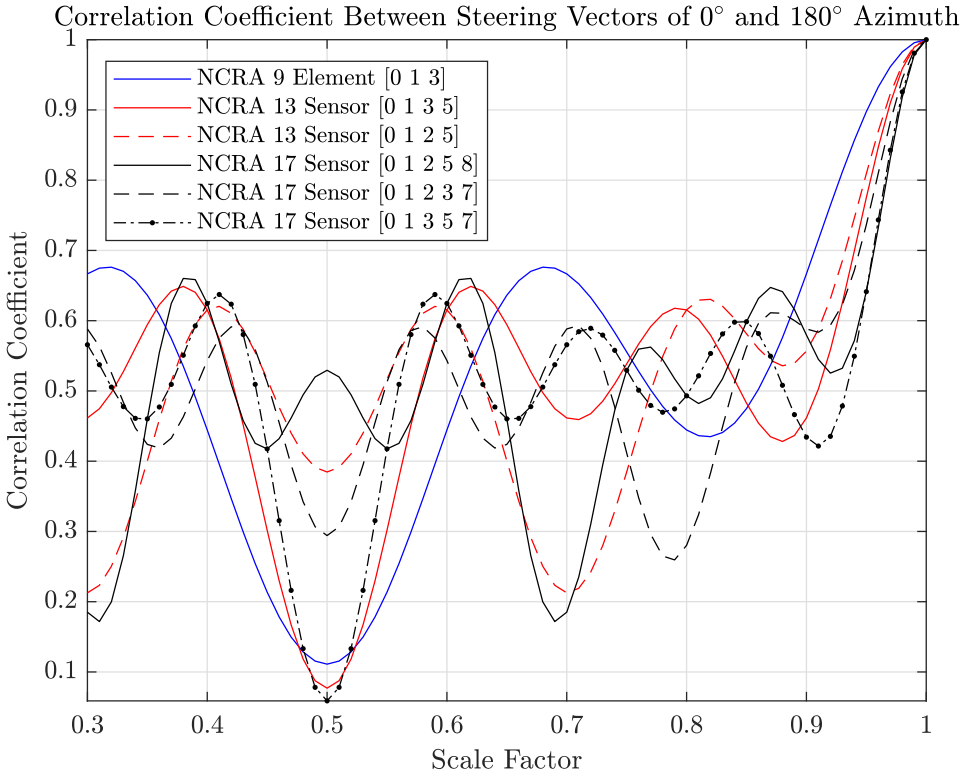

Figure F.2: Scaling effect for 4-arm NCRA configurations.